TECHNISCHE UNIVERSITÄT MÜNCHEN
Zentrum Mathematik

Feedback Loops With Time Scales

Stefan Brandt

TECHNISCHE UNIVERSITÄT MÜNCHEN
Zentrum Mathematik

Feedback Loops With Time Scales

Stefan Brandt

Vollständiger Abdruck der von der Fakultät für Mathematik der Technischen Universität München zur Erlangung des akademischen Grades eines

Doktors der Naturwissenschaften (Dr. rer. nat.)

genehmigten Dissertation.

Vorsitzender:		Univ.-Prof. Dr. Peter Rentrop
Prüfer der Dissertation:	1.	Univ.-Prof. Dr. Johannes Müller
	2.	Univ.-Prof. Dr. Jürgen Scheurle
	3.	Ao. Univ.-Prof. Dr. Peter Szmolyan Technische Universität Wien, Österreich (Schriftliche Beurteilung)

Die Dissertation wurde am 01. September 2009 bei der Technischen Universität München eingereicht und durch die Fakultät für Mathematik am 10. Februar 2010 angenommen.

Zusammenfassung

Rückkopplungsschleifen ("Feedback Loops") bilden ein zentrales Motiv in biologischen regulatorischen Netzwerken. Sie spielen außerdem eine wichtige Rolle im Auffinden von Hysterese-Effekten und/oder oszillativem Verhalten. In dieser Arbeit entwickeln wir ein allgemeines Model für gekoppelte Feedback Loops, wobei wir einen schnellen positiven mit einem langsamen negativen Feedback Loop verbinden. Das Einführen der verschiedenen Zeitskalen erlaubt eine tiefere mathematische Analyse eines drei-dimensionalen Prototyps. Wir beweisen die Existenz einer Linie von Hopf-Bifurkationen, einer Linie von homoklinen Orbits und Canard Orbits. Desweiteren untersuchen wir vier verschiedene generische Systeme in einem assoziierten planaren Fall numerisch. Als eine möglich Anwendung gekoppelter Feedback Loops analysieren wir ein Model für die Blutgerinnung.

Abstract

Feedback loops are a central motive in biological regulatory networks, playing an important role finding hysteresis effects and oscillatory behavior. In this thesis we develop a general system of coupled feedback loops, combining a fast positive feedback loop with a slow negative one. The introduction of different time scales allows a deeper investigation of a three-dimensional prototype. We prove the existence of a line of Hopf bifurcations, a line of homoclinic orbits, and canard cycles. Furthermore we give a numerical description of four generic cases in an associated planar case. As an application of coupled feedback loops we investigate a model of the blood coagulation system.

Acknowledgement

The last years have been an amazing, challenging and enjoyable experience. A lot of people contributed to that, and even if it is impossible to mention all of them here, I want them to know, that I am very thankful for all their help, all their encouragement and for numerous interesting discussions.

First and foremost, I sincerely thank my advisor Prof. Dr. Johannes Müller for introducing me into the field of biomathematics, for the constant support and for the continued helpful advice.

The research for this thesis was carried out at the Helmholtz Center Munich - German Research Center for Environmental Health. I am very grateful to Prof. Dr. Rupert Lasser for giving me the possibility to work at the Institute of Biomathematics and Biometry and for the excellent working conditions there.

A special thank goes to Prof. Dr. Peter Szmolyan for the opportunity to visit him at the TU Wien and for the fruitful discussions during my stay there.

Out of all the members at the IBB I wish to express my gratitude to Christina, Wolfgang, Burkhard, Moritz, Stefan, Kristine and Alexandra. A special thank goes to Georg for providing a constant support of coffee and for having an endless patience listening to my problems.

Last but not least I thank my parents, who always supported me. Their patience, understanding and encouragement were a great help, when it was most required.

Contents

1 Introduction **1**

2 Fundamental Setting And Requisites **3**
2.1 Biological Motivation 3
2.2 Tools From Geometric Singular Perturbation Theory 8

3 Coupled Feedback Loops **12**
3.1 General System 12
3.1.1 Fast And Slow System 12
3.1.2 The Layer Problem 14
3.2 Simplified System 18
3.2.1 Bifurcations In The Layer Problem 20
3.2.2 A Picture Of The Flow For $\varepsilon = 0$ 24

4 Two-dimensional Approach **30**
4.1 A New Time Scale 30
4.2 The Canard Point 33
4.2.1 The Flow Near The Canard Point 36
4.2.2 The Chart K_2 38
4.2.3 The Chart K_1 41
4.2.4 Outlines Of Proofs 46
4.3 The Homoclinic Point 49
4.4 Global Aspects Of The Flow 52

5 Three-dimensional Approach **59**
5.1 Local Flow Near The Canard Point 59
5.2 Periodic Orbits I 61
5.3 Homoclinic Orbit 64
5.4 Periodic Orbits II 68

6 Global Behavior Of Prototypical Examples **75**
6.1 Takens - Bogdanov Bifurcation 75
6.2 Unstable TB Orbits, A > 0 78
6.3 Unstable TB Orbits, A < 0 80
6.4 Stable TB Orbits, A < 0 83
6.5 Stable TB Orbits, A > 0 85

7 Application: The Extrinsic Coagulation System **89**
7.1 Motivation 89
7.2 Key Players 92
7.3 Threshold Behavior: A Minimal Model 95
7.4 Minimal Model For The Whole Story 104
7.5 Realistic coagulation models 108
7.6 Discussion 115

1 Introduction

Searching the internet for the term "feedback loop" one finds the following statement: "Scientists: 'Feedback Loops' Are the Single-Biggest Threat to Civilization From Global Warming" (abcNEWS, [52]). The thawing of the vast tundra reveals old decayed vegetation, which releases carbon dioxide influencing the warming of the atmosphere again. As it becomes clear, the knowledge about feedback loops is of central importance to understand physical and biological behavior, even if the example above is a little over the top. However, feedback loops arise often in biological networks and play an important role in the overall biological processes. Thus this work deals with the analysis of coupled feedback loops to get a better understanding of the underlying biological features.

In chapter 2 we give a short overview of feedback loops arising in biological systems. We derive systems of ordinary differential equations, describing positive as well as negative feedback loops. After the introduction of time scales we formulate our starting system of coupled feedback loops, which will be the subject of investigation throughout this work. Furthermore we are dealing with some mathematical tools from geometric singular perturbation theory used in the following chapters.

Chapter 3 is dedicated to some first investigations of general concepts underlying our system of coupled feedback loops. After analyzing steady states and their stabilities we reduce our system to three dimensions in order to get the possibility to treat our system analytically. The layer problem of this simplified system is investigated and bifurcations are determined.

In an approach to use known results from geometric singular perturbation theory we artificially introduce a third time scale to further reduce our system in chapter 4. We derive a singularly perturbed two-dimensional system, where the existence of a canard explosion is proven. Furthermore the small Hopf cycles local to the canard point grow to canard cycles and eventually end in an homoclinic orbit.

In chapter 5 we return to our three-dimensional system. With the help of center manifold theory we show that the flow local to the canard point remains equivalently to that in the two-dimensional case. We then recover Hopf cycles, which grow to canard cycles, as well as an homoclinic orbit. The approach remains the same as in the two-dimensional case, however, some additional statements are necessary.

Numerical simulations are the subject of chapter 6. We inspect four different systems, which lead to different bifurcation diagrams. It is shown, that under generical conditions these systems develop a Takens - Bogdanov bifurcation (TB) and that the canard bifurcation point and the TB are connected by a line of Hopf points. Numerical simulations show that the line of homoclinic orbits emanating at the canard bifurcation point also connects to the TB. We give a full numerical description of the flow for different regions in the parameter space.

A system of coupled feedback loops arises in modelling the extrinsic coagulation cascade. Chapter 7 focuses on the description of an modelling approach towards an explanation, why blood flow may play a crucial role in the biological coagulation system. It is meant as an application for the insight we got in the last chapters.

2 Fundamental Setting And Requisites

From a biomathematical viewpoint, the analysis of feedback loops are of central importance. We give a short introduction in modelling such loops, where we derive systems of ordinary differential equations for positive as well as negative feedback loops. Some basic properties of such systems are mentioned. Under the additional assumption of different time scales we then formulate a model for coupled feedback loops, i.e. the combination of a fast positive feedback loop with a slow negative one, which is the subject of investigation throughout this work. Afterwards we give a short overview of the tools from geometric singular perturbation theory used within our analysis.

2.1 Biological Motivation

Over the last years mathematics has become more and more important to model, describe and predict complex biological behavior. Biomathematics has proved to be useful not only to predict quantitative results but also to analyze biological systems qualitatively. In the meantime there are quite a few biomathematical models, which helped to understand general concepts underlying the biological universe. Examples of such successful mathematical descriptions of biological systems are, among others, the Hodgkin-Huxley and Fitzhugh-Nagumo models of neural firing, the Field-Noyes model of the Belousov-Zhabotinskii reaction and epidemic models with applications to HIV. A great summary of the achievements of mathematical biology can be found in the books of Murray, [43, 44] and also in the book of Jones and Sleeman [31]. The first important appearance of feedback control mechanisms in biological systems was in the model of Goodwin [19] for the repression of enzymes by certain metabolites. A few years later this model was analytically treated by Hastings [24], who showed the existence of periodic solutions, see also [20, 21]. An overview of both positive and negative feedback loops can be found in the paper of Tyson and Othmer, [51].

Feedback Loops

To explain the term "feedback loop" we start with the generalized system of Goodwin's model, see [43, chapter 7]. Consider an enzyme (E) reacting with a substrate to form a complex, which in turn is converted into a product P. The enzyme E is produced by transcription of DNA to messenger-RNA M. However, the product P represses this

transcription of DNA to M. A schematic picture of this situation is shown in figure 2.1.

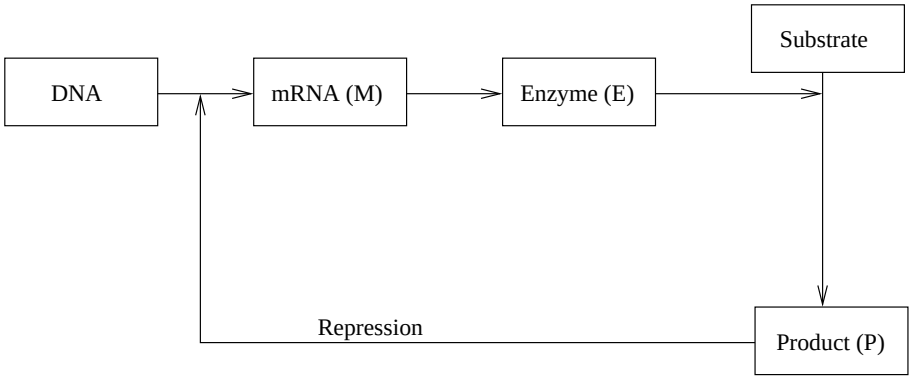

Figure 2.1: A sketch of Goodwin's model.

The mathematical model describing the above situation reads

$$\begin{aligned} \frac{dM}{dt} &= \frac{V}{D+P^m} - aM, \\ \frac{dE}{dt} &= bM - cE, \\ \frac{dP}{dt} &= dE - eP, \end{aligned}$$

where all parameters are positive constants. This model is a standard example for a negative feedback loop. The situation when output from an event in the past influences the same event in the present or future, we call that feedback. When such an event is part of a chain that forms a circuit, we call that a feedback loop. On a more abstract way feedback loops can schematically be seen as shown in figure 2.2. As for all biological substances there is a certain death rate involved, i.e. there is always a degradation term existent, here denoted by c_i.

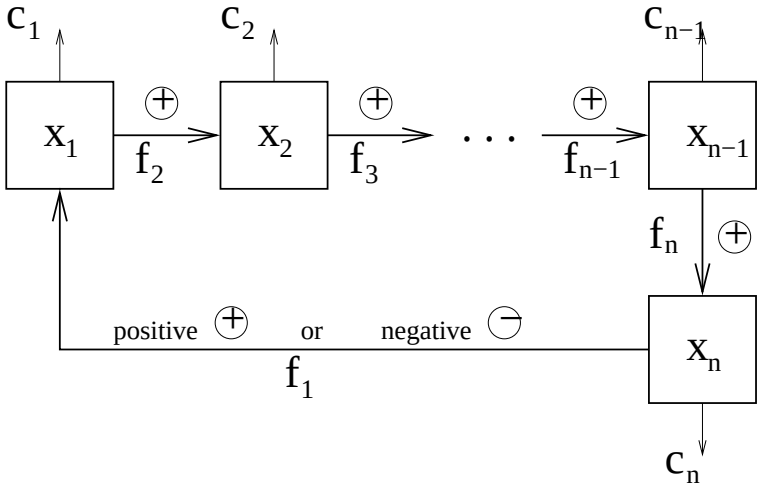

Figure 2.2: A sketch of a general feedback loop.

Deriving a mathematical model for feedback loops, we obtain

$$\begin{aligned} \dot{x}_1 &= f_1(x_n) - c_1 x_1, \\ \dot{x}_i &= f_i(x_{i-1}) - c_i x_i, \qquad i = 2, ..., n, \end{aligned} \tag{2.1}$$

where $c_i > 0$, $i = 1, ..., n$ and $f_i'(x) > 0$, $i = 2, ..., n$ for all $x \geq 0$. We call the feedback loop positive if $f_1'(x) > 0$ for all $x > 0$ and negative if $f_1'(x) < 0$ for all $x > 0$. From a biological viewpoint it is natural to assume that all substances involved are limited in the magnitude of their concentrations due to limited resources. Thus we always assume that the functions f_i are bounded. In most applications of feedback loops one concentrates on the case $f_i(x) = \alpha_i x$ for $i = 2, ..., n$, $\alpha_i > 0$ and Hill shapes for the activating function f_1. We note, that in most cases the above system can be reduced to such a problem, see [51]. It is now well known, that under these assumptions a positive feedback loop has a region of bistability considering the product of degradation rates as a bifurcation parameter. For negative feedback loops on the other hand oscillations may occur due to a Hopf bifurcation with the same bifurcation parameter considered. For a review of this behavior see the mentioned papers above. Since often feedback loops are only part of biological regulatory networks the question arises what qualitative behavior is present in coupled feedback loops, i.e. a combination of a positive with a negative one.

Some work is done in identifying non-coupled and coupled feedback loops as general network motifs in biological systems. They have been discussed in microRNAs, [49], cell-cycles, [47] and in diabetes, [4]. More general approaches can be found in the paper of Alon, [1] or in Kim et al, [34]. We are here interested in the case that the two involved loops live on different time scales, i.e. the negative feedback is considered to be very slow compared to the fast positive one.

Time Scales

Biochemical reactions are influenced by a lot of different factors. An important factor is the time it takes to complete the process. Take the above example of Goodwin's model. Here we have to take into account the time for each individual step, for example how much time does the transcription of DNA to M need or at what rate the enzyme binds to the substrate. In most cases one can assume one time scale for a whole process. However, if we couple different processes, we probably have to distinguish different time scales for each of them.

A positive feedback loop has the property to stay activated once a certain threshold is achieved and does not have the ability to down-regulate itself without further influence from outside. There are different possibilities for this influence, for example the limitation of resources. However, there are cases, where it is not possible to determine, how the down-regulation is achieved. This question gets particularly interesting in

trauma patients, considering shock or blood coagulation (see chapter 7). An interesting approach is the assumption, that the positive feedback loop itself starts another process, namely a negative feedback loop on a slow time scale. In the beginning of the whole process this negative feedback does not have any influence, but after some time passes gets stronger and finally is able to down-regulate the system. Time scales could be modelled differently. One possibility is to extend the length of the reaction chain for the negative feedback, another possibility would be to use some delay in the model. Here we take the approach of fast-slow systems, meaning we derive a singularly perturbed dynamical system.

Modelling approaches in biology with different time scales is not new, it is already used in the now famous FitzHugh-Nagumo model of neural firing, [15, 45] and in the Oregonator system of the Belousov-Zhabotinskii reaction, see for instance [50]. Especially the last one has had a great influence on analyzing singularly perturbed systems.

Coupling Of The Loops

As mentioned above we assume that a positive feedback loop gives rise to a negative one on a slow time scale. An abstract sketch of this situation is shown in figure 2.3.

We derive the following singularly perturbed system for coupled feedback loops.

$$\begin{aligned}
\dot{x}_1 &= f_1(x_n) - c_1 x_1; \\
\dot{x}_m &= f_m(x_{m-1}) - (c_m + h(y_l))x_m; \qquad 1 \leq m \leq n; \\
\dot{x}_i &= f_i(x_{i-1}) - c_i x_i; \qquad i = 2, ..., n;\ i \neq m; \\
\\
\dot{y}_1 &= \varepsilon[g_1(x_k) - d_1 y_1]; \\
\dot{y}_j &= \varepsilon[g_j(y_{j-1}) - d_j y_j]; \qquad j = 2, ..., l,
\end{aligned}$$

where $0 < \varepsilon \ll 1$. As before we assume that the constants $c_i > 0$ for all $i = 1, ..., n$ and $d_j > 0$ for all $j = 1, ..., l$. The positive feedback loop is written in $\mathbf{x}$, so that the functions f_i are strictly increasing functions and we assume that this holds even at the origin, i.e. we obtain $f_i'(x) > 0$ for all $i = 1, ..., n$ and $x \geq 0$. The assumption for g_j is equivalent, i.e. $g_j'(x) > 0$ for all $j = 1, ..., l$ and $x \geq 0$. The negative influence of the $\mathbf{y}$ chain is achieved by increasing the degradation rate of x_m by the function h. Since this negative influence should be increasing, when the negative feedback gets stronger we assume $h'(x) > 0$ for all $x \geq 0$. As already mentioned above, the general restrictions of resources (space) demand the functions f_i and g_j to be bounded, i.e.

$$\lim_{x \to \infty} f_i(x) < \infty, \quad \lim_{x \to \infty} g_j(x) < \infty,$$

for $i = 1, ..., n$, $j = 1, ..., l$. Since the negative feedback loop should be able to totally

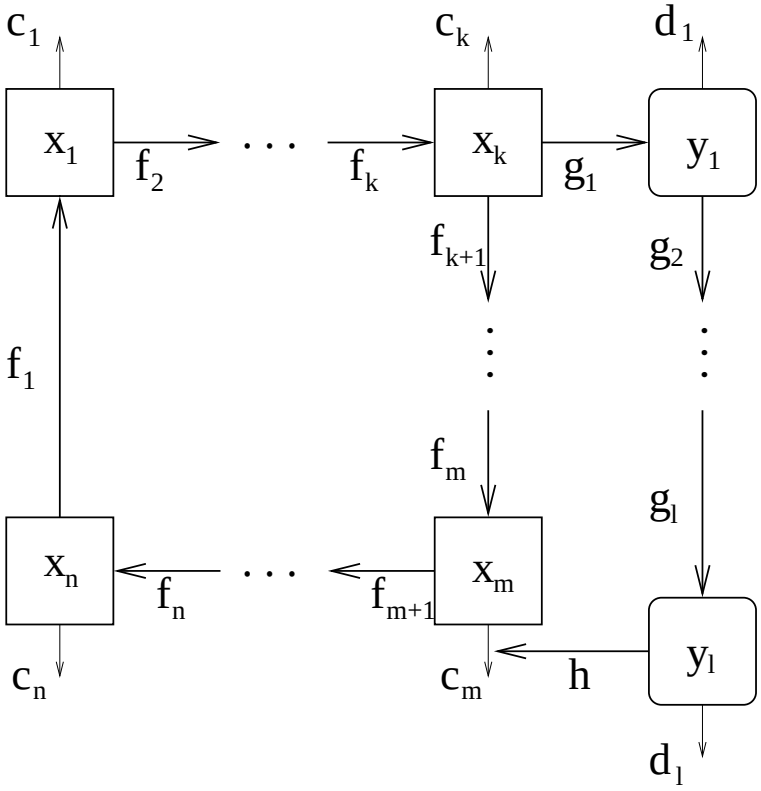

Figure 2.3: A sketch of a coupled feedback loop.

switch off the system, we assume for the function h

$$\lim_{x\to\infty} h(x) \to \infty.$$

Finally we assume that this system is not active at all, when there is no input, i.e. there is no activation of any substance as long as the concentration of the predecessor is zero. We obtain

$$f_i(0) = g_j(0) = h(0) = 0.$$

Despite the fact that for most statements smoothness of the functions is only required up to order three, we consider here for an easier mathematical treatment

$$f_i, g_j, h \in \mathcal{C}^\infty(\mathbb{R}_+, \mathbb{R}_+).$$

This system will be the starting point of our analysis beginning in chapter 2. Before we return to that we give a short introduction into the methods used within the next chapters.

2.2 Tools From Geometric Singular Perturbation Theory

Fast And Slow System

In this work we deal with singularly perturbed dynamical systems of the following form.

System (Fast System)

$$\begin{aligned} \dot{\mathbf{x}} &= F(\mathbf{x}, \mathbf{y}, \varepsilon, \lambda), \\ \dot{\mathbf{y}} &= \varepsilon \cdot G(\mathbf{x}, \mathbf{y}, \varepsilon, \lambda), \end{aligned} \tag{2.2}$$

with the definitions

$$\mathbf{x} \in \mathbb{R}^n, \quad \mathbf{y} \in \mathbb{R}^l, \quad \lambda \in \mathbb{R}, \quad 0 < \varepsilon \ll 1,$$
$$F \in \mathcal{C}^\infty(\mathbb{R}^n \times \mathbb{R}^l \times \mathbb{R} \times \mathbb{R}, \mathbb{R}^n), \quad G \in \mathcal{C}^\infty(\mathbb{R}^n \times \mathbb{R}^l \times \mathbb{R} \times \mathbb{R}, \mathbb{R}^l).$$

Here the dot, " $\dot{}$ ", means derivation by time t. The system (2.2) is called the fast system and the independent variable t is referred to as the fast time scale. By switching to the slow time scale we get an equivalent dynamical system. This is achieved by the time transformation $\tau = \varepsilon t$.

System (Slow System)

$$\begin{aligned} \varepsilon \cdot \mathbf{x}' &= F(\mathbf{x}, \mathbf{y}, \varepsilon, \lambda), \\ \mathbf{y}' &= G(\mathbf{x}, \mathbf{y}, \varepsilon, \lambda), \end{aligned} \tag{2.3}$$

This new equivalent system is called the slow system and the dash, " $'$ ", means derivation by time τ, which is referred to as the slow time scale. The general idea of analyzing systems of the form (2.2) is the description of the dynamics of the associated limiting problems for $\varepsilon = 0$ in both the fast system (2.2) and the slow system (2.3). From there one suitably combines the dynamics, i.e. one concatenates orbits of these two systems and proves, that orbits of the fast system (2.2) stay close to the concatenated structures and converge for $\varepsilon \to 0$ to them. Here we define the two limiting problems.

Definition 2.3 (Layer Problem, Reduced Problem)
The layer problem is defined as the limiting problem of the fast system (2.2) for $\varepsilon = 0$. It reads

$$\begin{aligned} \dot{\mathbf{x}} &= F(\mathbf{x}, \mathbf{y}, 0, \lambda), \\ \dot{\mathbf{y}} &= 0. \end{aligned} \tag{2.4}$$

The reduced problem is defined as the limiting problem of the slow system (2.3) for $\varepsilon = 0$. It reads

$$\begin{aligned} 0 &= F(\mathbf{x}, \mathbf{y}, 0, \lambda), \\ \mathbf{y}' &= G(\mathbf{x}, \mathbf{y}, 0, \lambda). \end{aligned} \tag{2.5}$$

For this first part we let λ be a constant. The construction of concatenated orbits can now be described the following way. First one analyzes the dynamics of the layer problem in dependence of $\mathbf{y} = \mathbf{y}_0$ with constant $\mathbf{y}_0$, which defines a flow. If this flow finally reaches a stationary point $(\mathbf{x}^*, \mathbf{y}_0)$, which is contained in the set $\{(\mathbf{x}, \mathbf{y}) \in \mathbb{R}^n \times \mathbb{R}^l : F(\mathbf{x}, \mathbf{y}, 0, \lambda) = 0\}$ the dynamics of the reduced problem takes over. This will generate a flow on the set $\{(\mathbf{x}, \mathbf{y}) \in \mathbb{R}^n \times \mathbb{R}^l : F(\mathbf{x}, \mathbf{y}, 0, \lambda) = 0\}$, which possibly reaches a stationary point of the reduced problem and from there the dynamics of the layer problem take over again. We see that the set $\{(\mathbf{x}, \mathbf{y}) \in \mathbb{R}^n \times \mathbb{R}^l : F(\mathbf{x}, \mathbf{y}, 0, \lambda) = 0\}$ plays a crucial role in the analysis of the combined dynamics. We define the critical manifold.

Definition 2.4 (Critical Manifold)
The critical manifold S is defined as the set

$$S := \{(\mathbf{x}, \mathbf{y}) \in \mathbb{R}^n \times \mathbb{R}^l : F(\mathbf{x}, \mathbf{y}, 0, \lambda) = 0\}, \tag{2.6}$$

which defines the set of stationary points of the layer problem and the phase space of the reduced problem.

Persistence Of Manifolds

This section is dedicated to the work of Fenichel in [13], see also [12]. He proved three important theorems, that, under certain conditions, give a complete description of the $\varepsilon \neq 0$ flow in the neighborhood of subsets of the critical manifold S. Here we follow [27], see also [28].

Definition 2.5 (Normally Hyperbolic Manifold)
A l-dimensional subset $S_0 \subset S$ is said to be normally hyperbolic, if the linearization of the layer problem (2.4) at each point $(\hat{x}, \hat{y}) \in \hat{S}_0$ has exactly l eigenvalues with zero real part, where $\hat{S}_0 \subset S$ is an l-dimensional manifold containing S_0 in its interior.

In the following we use the notation $x \cdot t$ to denote the application of a flow after time t to the initial condition x.

Definition 2.6 (Local Invariance)
A set S is locally invariant under the flow of (2.2) if it has a neighborhood V so that no trajectory can leave S without also leaving V. In other words, it is locally invariant if for all $x \in S$, $x \cdot [0, t] \subset V$ implies that $x \cdot [0, t] \subset M$, similarly with $[0, t]$ replaced by $[t, 0]$ when $t < 0$.

We make the following assumptions throughout this chapter:

(H1) The set S_0 is a compact manifold, possibly with boundary, and is normally hyperbolic relative to (2.4).

(H2) The set S_0 is given as the graph of the C^∞ function $s_0(y)$ for $y \in K$. The set K is a compact, simply connected domain whose boundary is a $(l-1)$ - dimensional C^∞ submanifold.

We state Fenichel's first theorem.

Theorem 2.7 (Fenichel's First Theorem)
If $\varepsilon > 0$, but sufficiently small, there exists a manifold S_ε that lies within $O(\varepsilon)$ of S_0 and is diffeomorphic to S_0. Moreover it is locally invariant under the flow of (2.2), and C^r, including in ε, for any $r < \infty$.

The manifold S_ε is referred to as the slow manifold. If the slow manifold S_ε is represented in terms of x given as a function of y, i.e. $x = s_\varepsilon(y)$, then the system governing the flow on S_ε can be written as

$$y' = g(s_\varepsilon(y), y, \varepsilon, \lambda). \tag{2.7}$$

and because $s_\varepsilon(y) \to s_0(y)$ as $\varepsilon \to 0$ the limit of this system is given by the flow of the reduced problem (2.5)

$$y' = g(s_0(y), y, 0, \lambda). \tag{2.8}$$

The great advantage of this approach is that equation (2.7) can be interpreted as a regular perturbation of (2.8) so that the singular nature of the perturbation has been suppressed. If we have some robust structure in the flow on the critical manifold (2.8) we can reasonably expect it to perturb to the flow on the slow manifold (2.7). Fenichel's first theorem now guarantees that under the above hypotheses (H1) and (H2) there exists such a function $s_\varepsilon(y)$ defined on K so that $S_\varepsilon = \{(x, y) : x = s_\varepsilon(y)\}$, see also Theorem 2 in [27].

Fenichel's first theorem gives a picture of the flow on the slow manifold but it is also important to understand the flow in a neighborhood of the slow manifold. Let $p \in S_0$ be a point on the critical manifold. The linearized flow at p has exactly l eigenvalues with zero real part as S_0 is normally hyperbolic. The corresponding l eigenvectors span the critical manifold. The normal directions are either stable or unstable. Therefor there is a stable manifold $W^s(p)$ attached to p spanned by the eigenvectors corresponding to the eigenvalues with negative real part and there is an unstable manifold $W^u(p)$ attached to p spanned by the eigenvectors corresponding to the eigenvalues with positive real part. These manifolds can be collected together to make manifolds for the full critical manifold S_0:

$$\begin{aligned} W^s(S_0) &= \cup_{p \in S_0} W^s(p), \\ W^u(S_0) &= \cup_{p \in S_0} W^u(p). \end{aligned}$$

The persistence of these manifolds for $\varepsilon \neq 0$ is described in Fenichel's second theorem.

Theorem 2.8 (Fenichel's Second Theorem)
If $\varepsilon > 0$ but sufficiently small, there exist manifolds $W^s(S_\varepsilon)$ and $W^u(S_\varepsilon)$ that lie within $O(\varepsilon)$ of, and are diffeomorphic to, $W^s(S_0)$ and $W^u(S_0)$ respectively. Moreover, they are each locally invariant under the flow of (2.2), and C^r, including in ε, for any $r < \infty$.

We use the terms stable and unstable manifolds for $W^s(S_\varepsilon)$ and $W^u(S_\varepsilon)$ respectively, which is justified by the connection with the corresponding objects when $\varepsilon = 0$. Recall the stable and unstable manifolds $W^s(p)$ and $W^u(p)$ for a point $p \in S_0$. Since their base points do not remain as critical points when $\varepsilon \neq 0$, it seems absurd that these manifolds perturb. The answer to this question gives the third theorem of Fenichel.

Theorem 2.9 (Fenichel's Third Theorem)
Let $\varepsilon > 0$ but sufficiently small. For every $p_\varepsilon \in S_\varepsilon$, there exists a manifold $W^s(p_\varepsilon) \subset W^s(S_\varepsilon)$, and a manifold $W^u(p_\varepsilon) \subset W^u(S_\varepsilon)$, lying within $O(\varepsilon)$ of, and diffeomorphic to, $W^s(p_0)$ and $W^u(p_0)$ respectively. The family $\{W^s(p_\varepsilon) : p_\varepsilon \in S_\varepsilon\}$is invariant in the sense that

$$W^s(p_\varepsilon) \cdot t \ \subset \ W^s(p_\varepsilon \cdot t),$$

and the family $\{W^u(p_\varepsilon) : p_\varepsilon \in S_\varepsilon\}$ is invariant in the sense that

$$W^u(p_\varepsilon) \cdot t \ \subset \ W^u(p_\varepsilon \cdot t).$$

Here $p_\varepsilon \cdot t$ denotes the trajectory through p_ε evolved after time t. The manifolds $W^s(p_\varepsilon)$ and $W^u(p_\varepsilon)$ for points $p \in S_\varepsilon$ are referred to as the Fenichel fibers.

Fenichel Normal Form

As a consequence of the theorems of Fenichel above, one derives the Fenichel Normal Form for singularly perturbed equations in the neighborhood of a slow manifold. Assume that $\dim W^s(S_0) = m$ and $\dim W^u(S_0) = k$, $m+k = n$. Then the Fenichel Normal Form reads

$$\begin{aligned} a' &= \Lambda(a,b,y,\varepsilon)a, \\ b' &= \Gamma(a,b,y,\varepsilon)b, \\ y' &= \varepsilon[h(y,\varepsilon) + H(a,b,y,\varepsilon)(a,b)], \end{aligned} \tag{2.9}$$

which holds in the set $D = \{(a,b,y,\varepsilon) : |a| \leq \Delta, |b| \leq \Delta, y \in K, \varepsilon \in [0,\varepsilon_0]\}$. Here $a \in \mathbb{R}^k$, $b \in \mathbb{R}^m$, Λ and Γ are matrices with $\Lambda(0,0,y,0) = A(y)$, where $A(y)$ is a matrix whose eigenvalues have positive real parts, and with $\Gamma(0,0,y,0) = B(y)$, where $B(y)$ is a matrix whose eigenvalues have negative real parts. $H(a,b,y,\varepsilon)$ is a bilinear function of a and b. This version of the normal form was derived in [29], a slightly different one in [30].

3 Coupled Feedback Loops

After introducing the modelling approach for coupled feedback loops in the last chapter, we now deal with the mathematical analysis of the resulting system. In this chapter we describe some of the properties of the layer problem in the general system. Afterwards, we concentrate our attention to the special case of a three-dimensional system and formulate assumptions which allow us to describe the picture of the flow for $\varepsilon = 0$ in the layer and the reduced problem.

3.1 General System

3.1.1 Fast And Slow System

To be precise about the assumptions, we start this chapter with restating the general system of coupled feedback loops developed in the last chapter.

System (Fast System)
The general system for coupled feedback loops is defined by

$$\begin{array}{lcll} \dot{x}_1 & = & f_1(x_n) - c_1 x_1; & \\ \dot{x}_m & = & f_m(x_{m-1}) - (c_m + h(y_l))x_m; & 1 \leq m \leq n; \\ \dot{x}_i & = & f_i(x_{i-1}) - c_i x_i; & i = 2, ..., n;\ i \neq m; \\ & & & \\ \dot{y}_1 & = & \varepsilon[g_1(x_k) - d_1 y_1]; & \\ \dot{y}_j & = & \varepsilon[g_j(y_{j-1}) - d_j y_j]; & j = 2, ..., l; \end{array} \tag{3.1}$$

where

$$\left.\begin{array}{l} c_i, d_j \in \mathbb{R}^+, \quad f_i, g_j, h \in \mathcal{C}^\infty(\mathbb{R}_+, \mathbb{R}_+), \\ f_i(0) = g_j(0) = h(0) = 0, \quad 0 < \varepsilon \ll 1, \\ f_i'(x), g_j'(x), h'(x) > 0 \quad \forall\, x \in \mathbb{R}_+, \\ \lim\limits_{x\to\infty} f_i(x) < \infty, \quad \lim\limits_{x\to\infty} g_j(x) < \infty, \\ \lim\limits_{x\to\infty} h(x) \to \infty \end{array}\right\} \quad \begin{array}{lcl} i & = & 1, ..., n; \\ j & = & 1, ..., l; \end{array}$$

and the initial values

$$\begin{pmatrix} \mathbf{x} \\ \mathbf{y} \end{pmatrix}(0) = \begin{pmatrix} \mathbf{x}_0 \\ \mathbf{y}_0 \end{pmatrix} \in \mathbb{R}^n_+ \times \mathbb{R}^l_+.$$

From a mathematical view this defines a singularly perturbed dynamical system as described in the previous chapters. Before we start with the analysis we slightly adapt the system, and extend it to allow negative values as well. Of course, this does not have a biological meaning but for the mathematical description it provides useful insight. At the end, we are only interested in the dynamics within the positive cone. This gives us the freedom to extend f_i, g_j and h to $\mathbb{R}$ in such a way that

$$\left.\begin{array}{l} f_i, g_j, h \in \mathcal{C}^\infty(\mathbb{R},\mathbb{R}), \\ f_i'(x), g_j'(x), h'(x) > 0 \quad \forall\, x \in \mathbb{R}, \\ \lim\limits_{x\to\pm\infty} |f_i(x)| < \infty, \quad \lim\limits_{x\to\pm\infty} |g_j(x)| < \infty, \\ \lim\limits_{x\to\infty} h(x) \to \infty, \quad \lim\limits_{x\to-\infty} h(x) \to -\infty. \end{array}\right\} \begin{array}{rcl} i &=& 1,...,n; \\ j &=& 1,...,l; \end{array}$$

Furthermore we now allow negative values for the initial values as well. The initial conditions then read

$$\mathbf{x}(0) = \mathbf{x}_0 \in \mathbb{R}, \quad y_j(0) = y_{j,0} \in \mathbb{R}, j = 1,...,l-1, \quad y_l(0) = y_{l,0} \in (h^{-1}(-c_m), \infty).$$

Remark 3.2 (Restriction)
We restrict the initial value of $y_{l,0} \in (h^{-1}(-c_m), \infty)$ to ensure, that $c_m + h(y_{l,0}) > 0$.

Recalling the terms of chapter 2 we introduce the equivalent slow system as well as the two limiting problems for $\varepsilon = 0$, i.e. the layer and the reduced problem. As before the dot " $\dot{}$ " means derivation by the fast time t whereas derivation by the slow time τ is denoted by the dash " $'$ ". Applying now the time transformation $\tau = \varepsilon t$ we get the slow system.

System (Slow System)
The slow system, which is equivalent to system (3.1), has the following form.

$$\begin{array}{rcll} \varepsilon x_1' &=& f_1(x_n) - c_1 x_1; & \\ \varepsilon x_m' &=& f_m(x_{m-1}) - (c_m + h(y_l))\, x_m; & 1 \le m \le n; \\ \varepsilon \dot{x}_i' &=& f_i(x_{i-1}) - c_i x_i; & i = 2,...,n;\ i \neq m; \\ & & & \\ y_1' &=& g_1(x_k) - d_1 y_1; & \\ y_j' &=& g_j(y_{j-1}) - d_j y_j; & j = 2,...,l; \end{array} \tag{3.2}$$

Letting $\varepsilon \to 0$ in both systems we get the limiting problems. In order to simplify the notation we define

$$\begin{array}{rcll} \tilde{c}_i &:=& c_i; & i = 1,...,n; \quad i \neq m; \\ \tilde{c}_m &:=& c_m + h(y_{l,0}). & \end{array} \tag{3.3}$$

With this notation the layer problem and the reduced problem can be written in the following form.

System (Layer Problem)
The layer problem is defined as the limiting problem of system (3.1) for $\varepsilon = 0$,

$$\dot{x}_i \;=\; f_i(x_{i-1}) - \tilde{c}_i x_i; \quad i = 1, ..., n;, \quad x_0 := x_n, \tag{3.4}$$

System (Reduced Problem)
The reduced problem is defined as the limiting problem of system (3.2) for $\varepsilon = 0$,

$$\begin{array}{lcll} 0 &=& f_1(x_n) - c_1 x_1; & \\ 0 &=& f_m(x_{m-1}) - (c_m + h(y_l))\, x_m; & 1 \le m \le n; \\ 0 &=& f_i(x_{i-1}) - c_i x_i; & i = 2, ..., n;\ i \neq m; \\ & & & \\ y_1' &=& g_1(x_k) - d_1 y_1; & \\ y_j' &=& g_j(y_{j-1}) - d_j y_j; & j = 2, ..., l; \end{array} \tag{3.5}$$

As stated before the next step in analyzing the dynamics of (3.1) is to suitably combine the dynamics of the layer problem (3.4) and the reduced problem (3.5). It is beneficial to analyze the dynamics of the layer problem (3.4) in this general setting first.

3.1.2 The Layer Problem

The layer problem (3.4) corresponds for all positive initial values and for $y_{l,0} \in (h^{-1}(-c_m), \infty)$ to the classical model of a positive feedback loop. A lot is known for such systems, see for example [20], [21] and [51]. We state some of the properties of such systems in order to use them during the analysis of the general system (3.1). A natural condition for a model describing biochemical densities is the invariance of the positive cone and the boundedness. We first state a (generalized) result first introduced by [20].

Theorem 3.6 (Absorbing Hypercubes)
Let

$$C = \max_{i,x} f_i(x) < \infty, \quad x \in \mathbb{R},\ i = 1, ..., n.$$

Then for all $\tilde{C} > C$ *the hypercubes defined by the two vertices* $(0, 0, ..., 0)$ *and* $(\frac{\tilde{C}}{\tilde{c}_1}, \frac{\tilde{C}}{\tilde{c}_2}, ..., \frac{\tilde{C}}{\tilde{c}_n})$ *are absorbing.*

Proof.
Let $K_{\tilde{C}}$ be the hypercube defined by the two vertices $(0, 0, ..., 0)$ and $(\frac{\tilde{C}}{\tilde{c}_1}, \frac{\tilde{C}}{\tilde{c}_2}, ..., \frac{\tilde{C}}{\tilde{c}_n})$ for some $\tilde{C} > C$. Then the flow on the faces of $K_{\tilde{C}}$ is directed inwards, since for any $1 \le i \le n$ with $x_i = 0$ it is

$$\dot{x}_i = f_i(x_{i-1}) \ge 0$$

and for any $1 \le i \le n$ with $x_i = \frac{\tilde{C}}{\tilde{c}_i}$ it is

$$\dot{x}_i = f_i(x_{i-1}) - \tilde{c}_i x_i \le C - \tilde{C} < 0.$$

■

One of the most interesting properties in the stability analysis of the layer problem (3.4) is the connection between equilibria (with their respective stability) and the solutions of a fixed point equation (with characteristics of their derivatives). In order to describe this relation we first introduce the Jacobian for an equilibrium $\mathbf{x}^* = (x_1^*, ..., x_n^*)^T \in \mathbb{R}^n$ of (3.4). It reads

$$J_{x^*} = \begin{pmatrix} -\tilde{c}_1 & 0 & \cdots & 0 & f_1'(x_n^*) \\ f_2'(x_1^*) & -\tilde{c}_2 & 0 & \cdots & 0 \\ \vdots & \ddots & \ddots & \ddots & \vdots \\ 0 & \cdots & f_{n-1}'(x_{n-2}^*) & -\tilde{c}_{n-1} & 0 \\ 0 & \cdots & 0 & f_n'(x_{n-1}^*) & -\tilde{c}_n \end{pmatrix}. \tag{3.6}$$

Throughout the rest of the chapter, we formally define $x_0^* := x_n^*$. Using

$$\beta_i = f_i'(x_{i-1}^*) \quad \forall i = 1, ..., n, \tag{3.7}$$

the characteristic polynomial reads

$$P(\lambda) = \det(J - \lambda I) = (-1)^n \, [\prod_{i=1}^{n} (\tilde{c}_i + \lambda) - \prod_{i=1}^{n} \beta_i]. \tag{3.8}$$

Now we are able to describe the previously mentioned relation between a fixed point equation and the equilibria of (3.4).

Theorem 3.7 (Fixed Point Equation)
Let

$$Q : \mathbb{R} \to \mathbb{R}, \quad Q(x) := \frac{1}{\tilde{c}_n} f_n(\frac{1}{\tilde{c}_{n-1}} f_{n-1}(\dots \frac{1}{\tilde{c}_2} f_2(\frac{1}{\tilde{c}_1} f_1(x)) \dots)). \tag{3.9}$$

Then there exists a bijective map between the set of solutions of the fixed point equation $x = Q(x)$ and the equilibria $\mathbf{x}^*$ of system (3.4). Especially, the n-th component x_n^* of $\mathbf{x}^*$ satisfies $x_n^* = Q(x_n^*)$. An equilibrium $\mathbf{x}^*$ is locally asymptotically stable if $Q'(x_n^*) < 1$ and locally unstable if $Q'(x_n^*) > 1$. If $\mathbf{x}^*$ is linearly stable, then $Q'(x_n^*) < 1$ and if $\mathbf{x}^*$ is linearly unstable, then $Q'(x_n^*) > 1$.

Proof.
The equilibria of (3.4) are given by

$$x_i^* = \frac{f_i(x_{i-1}^*)}{\tilde{c}_i} \quad \forall i = 1, ..., n. \tag{3.10}$$

Inserting iteratively into the equation for x_n^*, we obtain

$$x_n^* = \frac{1}{\tilde{c}_n} f_n(\frac{1}{\tilde{c}_{n-1}} f_{n-1}(\dots \frac{1}{\tilde{c}_2} f_2(\frac{1}{\tilde{c}_1} f_1(x_n^*)) \dots)).$$

Therefore we get a solution of the fixed point equation for every equilibrium of (3.4). If we have a solution of the fixed point equation, then it is possible to construct an equilibrium using (3.10). Now we investigate the correspondence between the local stability of equilibria and the derivative of Q.

$$\begin{aligned} Q'(x_n^*) &= \tfrac{1}{\tilde{c}_n} f_n'(\tfrac{1}{\tilde{c}_{n-1}} f_{n-1}(...(\tfrac{1}{\tilde{c}_2} f_2(\tfrac{1}{\tilde{c}_1} \cdot f_1(x_n^*)))...)) \\ &\quad \tfrac{1}{\tilde{c}_{n-1}} f_{n-1}'(\tfrac{1}{\tilde{c}_{n-2}} f_{n-2}(...(\tfrac{1}{\tilde{c}_2} f_2(\tfrac{1}{\tilde{c}_1} f_1(x_n^*)))...)) \\ &\quad \vdots \\ &\quad \tfrac{1}{\tilde{c}_1} f_1'(x_n^*) \end{aligned}$$

This equation together with equation (3.10) and notation (3.7) yields

$$Q'(x_n^*) = \frac{1}{\tilde{c}_n} f_n'(x_{n-1}^*) \frac{1}{\tilde{c}_{n-1}} \cdot f_{n-1}'(x_{n-2}^*) ... \frac{1}{\tilde{c}_1} \cdot f_1'(x_n^*) = \prod_{i=1}^{n} \frac{\beta_i}{\tilde{c}_i}.$$

Define the polynomial

$$\tilde{P}(\lambda) := \prod_{i=1}^{n} (\tilde{c}_i + \lambda) - \prod_{i=1}^{n} \beta_i.$$

Because the function $\tilde{P}(\lambda)$ is strictly increasing for $\lambda > 0$, there is a zero of $\tilde{P}(\lambda)$ (and therefore of the characteristic polynomial $P(\lambda)$) in $\mathbb{R}^+$ if and only if $\tilde{P}(0) < 0$. Since

$$Q'(x_n^*) > 1 \quad \Leftrightarrow \quad \tilde{P}(0) < 0,$$

the equilibrium $\mathbf{x}^*$ is unstable if $Q'(x_n^*) > 1$.

Next we show that $Q'(x_n^*) < 1$ implies that the corresponding equilibrium $\mathbf{x}^*$ is locally asymptotically stable. Let $\tilde{c} = (\max_i \tilde{c}_i) + 1$ and define $J_{\tilde{c},x^*} := J_{x^*} + \tilde{c}I$, where $I \in \mathbb{R}^{(n,n)}$ denotes the identity matrix. $J_{\tilde{c},x^*}$ is nonnegative and it follows (Perron-Frobenius-theorem for nonnegative matrices, see for instance Gantmacher [17]) for the spectrum $\sigma(J_{\tilde{c},x^*})$, that

$$\sigma(J_{\tilde{c},x^*}) \subset \{z : \Re(z) \leq \rho(J_{\tilde{c},x^*})\},$$

where $\rho(J_{\tilde{c},x^*})$ is the spectral radius. Moreover, the spectral radius $\rho(J_{\tilde{c},x^*})$ is a real eigenvalue of $J_{\tilde{c},x^*}$. For J_{x^*} we obtain

$$\sigma(J_{x^*}) \subset \{z : \Re(z) \leq \rho(J_{\tilde{c},x^*}) - \tilde{c} =: \mu_{x^*}\},$$

where μ_{x^*} is a real eigenvalue of J_{x^*}. Now consider

$$Q'(x_n^*) < 1 \quad \Leftrightarrow \quad \tilde{P}(0) > 0.$$

As a consequence of $\tilde{P}(0) > 0$ all real eigenvalues of J_{x^*} are negative and therefore μ_{x^*} is negative. We conclude, that all eigenvalues of J_{x^*} have negative real parts and therefore the equilibrium $\mathbf{x}^*$ is locally asymptotically stable. The last point to show is that a linearly stable equilibrium $\mathbf{x}^*$ forces the inequality $Q'(x_n^*) < 1$ and a linearly unstable equilibrium $\mathbf{x}^*$ forces the inequality $Q'(x_n^*) > 1$. If all eigenvalues of J_{x^*} have negative real parts, there is no real eigenvalue in $\mathbb{R}^+$. With $\lim_{\lambda\to\infty} \tilde{P}(\lambda) = \infty$ it is $\tilde{P}(0) > 0$. If all eigenvalues of J_{x^*} have positive real parts, we consider again $J_{\tilde{c},x^*} := J_{x^*} + \tilde{c}I$. Then the spectral radius $\rho(J_{\tilde{c},x^*})$ is a real eigenvalue of $J_{\tilde{c},x^*}$ and $\rho(J_{\tilde{c},x^*}) - \tilde{c}$ is a real eigenvalue of J_{x^*}, which is positive and therefore $\tilde{P}(0) < 0$. ∎

We will show an ordering property of the stationary points. Therefore we define the partial ordering on $\mathbb{R}^n$.

Definition 3.8 (Partial Ordering on $\mathbb{R}^n$ generated by an orthant)
Let $x, y \in \mathbb{R}^n$, $\mathbf{p} = (p_1, p_2, ..., p_n)$, $p_i \in \{0, 1\}$, $1 \le i \le n$ and $K_p = \{x \in \mathbb{R}^n : (-1)^{p_i} x_i \ge 0, 1 \le i \le n\}$. Then we define $\preceq_{K_p}$ as

$$x \preceq_{K_p} y \Leftrightarrow y - x \in K_p.$$

If $p_i = 0$, $1 \le i \le n$, this is the usual partial ordering on $\mathbb{R}^n$ and we write $x \le y$, if and only if $y - x \in \mathbb{R}^n_+$.

Remark 3.9
Note, that

$$Q(x) - x \in \mathcal{C}^\infty, \quad \lim_{x\to\pm\infty} |Q(x) - x| \to \infty.$$

Therefore, if all zeros of $Q(x) - x$ are simple, then there exists only a finite number of zeros of $Q(x) - x$.

By using the fixed point equation, we now get another statement for the equilibria of system (3.4).

Corollary 3.10 (Ordering Of Equilibria)
Assume that all zeros of $Q(x) - x$ are simple and ordered, $x_n^{(1)} \le ... \le x_n^{(\tilde{m})}$. Then the corresponding equilibria in $\mathbb{R}^n$ are also ordered, $x^{(1)} \le ... \le x^{(\tilde{m})}$, and the stability of the equilibria alternates, i.e.

$$\left.\begin{array}{lcl} \mathbf{x}^{(q)} \text{ stable} & \Rightarrow & \mathbf{x}^{(q+1)} \text{ unstable} \\ \mathbf{x}^{(q)} \text{ unstable} & \Rightarrow & \mathbf{x}^{(q+1)} \text{ stable} \end{array}\right\} 1 \le q < \tilde{m}.$$

The equilibria $\mathbf{x}^{(1)}$ and $\mathbf{x}^{(\tilde{m})}$ are locally asymptotically stable. As a consequence there is an odd number of equilibria.

Proof.
Since $f_i(x)$ is strictly increasing for all $i = 1, ..., n$ we conclude for all $1 \leq q < \tilde{m}$ using (3.10), that

$$x_n^{(q)} < x_n^{(q+1)} \Rightarrow x_i^{(q)} < x_i^{(q+1)} \quad \forall\, i = 1, ..., n.$$

As $x_n^{(q)}$ is a simple root of $Q(x) - x$ the derivative $Q'(x_n^{(q)}) < 1$ implies $Q'(x_n^{(q+1)}) > 1$ and vice versa. Because

$$\lim_{x \to \pm\infty} |Q(x)| < \infty,$$

the equilibria $\mathbf{x}^{(1)}$ with $x_n^{(1)} = \min\{x : Q(x) - x = 0\}$ and $\mathbf{x}^{(\tilde{m})}$ with $x_n^{(\tilde{m})} = \max\{x : Q(x) - x = 0\}$ are stable. ∎

3.2 Simplified System

A complete analysis of the high-dimensional system (3.1) is out of the scope of the present work. Therefore we consider the special case $\mathbf{x} \in \mathbb{R}^2$ and $\mathbf{y} \in \mathbb{R}$. We first recall some terms and formulate assumptions on the layer problem.

System (Simplified System)
The simplified system reads

$$\begin{aligned} \dot{x}_1 &= f_1(x_2) - c_1 x_1; \\ \dot{x}_2 &= f_2(x_1) - (c_2 + h(y)) x_2; \\ \dot{y} &= \varepsilon[g(x_1) - dy]; \end{aligned} \tag{3.11}$$

where, like before,

$$\left.\begin{array}{l} c_i, d \in \mathbb{R}^+, \quad f_i, g, h \in \mathcal{C}^\infty(\mathbb{R}), \\ f_i(0) = g(0) = h(0) = 0, \quad 0 < \varepsilon \ll 1, \\ f_i'(x), g'(x), h'(x) > 0 \quad \forall\, x \in \mathbb{R}, \\ \lim\limits_{x \to \pm\infty} |f_i(x)| < \infty, \quad \lim\limits_{x \to \pm\infty} |g(x)| < \infty, \\ \lim\limits_{x \to \infty} h(x) \to \infty, \quad \lim\limits_{x \to -\infty} h(x) \to -\infty \end{array}\right\} \; i \;=\; 1, 2$$

and we consider initial values

$$\mathbf{x}(0) = \mathbf{x}_0 \in \mathbb{R}^2 \quad y(0) = y_0 \in (h^{-1}(-c_2, \infty)).$$

We proceed with the analysis of the layer problem, which now reads

$$\begin{aligned} \dot{x}_1 &= f_1(x_2) - c_1 x_1; \\ \dot{x}_2 &= f_2(x_1) - (c_2 + h(y_0))x_2. \end{aligned} \tag{3.12}$$

The initial value $y_0 = 0$ is of special interest. In this case, we obtain

$$\begin{aligned} \dot{x}_1 &= f_1(x_2) - c_1 x_1; \\ \dot{x}_2 &= f_2(x_1) - c_2 x_2. \end{aligned} \tag{3.13}$$

For the system (3.12), the fixed point equation (3.9) introduced in the previous section reads

$$Q(x) = \frac{1}{c_2 + h(y_0)} f_2(\frac{1}{c_1} f_1(x)) = x. \tag{3.14}$$

In order to get a deeper insight in the dynamics of the layer problem (3.12), we superimpose additional assumptions, which are usually given in biomathematical applications.

(A1') There are exactly three equilibria in the system (3.13) and the corresponding zeros of $Q(x) - x$ are simple. The two non-trivial zeros are positive.

(A2') For any $y_0 \in (h^{-1}(-c_2), \infty)$ there are not more than three equilibria in the system (3.12).

(A3') If there are three equilibria in the system (3.12) for any $y_0 \in (h^{-1}(-c_2), \infty)$, then these equilibria are normally hyperbolic.

(A4') All emerging bifurcations in the system (3.12) are generic.

Remark 3.12
The assumption [(A4')] will be specified throughout this chapter, see assumption [(A4)].

These assumptions allow us to analyze the system mathematically, but are not too restrictive for biological applications.

Remark 3.13 (Stability Of The Origin)
The assumptions imply that the trivial equilibrium $\mathbf{x} = \mathbf{0}$ is locally asymptotically stable in the system (3.13) according to corollary (3.10).

Most approaches in modelling feedback loops use a Hill shape for the activating function, which implies the assumptions [(A1') - (A4')], see for example [51]. It turns out, that it is useful to rewrite our assumptions in terms of the fixed point equation with help of theorem (3.7). For that purpose, we define the following associated function.

$$F : \mathbb{R} \times (h^{-1}(-c_2), \infty) \to \mathbb{R}, \quad F(x, y) := f_2(\tfrac{1}{c_1} f_1(x)) - (c_2 + h(y))x. \tag{3.15}$$

Obviously the following relations are true, since $F(x, y_0) = (c_2 + h(y_0))(Q(x) - x)$.

$$F(x, y_0) = 0 \Leftrightarrow Q(x) = x, \quad \tfrac{\partial}{\partial x} F(x, y_0) \gtrless 0 \Leftrightarrow Q'(x) \gtrless 1.$$

Notation 3.14
In the following, we will talk about zeros of $F(x, y_0)$. Here we interpret y_0 as a given parameter and aim - for given y_0 - to find $x \in \mathbb{R}$ so that $F(x, y_0) = 0$. Accordingly, we call x a simple zero of $F(x, y_0)$ if $F(x, y_0) = 0$ and $\frac{\partial}{\partial x} F(x, y_0) \neq 0$.

In terms of this function, our assumptions read:

(A1) There are exactly three simple zeros of $F(x, 0)$. The two non-trivial zeros are positive.

(A2) For any $y_0 \in (h^{-1}(-c_2), \infty)$ there are not more than three zeros of $F(x, y_0)$.

(A3) Let $y_0 \in (h^{-1}(-c_2), \infty)$. If there are three zeros of $F(x, y_0)$, then they are simple.

(A4) Let $y_0 \in (h^{-1}(-c_2), \infty)$. For every non-simple zero x_b of $F(x, y_0)$ we require $\frac{\partial^2}{\partial x^2} F(x_b, 0) \neq 0$.

Remark 3.15
It is not obvious, that the previous assumption [(A4')] can be written in terms of our associated function F. However, we will see in the next section, that there exists a saddle-node and a transcritical bifurcation in the layer problem, for which assumption [(A4)] guarantees that the non-degeneracy conditions are fulfilled.

Our assumptions now allow us to analyze the layer problem with respect to the description of bifurcations.

3.2.1 Bifurcations In The Layer Problem

If one only considers the layer problem, then y_0 can be treated as a bifurcation parameter. This will give a picture of the flow in this system. We show that there exists a saddle - node bifurcation as well as a transcritical bifurcation. The first lemma is connected to the saddle - node bifurcation.

Lemma 3.16
Suppose [(A1) - (A3)] hold. Then there exists a $y_c > 0$, so that:

a) For $y_0 \in [0, y_c)$ there exist exactly three simple zeros of $F(x, y_0)$.

b) There exist exactly two zeros of $F(x, y_c)$.

c) For $y_0 \in (y_c, \infty)$ there exists only the trivial zero of $F(x, y_0)$.

Let x_c be the nontrivial zero of $F(x, y_c)$. Then

$$y_c := h^{-1}\left(\frac{1}{c_1} f_1'(x_c) f_2'(\frac{1}{c_1} f_1(x_c)) - c_2\right).$$

Proof.
$F(x,0)$ has exactly three distinct ordered zeros. We denote them by $x^{(1)} = 0 < x^{(2)} < x^{(3)}$. The assumption [(A1)] together with corollary (3.10) guarantees that

$$\frac{\partial}{\partial x}F(0,0) < 0, \quad \frac{\partial}{\partial x}F(x^{(2)},0) > 0, \quad \frac{\partial}{\partial x}F(x^{(3)},0) < 0.$$

We conclude that $F(x,0) \geq 0$ for $x \leq 0$ and for $x \in [x^{(2)}, x^{(3)}]$ and that $F(x,0) \leq 0$ for $x \in [0, x^{(2)}]$ and for $x \geq x^{(3)}$.

Note that $F(x,y_0) = F(x,0) - h(y_0)x$. For every $y_0 \geq 0$ it is also $h(y_0) \geq 0$ because of the definition of the function h. As a consequence we get that $F(x,y_0) > 0$ for $x < 0$ and that $F(x,y_0) < 0$ for $x \in (0, x^{(2)}]$ and for $x \geq x^{(3)}$. If there are more zeros than the trivial one, we find them in the interval $(x^{(2)}, x^{(3)})$.

As $F(x,y_0) \in \mathcal{C}^0$, this function is bounded in the interval $[x^{(2)}, x^{(3)}]$. Let $C = \max\{F(x,y_0) : x \in [x^{(2)}, x^{(3)}]\}$. It is

$$F(x,y_0) = F(x,0) - h(y_0)x < C - h(y_0)x^{(2)}, \quad x \in (x^{(2)}, x^{(3)}).$$

Now if there exists a $x \in (x^{(2)}, x^{(3)})$ so that $F(x,y_0) = 0$ for a y_0, then

$$0 < C - h(y_0)x^{(2)} \quad \Leftrightarrow \quad h(y_0) < \tfrac{C}{x^{(2)}} \quad \Leftrightarrow \quad y_0 < h^{-1}(\tfrac{C}{x^{(2)}}).$$

Now let $y^* = h^{-1}(\frac{C}{x^{(2)}})$. We have shown, that for all $y_0 \geq y^*$ there is no zero of $F(x,y_0)$ in the interval $(x^{(2)}, x^{(3)})$.

Since $F(x,y^*)$ has no zero in the interval $(x^{(2)}, x^{(3)})$ and $F(x,0)$ has two zeros in this interval, we conclude, that there exists a $y_c \in (0, y^*)$ so that for every $y_0 > y_c$ there is no zero of $F(x,y_0)$ in the interval $(x^{(2)}, x^{(3)})$ and $F(x,y_c)$ has at least one zero in this interval. We show by contradiction that there is exactly one zero of $F(x,y_c)$ in $(x^{(2)}, x^{(3)})$.

Assumption [(A2)] allows only one or two zeros of $F(x,y_c)$ in the interval $(x^{(2)}, x^{(3)})$. Assume there are two zeros. Then the assumption [A(3)] guarantees, that these zeros are simple and with corollary (3.10), that $F(x,y_c) > 0$ in the closed interval bounded by the two zeros. Since $F(x,y_c)$ is continuous, there exists a local maximum in this interval, which we denote by (x_{max}, y_{max}). Let $0 < b < \min\{\frac{y_{max}}{x_{max}}, h(y_c)\}$ and $y^{**} = h^{-1}(h(y_c) + b) > y_c$ so that

$$F(x,y_c) - bx = F(x,0) - (h(y_c) + b)x = F(x,0) - h(y^{**})x = F(x,y^{**}).$$

Then obviously $F(x,y^{**})$ has two zeros in $(x^{(2)}, x^{(3)})$, which is a contradiction to the choice of y_c.

With a parallel argument one concludes, that there are exactly two zeros in the interval $(x^{(2)}, x^{(3)})$ for every $y_0 \in [0, y_c)$.

Denote the one zero of $F(x, y_c)$ in the interval $(x^{(2)}, x^{(3)})$ by x_c. Since x_c is a local maximum of $F(x, y_c)$ it is $\frac{\partial}{\partial x}F(x_c, y_c) = 0$. Hence

$$h(y_c) = \tfrac{\partial}{\partial x}F(x_c, 0) = \tfrac{1}{c_1}f_1'(x_c)f_2'(\tfrac{1}{c_1}f_1(x_c)) - c_2,$$

and

$$y_c \;:=\; h^{-1}\left(\frac{1}{c_1}f_1'(x_c)f_2'(\frac{1}{c_1}f_1(x_c)) - c_2\right).$$

which concludes the statement. ∎

Next we prove a lemma related to a transcritical bifurcation in system (3.12).

Lemma 3.17
Suppose [(A1) - (A3)] hold and let $y_{tr} = h^{-1}(\frac{1}{c_1}f_1'(0)f_2'(0) - c_2) \in (h^{-1}(-c_2), 0)$. *Then:*

a) There exist exactly two zeros of $F(x, y_{tr})$.

b) For $y_0 \in (h^{-1}(-c_2), 0)$, $y_0 \neq y_{tr}$ *there are exactly three zeros of* $F(x, y_0)$.

Proof.
We mainly use the Intermediate Value Theorem. Let $x^{(1)} = 0 < x^{(2)} < x^{(3)}$ be again the three distinct ordered zeros of $F(x, 0)$. As before we note that $F(x, 0) \geq 0$ for $x \in (-\infty, 0] \cup [x^{(2)}, x^{(3)}]$ and that $F(x, 0) \leq 0$ for $x \in [0, x^{(2)}] \cup [x^{(3)}, \infty)$. Furthermore

$$\begin{aligned}\lim_{x\to+\infty} F(x, y_0) &= \lim_{x\to+\infty} f_2(\tfrac{1}{c_1}f_1(x)) - (c_2 + h(y_0))x \to -\infty,\\ \lim_{x\to-\infty} F(x, y_0) &= \lim_{x\to-\infty} f_2(\tfrac{1}{c_1}f_1(x)) - (c_2 + h(y_0))x \to +\infty,\end{aligned}$$

since $c_2 + h(y_0) > 0$ and $f_2(\frac{1}{c_1}f_1(x))$ is bounded.

Since $h(y_0) < 0$ for $y_0 \in (h^{-1}(-c_2), 0)$, we conclude, that $F(x^{(3)}, y_0) = F(x^{(3)}, 0) - h(y_0)x^{(3)} > 0$. And we conclude, that for all $y_0 \in (h^{-1}(-c_2), 0)$ there exists at least on zero of $F(x, y_0)$ in the interval $(x^{(3)}, \infty)$.

The choice of y_{tr} guarantees, that

$$\begin{aligned}&\tfrac{\partial}{\partial x}F(0, y_0) > 0 \quad \text{for } y_0 \in (h^{-1}(-c_2), y_{tr}),\\ &\tfrac{\partial}{\partial x}F(0, y_{tr}) = 0,\\ &\tfrac{\partial}{\partial x}F(0, y_0) < 0 \quad \text{for } y_0 \in (y_{tr}, 0).\end{aligned}$$

Let $y_0 \in (h^{-1}(-c_2), y_{tr})$, then $F(x_-, y_0) < 0$ for some $x_- \in (-\infty, 0)$. And we obtain that for all $y_0 \in (h^{-1}(-c_2), y_{tr})$ there exists at least one zero of $F(x, y_0)$ in the interval $(-\infty, 0)$.

Let $y_0 \in (y_{tr}, 0)$, then $F(x_+, y_0) < 0$ for some $x_+ \in (0, x^{(2)})$ and $F(x^{(2)}, y_0) > 0$. And we get that for all $y_0 \in (y_{tr}, 0)$ there exists at least one zero of $F(x, y_0)$ in the interval $(0, x^{(2)})$.

The statements above together with assumption [A(2)] prove b). Finally, since 0 is a double zero of $F(x, y_{tr})$, assumption [A(3)] guarantees, that there are exactly two zeros of $F(x, y_{tr})$. This proves a). ∎

The last two lemmata give rise to a saddle-node and a transcritical bifurcation in the layer problem. We state our main theorem.

Theorem 3.18 (Bifurcation Points)
Consider system (3.12) and suppose [(A1) - (A4)] hold. Then there exist a $x_c > 0$, so that there is a saddle-node bifurcation at point $(x_1, x_2, y_0) = (\frac{1}{c_1} f_1(x_c), x_c, y_c)$, where

$$y_c = h^{-1}\left(\frac{1}{c_1} f_1'(x_c) f_2'(\frac{1}{c_1} f_1(x_c)) - c_2\right). \tag{3.16}$$

Furthermore there is a transcritical bifurcation at point $(x_1, x_2, y_0) = (0, 0, y_{tr})$, where

$$y_{tr} = h^{-1}\left(\frac{1}{c_1} f_1'(0) f_2'(0) - c_2\right). \tag{3.17}$$

It is $0 < y_c < \infty$ and $h^{-1}(-c_2) < y_{tr} < 0$.

Proof.
At both points there exist center manifolds. Center manifold reduction methods (see for instance [23]) lead to the following statements.

Assumption [(A4)], i.e. $\frac{\partial^2}{\partial x^2} F(0,0) \neq 0$ guarantees, that in a neighborhood of the point $(0, 0, y_{tr})$ system (3.12) is locally topologically equivalent to the system

$$\begin{aligned} \dot{u} &= -(\tfrac{1}{c_1} f_1'(0) f_2'(0) + c_1) u, \\ \dot{v} &= \tfrac{1}{2} \tfrac{c_1^2}{f_1'(0) f_2'(0) + c_1^2} [\tfrac{\partial^2}{\partial x^2} F(0,0) v^2 - 2(h(y_0) - \tfrac{\partial}{\partial x} F(0,0) v)]. \end{aligned}$$

The equation for $\dot{v}$ is the restriction to the center manifold and defines the normal form of the transcritical bifurcation. Let

$$\tilde{g}(v, y_0) = \tfrac{\partial^2}{\partial x^2} F(0,0) v^2 - 2(h(y_0) - \tfrac{\partial}{\partial x} F(0,0)) v.$$

Indeed the conditions for a transcritical bifurcation at $(0,0,y_{tr})$ are satisfied. Since $\frac{1}{2}\frac{c_1^2}{f_1'(0)f_2'(0)+c_1^2} > 0$ they read (see for instance [37])

$$\tilde{g}(0,y_{tr}) = 0, \quad \frac{\partial}{\partial v}\tilde{g}(0,y_{tr}) = 2(\frac{\partial}{\partial x}F(0,0) - h(y_{tr})) = 0,$$
$$\frac{\partial}{\partial y_0}\tilde{g}(0,y_{tr}) = 0.$$

The non-degeneracy conditions are

$$\frac{\partial^2}{\partial v^2}\tilde{g}(0,y_{tr}) = \frac{\partial^2}{\partial x^2}F(0,0) \neq 0,$$
$$\frac{\partial^2}{\partial v \partial y_0}\tilde{g}(0,y_{tr}) = -2h'(y_{tr}) \neq 0.$$

This proves the statement about the transcritical bifurcation.

Again assumption [(A4)], here $\frac{\partial^2}{\partial x^2}F(x_c,0) \neq 0$, guarantees that in a neighborhood of the point $(\frac{1}{c_1}f_1(x_c), x_c, y_c)$ system (3.12) is locally topologically equivalent to the system

$$\begin{aligned}\dot{u} &= -(\tfrac{1}{c_1}f_1'(x_c)f_2'(\tfrac{1}{c_1}f_1(x_c)) + c_1)(u - \tfrac{1}{c_1}f_1(x_c)),\\ \dot{v} &= \tfrac{1}{2}\tfrac{c_1^2}{f_1'(x_c)f_2'(\frac{1}{c_1}f_1(x_c))+c_1^2}[\tfrac{\partial^2}{\partial x^2}F(x_c,0)(v-x_c)^2 - 2x_c(h(y_0) - \tfrac{\partial}{\partial x}F(x_c,0))].\end{aligned}$$

And again the equation for $\dot{v}$ is the restriction to the center manifold. Here it defines the normal form of the saddle-node bifurcation. Analogously to the transcritical bifurcation, one can show that the conditions for the saddle-node bifurcation hold. ∎

The previous analysis gives a description of the flow in the layer problem, i.e. a description of the critical manifold. However, to get a description for the flow of the full system (3.11) for $\varepsilon = 0$ one has to describe the flow on the critical manifold as well. This will be done in the next section.

3.2.2 A Picture Of The Flow For $\varepsilon = 0$

As stated above the analysis in the last section characterize the critical manifold of system (3.11), which we call S_{3D}. We have also investigated the stability of points in S_{3D} considered as equilibrium points of the layer problem. The critical manifold can be written as

$$S_{3D} := \{(x_1,x_2,y) \in \mathbb{R}^2 \times (h^{-1}(-c_2),\infty) : F(x_2,y) = 0, \quad x_1 = \tfrac{1}{c_1}f_1(x_2)\}. \quad (3.18)$$

We note that we can divide the critical manifold into two branches.

Remark 3.19
It is $f_2(\frac{1}{c_1}f_1(x)) \in \mathcal{C}^\infty(\mathbb{R},\mathbb{R})$ and $f_2(\frac{1}{c_1}f_1(0)) = 0$. Thus a function $\tilde{f}(x) \in \mathcal{C}^\infty(\mathbb{R},\mathbb{R})$ exists with

$$f_2(\tfrac{1}{c_1}f_1(x)) \;=\; \tilde{f}(x)x.$$

This leads to the following description of S_{3D}.

$$\begin{aligned} S_{3D} \;=\; & \{(x_1,x_2,y) \in \mathbb{R}^2 \times (h^{-1}(-c_2),\infty) : x_1 = x_2 = 0\} \quad \cup \\ & \{(x_1,x_2,y) \in \mathbb{R}^2 \times (h^{-1}(-c_2),\infty) : \\ & \qquad x_2 \neq 0, \quad x_1 = \tfrac{1}{c_1}f_1(x_2), \quad y = h^{-1}(\tilde{f}(x_2) - c_2)\}. \end{aligned}$$

We draw a first sketch of the critical manifold, see figure 3.1.

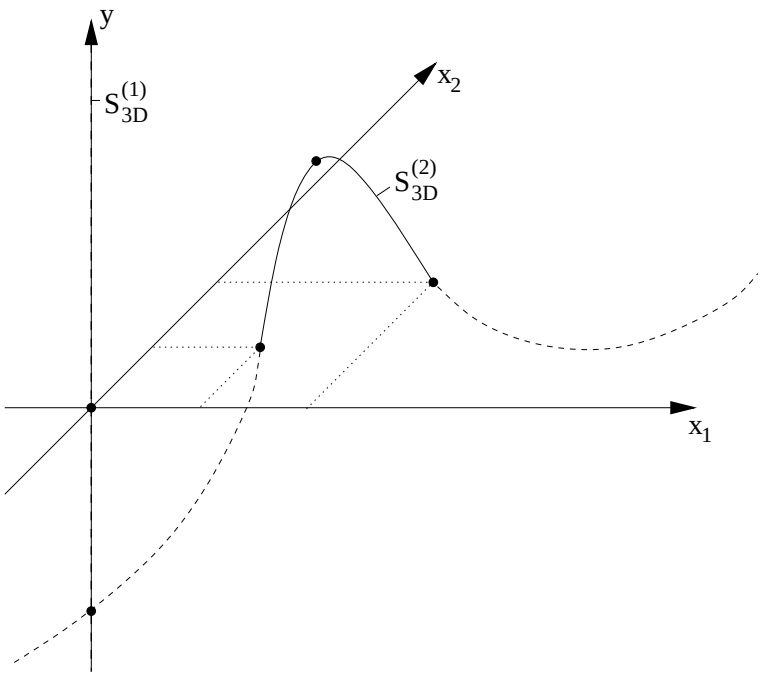

Figure 3.1: A picture of the critical manifold.

System (Slow System)
The slow system equivalent to system 3.1 is given by

$$\begin{aligned} \varepsilon\dot{x}_1 &= f_1(x_2) - c_1x_1; \\ \varepsilon\dot{x}_2 &= f_2(x_1) - (c_2 + h(y))x_2; \\ \dot{y} &= g(x_1) - dy. \end{aligned} \tag{3.19}$$

Again letting formally $\varepsilon \to 0$ this reduces to

System (Reduced Problem)

$$\begin{aligned} 0 &= f_1(x_2) - c_1 x_1; \\ 0 &= f_2(x_1) - (c_2 + h(y))x_2; \\ \dot{y} &= g(x_1) - dy. \end{aligned} \tag{3.20}$$

This system can equivalently be written as

$$\begin{aligned} 0 &= F(x_2, y); \\ \dot{y} &= g(\tfrac{1}{c_1} f_1(x_2)) - dy. \end{aligned}$$

To analyze the flow on the critical manifold S_{3D}, which is given by the flow of the reduced problem, we describe the zero set of $g(\frac{1}{c_1} f_1(x_2)) - d\,y$.

We introduce a new parameter λ by $d = c_3 + \lambda$ with

$$c_3 := \tfrac{1}{y_c} g(\tfrac{1}{c_1} f_1(x_c)). \tag{3.21}$$

The idea is to use ε and λ as bifurcation parameters in the analysis of system (3.11). The zero set Z_{3D}^{λ} of $g(\frac{1}{c_1} f_1(x_2)) - (c_3 + \lambda)y$ for $c_3 + \lambda \neq 0$ can be written as

$$Z_{3D}^{\lambda} = \{(x_1, x_2, y) \in \mathbb{R}^2 \times (h^{-1}(-c_2), \infty) : y = \tfrac{1}{c_3 + \lambda} g(\tfrac{1}{c_1} f_1(x_2))\}.$$

We directly conclude, that

$$(0, 0, 0) \in S_{3D} \cap Z_{3D}^{\lambda},$$

and with the help of the definition of c_3 we also find, that

$$(\tfrac{1}{c_1} f_1(x_c), x_c, y_c) \in S_{3D} \cap Z_{3D}^{0}.$$

Furthermore it is trivial to see that there has to be at least one more intersection point of S_{3D} and Z_{3D}^{0} for $x_2 \in (0, x_c)$ using again the Intermediate Value Theorem. According to this observations we formulate our assumptions for the zero set Z_{3D}^{λ}.

(A5) There exist exactly three intersection points of S_{3D} and Z_{3D}^{0}.

(A6) For every λ with $|\lambda| < c_3$ there exist not more than three intersection points of S_{3D} and Z_{3D}^{λ}.

Remark 3.22 (Assumptions)
For all further calculations and results, we implicitly assume, that all assumptions (A1) - (A6) hold.

The intersection points of S_{3D} and Z^0_{3D} are $(0,0,0)$, $(\frac{1}{c_1}f_1(x_c), x_c, y_c)$ and a third point, which we denote by $(\frac{1}{c_1}f_1(x_h), x_h, y_h)$, where $y_h = \frac{1}{c_3}g(\frac{1}{c_1}f_1(x_h))$.

As stated above the critical manifold can be divided into two branches. Let

$$S^{(1)}_{3D} := \{(x_1, x_2, y) \in \mathbb{R}^2 \times (h^{-1}(-c_2), \infty) : x_1 = x_2 = 0\}$$

and

$$\begin{aligned} S^{(2)}_{3D} \;:=\; & \{(x_1, x_2, y) \in \mathbb{R}^2 \times (h^{-1}(-c_2), \infty) : \\ & x_2 \neq 0, \quad x_1 = \tfrac{1}{c_1}f_1(x_2), \quad y = h^{-1}(\tilde{f}(x_2) - c_2)\}, \end{aligned}$$

so that $S_{3D} = S^{(1)}_{3D} \cup S^{(2)}_{3D}$.

Lemma 3.23 (Flow On The Critical Manifold)
Consider system (3.20) for $\lambda = 0$. For the flow on $S^{(1)}_{3D}$ it is $\dot{y} < 0$ for $y > 0$ and $\dot{y} > 0$ for $y < 0$. For the flow on $S^{(2)}_{3D}$ it is $\dot{x}_2 < 0$ for $x_2 > x_h$ and $\dot{x}_2 > 0$ for $x_2 < x_h$.

Proof.
The flow on $S^{(1)}_{3D}$ is given by the equation $\dot{y} = -c_3 y$, which proves the first statement.

Let $\varphi(x) = h^{-1}(\tilde{f}(x) - c_2)$. Then

$$\varphi'(x) \;=\; [h^{-1}]'(\tilde{f}(x) - c_2)\tilde{f}'(x)$$

Since $\tilde{f}(x) = \frac{1}{x}f_2(\frac{1}{c_1}f_1(x))$ for every $x \neq 0$, it follows that

$$\varphi'(x) \;=\; \tfrac{[h^{-1}]'(\tilde{f}(x)-c_2)}{x^2}[\tfrac{1}{c_1}f_1'(x)f_2'(\tfrac{1}{c_1}f_1(x))x - f_2(\tfrac{1}{c_1}f_1(x))].$$

Substituting $y = \varphi(x_2)$, i.e. the y component of $S^{(2)}_{3D}$, into system (3.20) we obtain for the flow on $S^{(2)}_{3D}$ with $x_2 \neq 0$

$$\begin{aligned} \dot{x}_2 \;&=\; \tfrac{1}{\varphi'(x_2)}[g(\tfrac{1}{c_1}f_1(x_2)) - c_3\varphi(x_2)] = \\ &=\; \tfrac{x_2^2}{[h^{-1}]'(\tilde{f}(x_2)-c_2)} \quad \tfrac{g(\frac{1}{c_1}f_1(x_2))-c_3\varphi(x_2)}{\frac{1}{c_1}f_1'(x_2)f_2'(\frac{1}{c_1}f_1(x_2))x_2-f_2(\frac{1}{c_1}f_1(x_2))}. \end{aligned}$$

We are only interested in the changes of the sign of $\dot{x}_2$. There are only two possibilities, where these changes can happen. The first one is at intersection points of $S^{(2)}_{3D}$ and Z^0_{3D}, i.e. for $x_2 = x_h$ and for $x_2 = x_c$. The second one is at the bifurcation points of the layer problem, i.e. for $x_2 = 0$ and again for $x_2 = x_c$. Since $(\frac{1}{c_1}f_1(x_c), x_c, y_c)$ is an intersection point as well as a bifurcation point in the layer problem, we show that there is no change of the sign of $\dot{x}_2$ at $x_2 = x_c$, i.e. both numerator and denominator change sign at $x_2 = x_c$.

We note that

$$g(\tfrac{1}{c_1}f_1(x_2)) - c_3\varphi(x_2) > 0, \quad \forall x_2 \in (-\infty, x_h) \cup (x_c, \infty),$$
$$g(\tfrac{1}{c_1}f_1(x_2)) - c_3\varphi(x_2) < 0, \quad \forall x_2 \in (x_h, x_c)$$

and

$$\tfrac{x_2^2}{[h^{-1}]'(\tilde{f}(x_2)-c_2)} > 0, \quad \forall x_2 \neq 0.$$

Furthermore

$$\tfrac{\partial^2}{\partial x^2}F(x,y) = \tfrac{\partial^2}{\partial x^2}F(x,0) = \tfrac{d^2}{dx^2}[f_2(\tfrac{1}{c_1}f_1(x))] = \tfrac{d}{dx}[\tfrac{1}{c_1}f_1'(x)f_2'(\tfrac{1}{c_1}f_1(x))]. \tag{3.22}$$

We find $\tfrac{d}{dx}[\tfrac{1}{c_1}f_1'(x)f_2'(\tfrac{1}{c_1}f_1(x))]|_{x=x_c} < 0$ since x_c is a maximum of $F(x,0)$. We define

$$\hat{f}(x) \;:=\; \tfrac{1}{c_1}f_1'(x)f_2'(\tfrac{1}{c_1}f_1(x))x - f_2(\tfrac{1}{c_1}f_1(x)).$$

Then $\hat{f}(x_c) = 0$, since $y_c = h^{-1}(\tfrac{1}{c_1}f_1'(x_c)f_2'(\tfrac{1}{c_1}f_1(x_c)) - c_2) = h^{-1}(\tilde{f}(x_c) - c_2)$. As

$$\begin{aligned}\hat{f}'(x) &= \tfrac{1}{c_1}f_1'(x)f_2'(\tfrac{1}{c_1}f_1(x)) + x\tfrac{d}{dx}[\tfrac{1}{c_1}f_1'(x)f_2'(\tfrac{1}{c_1}f_1(x))] - \tfrac{1}{c_1}f_1'(x)f_2'(\tfrac{1}{c_1}f_1(x)) = \\ &= x\tfrac{d}{dx}[\tfrac{1}{c_1}f_1'(x)f_2'(\tfrac{1}{c_1}f_1(x))]\end{aligned}$$

we conclude that $\hat{f}'(x_c) < 0$. There exists a sufficiently small $\kappa > 0$, so that $\hat{f}(x) > 0$ for $x \in (x_c - \kappa, x_c)$ and $\hat{f}(x) < 0$ for $x \in (x_c, x_c + \kappa)$. Consequently, since the expression for $\dot{x}_2$ does not have a singularity at $x_2 = x_c$, we get

$$\dot{x}_2 < 0, \quad x_2 \in (x_h, \infty).$$

We proceed to show the change of sign at $x_2 = x_h$, which corresponds to show that $\hat{f}(x_h) > 0$. Obviously it is $y_h \in (0, y_c)$ and x_h is a simple zero of $F(x, y_h)$ for y_h fixed, indeed it is the middle zero of the three ordered zeros of $F(x, y_h)$. We obtain

$$\begin{aligned}0 < \tfrac{\partial}{\partial x}F(x,y_h)|_{x=x_h} &= \tfrac{\partial}{\partial x}F(x,0)|_{x=x_h} - h(y_h) = \\ &= \tfrac{1}{c_1}f_1'(x_h)f_2'(\tfrac{1}{c_1}f_1(x_h)) - c_2 - h(h^{-1}(\tilde{f}(x_h) - c_2)) = \\ &= \tfrac{1}{c_1}f_1'(x_h)f_2'(\tfrac{1}{c_1}f_1(x_h)) - \tilde{f}(x_h) = \\ &= \tfrac{1}{x_h}[\tfrac{1}{c_1}f_1'(x_h)f_2'(\tfrac{1}{c_1}f_1(x_h))x_h - f_2(\tfrac{1}{c_1}f_1(x_h))] = \\ &= \tfrac{1}{x_h}\hat{f}(x_h).\end{aligned} \tag{3.23}$$

Finally we get

$$\dot{x}_2 < 0, \quad x_2 \in (0, x_h).$$

The last thing remaining to show is, that there is no change of sign at $x_2 = 0$. For every point on $S_{3D}^{(2)}$ which satisfies $x_2 < 0$, it is

$$\frac{\partial}{\partial x} F(x, h^{-1}(\tilde{f}(x) - c_2))|_{x=x_2} < 0,$$

since the x_2 - component of such a point on $S_{3D}^{(2)}$ is the left zero of the three ordered zeros of $F(x, y_0)$ for fixed $y_0 = h^{-1}(\tilde{f}(x_2) - c_2)$. As $\frac{\partial}{\partial x} F(x, h^{-1}(\tilde{f}(x) - c_2))|_{x=x_2} = \frac{1}{x_2}\hat{f}(x_2)$ with the same computation as in (3.23) it follows that

$$\dot{x}_2 < 0, \quad x_2 \in (-\infty, x_h),$$

since again the expression for $\dot{x}_2$ does not have a singularity at $x_2 = 0$. ∎

The last lemma now guarantees, that the flow for $\varepsilon = 0$ is as shown in figure 3.2 (left panel) for $\lambda = 0$ and in figure 3.2 (right panel) for $\lambda < 0$.

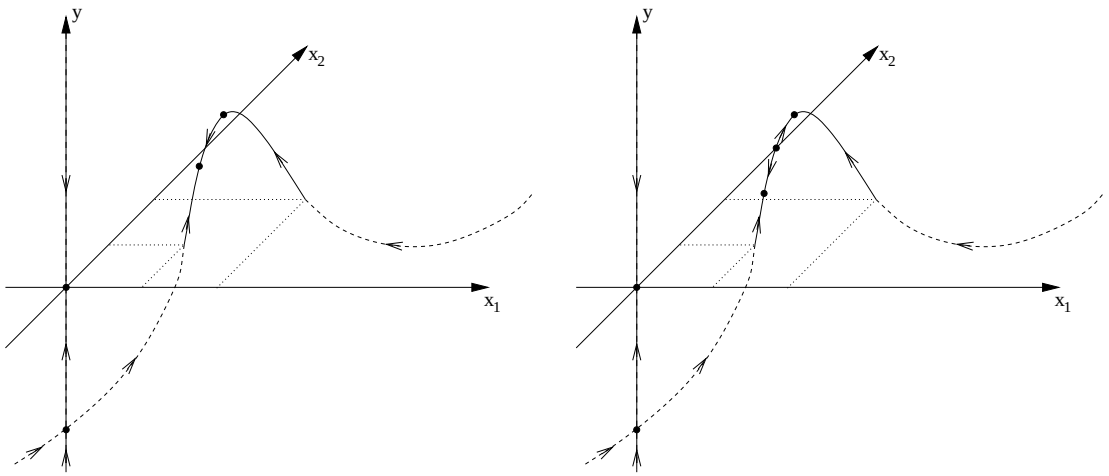

Figure 3.2: The flow on the critical manifold for $\lambda = 0$ (left panel) and for $\lambda < 0$ (right panel).

To further analyze system (3.11), it is beneficial to first describe a closely related two-dimensional system. Therefore we change our focus here and continue with a two-dimensional approach.

4 Two-dimensional Approach

This chapter is dedicated to the study of a two-dimensional system, which is closely related to the three-dimensional system of the last chapter. We first introduce artificially a new time scale, that allows us to reduce the three-dimensional system to a two-dimensional one. After some transformations, we investigate the flow in neighborhoods of both the canard point and the homoclinic point. This leads to the description of properties of the global flow. We prove the transition of small periodic orbits emanating from the canard point to a homoclinic orbit with respect to the homoclinic point for every small $\varepsilon > 0$ as λ varies.

4.1 A New Time Scale

We assume that the activation of a substance with concentration x_2 is much slower than the activation of the substance with concentration x_1 but still much faster than the negative feedback. This assumption is not motivated by the application but mainly by technical considerations. This structure leads to the introduction of a new time scale in the fast system (3.11) of the last chapter. We consider two time scale parameters ε_1 and ε_2, $0 < \varepsilon_i \ll 1$, $i = 1, 2$ and define our new system according to

System (Three Time Scales System)

$$\begin{aligned} \dot{x}_1 &= f_1(x_2) - c_1 x_1, \\ \dot{x}_2 &= \varepsilon_2[f_2(x_1) - (c_2 + h(y))x_2], \\ \dot{y} &= \varepsilon_1\varepsilon_2[g(x_1) - (c_3 + \lambda)y]. \end{aligned} \tag{4.1}$$

Rescaling according to the time transformation $t = \varepsilon_2\tau$ the equivalent system reads

$$\begin{aligned} \varepsilon_2\dot{x}_1 &= f_1(x_2) - c_1 x_1, \\ \dot{x}_2 &= f_2(x_1) - (c_2 + h(y))x_2, \\ \dot{y} &= \varepsilon_1[g(x_1) - (c_3 + \lambda)y] \end{aligned}$$

and taking the limit $\varepsilon_2 = 0$ this reduces to

$$\begin{aligned} x_1 &= \tfrac{1}{c_1} f_1(x_2), \\ \dot{x}_2 &= f_2(x_1) - (c_2 + h(y))x_2, \\ \dot{y} &= \varepsilon_1[g(x_1) - (c_3 + \lambda)y], \end{aligned}$$

which can equivalently be written as the two-dimensional system.

$$\begin{aligned} \dot{x}_2 &= f_2(\tfrac{1}{c_1} f_1(x_2)) - (c_2 + h(y))x_2, \\ \dot{y} &= \varepsilon_1[g(\tfrac{1}{c_1} f_1(x_2)) - (c_3 + \lambda)y]. \end{aligned}$$

We implicitly assume that the activation of the substance with concentration x_1 is sufficiently fast so that it changes its state almost immediately. Thus we can assume that x_1 is in its steady state. The relation of this system to our three-dimensional system (3.11) can easily be seen, since $\dot{x}_2 = F(x_2, y)$. In the following we will analyze the dynamics of this system, starting with the description of the flow for $\varepsilon_1 = 0$ and $\lambda = 0$. To simplify the notation, we drop the subscripts on ε_1 and x_2 and define

$$G(x, y, \lambda) := g(\tfrac{1}{c_1} f_1(x)) - (c_3 + \lambda)y,$$

so that our basic system for this chapter is the following one.

System (Two-dimensional System)

$$\begin{aligned} \dot{x} &= F(x, y), \\ \dot{y} &= \varepsilon G(x, y, \lambda). \end{aligned} \tag{4.2}$$

We use the observations of the last chapter to describe the critical manifold, which leads to

$$S_{2D} := \{(x, y) \in \mathbb{R} \times (h^{-1}(-c_2), \infty) : F(x, y) = 0\}.$$

We divide the critical manifold as before into two branches $S_{2D}^{(1)}$ and $S_{2D}^{(2)}$ defined analogously to $S_{3D}^{(1)}$ and $S_{3D}^{(2)}$. Let Z_{2D}^{λ} also be defined analogously to Z_{3D}^{λ}. Lemma 3.16, lemma 3.17 as well as lemma 3.23 guarantee, that the flow for $\varepsilon = 0$, $\lambda = 0$ is as shown in figure 4.1.

Our previous analysis assures that the point (x_c, y_c) defines a canard point for $\lambda = 0$ as the following lemma shows.

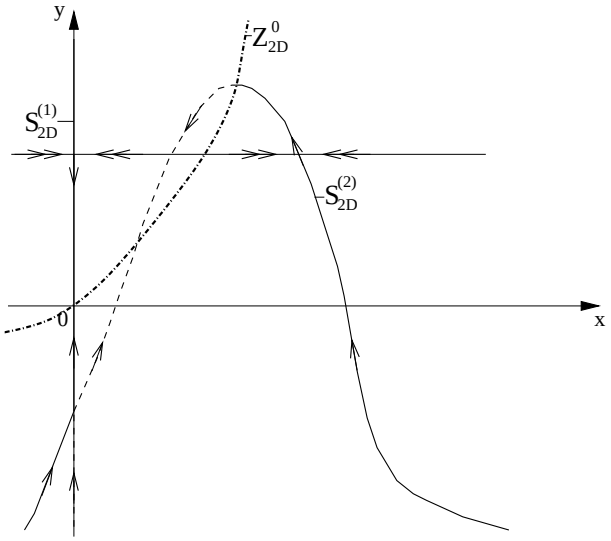

Figure 4.1: A picture for the flow for $\varepsilon = 0$, $\lambda = 0$.

Lemma 4.3 (Canard Point)
For $\lambda = 0$ the point (x_c, y_c) defines a non-degenerated canard point for system (4.2) .

Proof.
We prove the defining equations (see [36]) in the definition of the canard point.

(x_c, y_c) is an intersection point of $S^{(2)}_{2D}$ and Z^0_{2D} and x_c is a maximum of $F(x, y_c)$. This and the definition of c_3 leads to

$$\begin{aligned} &F(x_c, y_c) = 0, \quad \tfrac{\partial}{\partial x} F(x_c, y_c) = 0, \\ &G(x_c, y_c, 0) = g(\tfrac{1}{c_1} f_1(x_c)) - c_3 y_c = 0. \end{aligned} \tag{4.3}$$

The non-degeneracy conditions are also satisfied. With $x_c, y_c > 0$, $h'(y_c) > 0$, $g'(\frac{1}{c_1} f_1(x_c)) > 0$ and $f_1'(x_c) > 0$ we obtain

$$\begin{aligned} &\tfrac{\partial^2}{\partial x^2} F(x_c, y_c) < 0, \quad \tfrac{\partial}{\partial y} F(x_c, y_c) = -h'(y_c) x_c < 0. \\ &\tfrac{\partial}{\partial x} G(x_c, y_c, 0) = \tfrac{1}{c_1} g'(\tfrac{1}{c_1} f_1(x_c)) f_1'(x_c) > 0, \quad \tfrac{\partial}{\partial \lambda} G(x_c, y_c, 0) = -y_c < 0. \end{aligned} \tag{4.4}$$

This concludes the statement. ∎

As stated at the beginning we continue with the analysis of the local flow near the canard point. This is done analogously to the paper of Krupa and Szmolyan, [36].

4.2 The Canard Point

We transform our system such that we derive the canonical form (3.3) in [36]. We obtain the following statement.

Lemma 4.4 (Canonical Form)
In a neighborhood of the non-degenerated canard point system (4.2) can be transformed to the following canonical form.

$$\begin{aligned} \dot{\xi} &= -\eta h_1(\xi,\eta) + \xi^2 h_2(\xi,\eta), \\ \dot{\eta} &= \tilde{\varepsilon}[\xi h_3(\xi,\eta) - \tilde{\lambda} h_4(\xi,\eta) + \eta h_5(\xi,\eta)], \end{aligned} \tag{4.5}$$

where

$$h_j(\xi,\eta) = 1 + O(\xi,\eta), \quad j = 1,...,4.$$

Proof.
We use the Taylor expansions of F with respect to (x_c, y_c) and of G with respect to $(x_c, y_c, 0)$. Note that

$$\begin{aligned} &\tfrac{\partial^3}{\partial x^2 \partial y} F(x,y) = 0, \quad \tfrac{\partial^2}{\partial x \partial y} G(x,y,\lambda) = 0, \\ &\tfrac{\partial^2}{\partial x \partial \lambda} G(x,y,\lambda) = 0, \quad \tfrac{\partial^2}{\partial y^2} G(x,y,\lambda) = 0, \end{aligned}$$

which is a direct consequence of the definitions of F and G. This fact and the equations defining the canard point (4.3) lead to the system

$$\begin{aligned} \dot{\tilde{x}} &= a_1\tilde{x}^2 + a_2\tilde{x}^3 + a_3\tilde{y} + a_4\tilde{y}^2 + a_5\tilde{y}^3 + a_6\tilde{x}\tilde{y} + a_7\tilde{x}\tilde{y}^2 + O(\tilde{x}^4 + |\tilde{x}\tilde{y}^3| + \tilde{y}^4), \\ \dot{\tilde{y}} &= \varepsilon[b_1\tilde{x} + b_2\tilde{x}^2 + b_3\lambda + b_4\tilde{y} + O(\tilde{x}^3)], \end{aligned}$$

where the constants are defined by

$$\begin{aligned} a_1 = \tfrac{1}{2}\tfrac{\partial^2}{\partial x^2}F(x_c,y_c), \quad a_2 = \tfrac{1}{6}\tfrac{\partial^3}{\partial x^3}F(x_c,y_c), \\ a_3 = \tfrac{\partial}{\partial y}F(x_c,y_c), \quad a_4 = \tfrac{\partial^2}{\partial y^2}F(x_c,y_c), \quad a_5 = \tfrac{\partial^3}{\partial y^3}F(x_c,y_c), \\ a_6 = \tfrac{\partial^2}{\partial x \partial y}F(x_c,y_c), \quad a_7 = \tfrac{\partial^3}{\partial x \partial y^2}F(x_c,y_c). \end{aligned}$$

and

$$\begin{aligned} b_1 = \tfrac{\partial}{\partial x}G(x_c,y_c,0), \quad b_2 = \tfrac{1}{2}\tfrac{\partial^2}{\partial x^2}G(x_c,y_c,0), \\ b_3 = \tfrac{\partial}{\partial \lambda}G(x_c,y_c,0), \quad b_4 = \tfrac{\partial}{\partial y}G(x_c,y_c,0). \end{aligned}$$

Due to the non - degeneracy conditions of the canard point (4.4) we find $a_1 < 0$, $a_3 < 0$, $b_1 > 0$ and $b_3 < 0$. We define the parameters

$$\theta_1 = a_1, \quad \theta_2 = -a_1 a_3, \quad \theta_3 = -a_3 b_1, \quad \theta_4 = -\tfrac{a_1 b_3}{b_1}. \tag{4.6}$$

Scaling the system according to $\xi = \theta_1 \tilde{x}$, $\eta = \theta_2 \tilde{y}$, $\tilde{\varepsilon} = \theta_3 \varepsilon$ and $\tilde{\lambda} = \theta_4 \lambda$, it reads

$$\begin{aligned}
\tfrac{1}{\theta_1}\dot{\xi} &= \tfrac{1}{\theta_1^2}\xi^2[a_1 + a_2 \tfrac{1}{\theta_1}\xi + O(\xi^2)] \\
&\quad -\tfrac{1}{\theta_2}\eta[-a_3 - a_4 \tfrac{1}{\theta_2}\eta - a_5 \tfrac{1}{\theta_2^2}\eta^2 - a_6 \tfrac{1}{\theta_1}\xi - a_7 \tfrac{1}{\theta_1}\xi \tfrac{1}{\theta_2}\eta + O(\xi\eta^2) + O(\eta^3)], \\
\tfrac{1}{\theta_2}\dot{\eta} &= \tfrac{1}{\theta_3}\tilde{\varepsilon}[\tfrac{1}{\theta_1}\xi(b_1 + b_2 \tfrac{1}{\theta_1}\xi + O(\xi^2)) + \tfrac{1}{\theta_4}\tilde{\lambda}(b_3) + \tfrac{1}{\theta_2}\eta(b_4)].
\end{aligned}$$

and finally

$$\begin{aligned}
\dot{\xi} &= -\eta[1 + \alpha_{02}\eta + \alpha_{11}\xi + O(\xi\eta) + O(\eta^2)] + \xi^2[1 + \alpha_{30}\xi + O(\xi^2)], \\
\dot{\eta} &= \tilde{\varepsilon}[\xi(1 + \beta_{20}\xi + O(\xi^2)) - \tilde{\lambda}(1) + \eta(\beta_{01})],
\end{aligned}$$

where

$$\begin{gathered}
\alpha_{02} = \tfrac{a_4}{a_1 a_3^2}, \quad \alpha_{11} = -\tfrac{a_6}{a_1 a_3}, \quad \alpha_{30} = \tfrac{a_2}{a_1^2}, \\
\beta_{20} = \tfrac{b_2}{a_1 b_1}, \quad \beta_{01} = -\tfrac{b_4}{a_3 b_1}.
\end{gathered}$$

This concludes the statement. ∎

This lemma allows us to follow the paper of Krupa and Szmolyan [36] for the description of the flow near the canard point. We proceed with translating their results into our setting. We have

$$\begin{gathered}
h_1(\xi,\eta) = 1 + \alpha_{02}\eta + \alpha_{11}\xi + O(\xi\eta) + O(\eta^2), \quad h_2(\xi,\eta) = 1 + \alpha_{30}\xi + O(\xi^2), \\
h_3(\xi,\eta) = 1 + \beta_{20}\xi + O(\xi^2), \quad h_4(\xi,\eta) = 1, \quad h_5(\xi,\eta) = \beta_{01}.
\end{gathered} \tag{4.7}$$

Let

$$\begin{aligned}
k_1 &:= \tfrac{\partial}{\partial\xi} h_1(0,0) = \alpha_{11}, \quad k_2 := \tfrac{\partial}{\partial\xi} h_2(0,0) = \alpha_{30}, \\
k_3 &:= \tfrac{\partial}{\partial\xi} h_3(0,0) = \beta_{20}, \quad k_4 := h_5(0,0) = \beta_{01}
\end{aligned}$$

and define the constant

$$A = -k_1 + 3k_2 - 2k_3 - 2k_4 = -\alpha_{11} + 3\alpha_{30} - 2(\beta_{20} + \beta_{01}). \tag{4.8}$$

The sign of A plays an important role in the dynamic phenomena related to the flow near the canard point. The main tool to analyze this flow is the technique of blow-up

transformations. The transformation, which is used to desingularize the flow near the canard point, is defined by

$$\Phi : S^3 \times [0, \rho] \to \mathbb{R}^4$$

given by

$$\xi = \overline{r}\,\overline{\xi}, \quad \eta = \overline{r}^2\,\overline{\eta}, \quad \tilde{\varepsilon} = \overline{r}^2\,\overline{\varepsilon}, \quad \tilde{\lambda} = \overline{r}\,\overline{\lambda}, \quad (\overline{\xi}, \overline{\eta}, \overline{\lambda}, \overline{\varepsilon}) \in S^3.$$

We will use two charts here, K_1 and K_2. K_1 is given by

$$\xi = r_1\xi_1, \quad \eta = r_1^2, \quad \tilde{\varepsilon} = r_1^2\varepsilon_1, \quad \tilde{\lambda} = r_1\lambda_1 \tag{4.9}$$

and K_2 is given by

$$\xi = r_2\xi_2, \quad \eta = r_2^2\eta_2, \quad \tilde{\varepsilon} = r_2^2, \quad \tilde{\lambda} = r_2\lambda_2. \tag{4.10}$$

Let $\Phi_1(\xi_1, r_1, \varepsilon_1, \lambda_1)$ be the map defined by K_1. As the domain of Φ_1 we use the set V_1 given by

$$V_1 \;=\; (-\xi_{1,0}, \xi_{1,0}) \times (-\rho, \rho) \times [0, 1) \times (-\mu, \mu),$$

with $\xi_{1,0} > 0$ sufficiently large and $\rho > 0$, $\mu > 0$ sufficiently small and define

$$V_{1,\tilde{\varepsilon}} \;=\; \{(\xi_1, r_1, \varepsilon_1, \lambda_1) \in V_1 : \tilde{\varepsilon} = r_1^2\varepsilon_1\}.$$

Let $P_{(\xi,\eta)}$ be the projection onto the (ξ, η) coordinates, then

$$P_{(\xi,\eta)}(\Phi_1(V_{1,\tilde{\varepsilon}})) \;=\; \{(\xi, \eta) : \eta \in (\tilde{\varepsilon}, \rho^2), \xi \in (-\xi_{1,0}\sqrt{\eta}, \xi_{1,0}\sqrt{\eta})\}.$$

Let $\Phi_2(\xi_2, \eta_2, r_2, \lambda_2)$ the map defined by K_2. As the domain of Φ_2 we use the set

$$V_2 \;=\; D \times [0, \rho) \times (-\mu, \mu),$$

where D is a disk of large radius centered at the origin and μ is small and define

$$V_{2,\tilde{\varepsilon}} \;=\; \{(\xi_2, \eta_2, \sqrt{\tilde{\varepsilon}}, \lambda_2) \in V_2\}.$$

Then $P_{(\xi,\eta)}(\Phi_2(V_{2,\tilde{\varepsilon}}))$ is a neighborhood of the origin of size $O(\sqrt{\tilde{\varepsilon}})$ in ξ-direction and $O(\tilde{\varepsilon})$ in η-direction. We define

$$V_{\tilde{\varepsilon}} \;=\; P_{(\xi,\eta)}(\Phi_1(V_{1,\tilde{\varepsilon}}) \cup \Phi_2(V_{2,\tilde{\varepsilon}})).$$

Before we state the main theorems for the flow in a neighborhood $V = V_{\varepsilon_0}$ of the origin, we concentrate again on the critical manifold S_{2D}. From our previous observations it is clear that for $\varepsilon_0 > 0$ sufficiently small, only a part of $S_{2D}^{(2)}$ lies in the neighborhood V_{ε_0} and is defined by the solution of

$$\begin{aligned}&-\eta h_1(\xi,\eta) + \xi^2 h_2(\xi,\eta) = \\ &-\eta[1 + \alpha_{02}\eta + \alpha_{11}\xi + O(\xi\eta) + O(\eta^2)] + \xi^2[1 + \alpha_{30}\xi + O(\xi^2)] = 0.\end{aligned}$$

Then the critical manifold in V can be written as

$$\eta = \varphi_S(\xi) = \xi^2(1 + O(\xi))$$

and we can split the critical manifold in V into the two branches S_l and S_r, defined by

$$\begin{aligned}S_l &:= \{(\xi, \varphi_s(\xi)) : \xi < 0\}, \\ S_r &:= \{(\xi, \varphi_s(\xi)) : \xi > 0\}.\end{aligned} \tag{4.11}$$

The fast and slow flow for $\tilde{\varepsilon} = 0$, $\tilde{\lambda} = 0$ in V is as shown in figure 4.2. We are now able to describe the flow near the canard point.

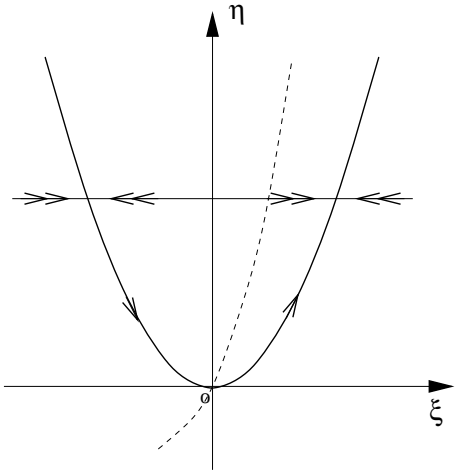

Figure 4.2: Fast and slow flow in V.

4.2.1 The Flow Near The Canard Point

The following results are taken from the paper of Szmolyan and Krupa [36]. The first statement is the existence of a Hopf bifurcation.

Theorem 4.5
There exists $\varepsilon_0 > 0$, $\lambda_0 > 0$ such that for each $0 < \tilde{\varepsilon} < \varepsilon_0$, $|\tilde{\lambda}| < \lambda_0$ equation (4.5) has precisely one equilibrium $p_e \in V$ which converges to the canard point as $(\tilde{\varepsilon}, \tilde{\lambda}) \to 0$.

Moreover, there exists a curve $\lambda_H(\sqrt{\tilde{\varepsilon}})$ *such that* p_e *is stable for* $\tilde{\lambda} < \lambda_H(\sqrt{(\tilde{\varepsilon})})$ *and loses stability through a Hopf bifurcation as* $\tilde{\lambda}$ *passes through* $\lambda_H(\sqrt{\tilde{\varepsilon}})$*. The curve* $\lambda_H(\sqrt{\tilde{\varepsilon}})$ *has the expansion*

$$\lambda_H(\sqrt{\tilde{\varepsilon}}) \;=\; -\tfrac{k_4}{2}\tilde{\varepsilon} + O(\tilde{\varepsilon}^{\frac{3}{2}}).$$

The Hopf bifurcation is non-degenerate if the constant A *defined in (4.8) is nonzero. It is supercritical if* $A < 0$ *and subcritical if* $A > 0$*.*

By Fenichel theory both S_l and S_r perturb as normally hyperbolic pieces of the critical manifold to nearby invariant manifolds $S_{l,\tilde{\varepsilon}}$ and $S_{r,\tilde{\varepsilon}}$. Under perturbation the critical manifold will break up at the non-hyperbolic canard point. However, the next statement shows that the connection of $S_{l,\tilde{\varepsilon}}$ and $S_{r,\tilde{\varepsilon}}$ is valid for a specific $\tilde{\lambda}$.

Theorem 4.6
Consider system (4.5). There exists a smooth function $\lambda_c(\sqrt{\tilde{\varepsilon}})$ *such that a solution starting in* $S_{l,\tilde{\varepsilon}}$ *connects to* $S_{r,\tilde{\varepsilon}}$*, if and only if* $\tilde{\lambda} = \lambda_c(\sqrt{\tilde{\varepsilon}})$*. The function* $\lambda_c(\sqrt{\tilde{\varepsilon}})$ *has the expansion*

$$\lambda_c(\sqrt{\tilde{\varepsilon}}) \;=\; -(\tfrac{k_4}{2} + \tfrac{1}{8}A)\tilde{\varepsilon} + O(\tilde{\varepsilon}^{\frac{3}{2}}).$$

As we see, the sign of A is essential for the dynamics near the canard point. The following two theorems now describe the flow near the canard point for both cases, $A < 0$ and $A > 0$. For $A < 0$ we get the following statement.

Theorem 4.7
Suppose ε_0*,* λ_0 *and* $V = V_{\varepsilon_0}$ *are sufficiently small and* $A < 0$*. Fix* $\tilde{\varepsilon} \in (0, \varepsilon_0]$*. Then the following statements hold:*

(i) For $\tilde{\lambda} \in (-\lambda_0, \lambda_H(\sqrt{\tilde{\varepsilon}}))$ *all orbits starting in* V *converge to* p_e *or leave* V*.*

(ii) There exists a curve $\tilde{\lambda} = \lambda_{sc}(\sqrt{\tilde{\varepsilon}})$ *and a constant* $K > 0$*, with*

$$0 < \lambda_c(\sqrt{\tilde{\varepsilon}}) - \lambda_{sc}(\sqrt{\tilde{\varepsilon}}) = O(e^{-\frac{K}{\tilde{\varepsilon}}}),$$

such that for each $\tilde{\lambda} \in (\lambda_H(\sqrt{\tilde{\varepsilon}}), \lambda_{sc}(\sqrt{\tilde{\varepsilon}}))$ *equation (4.5) has a unique, attracting limit cycle* $\Gamma_{(\tilde{\lambda},\tilde{\varepsilon})}$ *contained in* V*. All orbits starting in* V*, except for* p_e*, either leave* V *or are attracted to* $\Gamma_{(\tilde{\lambda},\tilde{\varepsilon})}$*.*

(iii) For $\tilde{\lambda} \in (\lambda_{sc}(\sqrt{\tilde{\varepsilon}}), \lambda_0]$ *all orbits starting in* V*, except for* p_e *leave* V*.*

Similarly, for $A > 0$ we get the next statement.

Theorem 4.8
Suppose ε_0, λ_0 and $V = V_{\varepsilon_0}$ are sufficiently small and $A > 0$. Fix $\tilde{\varepsilon} \in (0, \varepsilon_0]$. Then the following statements hold:

(i) There exists a curve $\tilde{\lambda} = \lambda_{sc}(\sqrt{\tilde{\varepsilon}})$ and a constant $K > 0$, with

$$0 < \lambda_{sc}(\sqrt{\tilde{\varepsilon}}) - \lambda_c(\sqrt{\tilde{\varepsilon}}) = O(e^{-\frac{K}{\tilde{\varepsilon}}}),$$

such that for each $\tilde{\lambda} \in (\lambda_{sc}(\sqrt{\tilde{\varepsilon}}), \lambda_H(\sqrt{\tilde{\varepsilon}}))$ equation (4.5) has a unique, repelling limit cycle $\Gamma_{(\tilde{\lambda},\tilde{\varepsilon})}$ contained in V.

(ii) For $\tilde{\lambda} \in (-\lambda_0, \lambda_H(\sqrt{\tilde{\varepsilon}}))$ all orbits starting in V, except for $\Gamma_{(\tilde{\lambda},\tilde{\varepsilon})}$ either leave V or are attracted to p_e.

(iii) For $\tilde{\lambda} \in [\lambda_H(\sqrt{\tilde{\varepsilon}}), \lambda_0)$ all orbits starting in V, except for p_e, leave V.

Based on the results of these theorems we can draw phase portraits, for both cases $A < 0$ and $A > 0$, for the dynamics near the canard point. These corresponding phase portraits are shown in figure 4.4 for $A < 0$ and in figure 4.5 for $A > 0$. Figure 4.3 shows the $(\tilde{\lambda}, \tilde{\varepsilon})$ - plane for both cases, $A < 0$ in the left and $A > 0$ in the right panel.

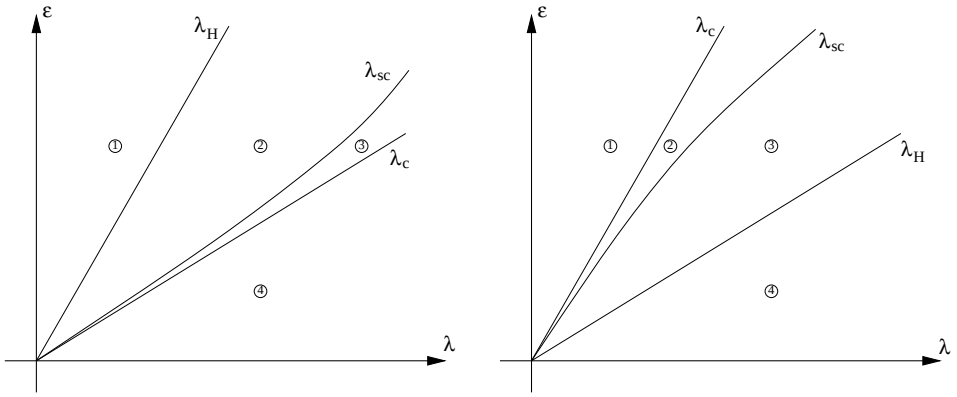

Figure 4.3: Bifurcation curves for $A < 0$ (left) and $A > 0$ (right).

For both the convenience of the reader and the use of some of the results in the description of aspects of the global flow, we outline the strategy for proving the results for the local dynamics near the canard point as developed by Krupa and Szmolyan [36, 35]. As already mentioned, the results are carried out with the help of the two charts of the blow-up transformation.

4.2.2 The Chart K_2

In this subsection we discuss some aspects for the flow in K_2. We first transform our system to K_2.

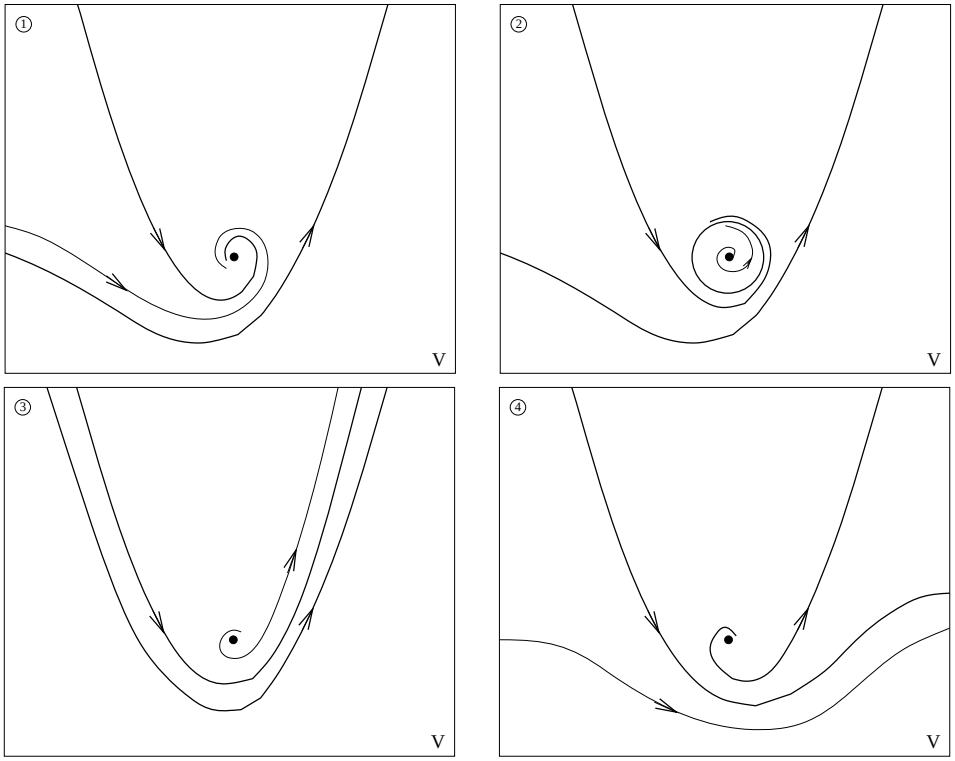

Figure 4.4: Phase portraits for $A < 0$ in the regions 1 to 4.

Lemma 4.9 (K_2 System)
Our system transformed to K_2 has the form

$$\begin{aligned} \dot{\xi}_2 &= \xi_2^2 - \eta_2 + r_2 G_1(\xi_2, \eta_2) + O(r_2^2), \\ \dot{\eta}_2 &= \xi_2 - \lambda_2 + r_2 G_2(\xi_2, \eta_2) + O(r_2^2), \end{aligned} \tag{4.12}$$

where

$$\begin{aligned} G_1(\xi_2, \eta_2) &= -k_1 \xi_2 \eta_2 + k_2 \xi_2^3, \\ G_2(\xi_2, \eta_2) &= k_3 \xi_2^2 + k_4 \eta_2. \end{aligned}$$

Proof.
Applying the transformation of K_2 we get

$$\begin{aligned} \xi_2 \dot{r}_2 + r_2 \dot{\xi}_2 &= -r_2^2 \eta_2 (1 + k_1 r_2 \xi_2 + O(r_2^2)) + r_2^2 \xi_2^2 (1 + k_2 r_2 \xi_2 + O(r_2^2)), \\ 2 r_2 \eta_2 \dot{r}_2 + r_2^2 \dot{\eta}_2 &= r_2^2 [r_2 \xi_2 (1 + k_3 r_2 \xi_2 + O(r_2^2)) - r_2 \lambda_2 (1 + O(r_2^2)) + k_4 r_2^2 \eta_2], \\ 2 r_2 \dot{r}_2 &= 0, \\ \lambda_2 \dot{r}_2 + r_2 \dot{\lambda}_2 &= 0, \end{aligned}$$

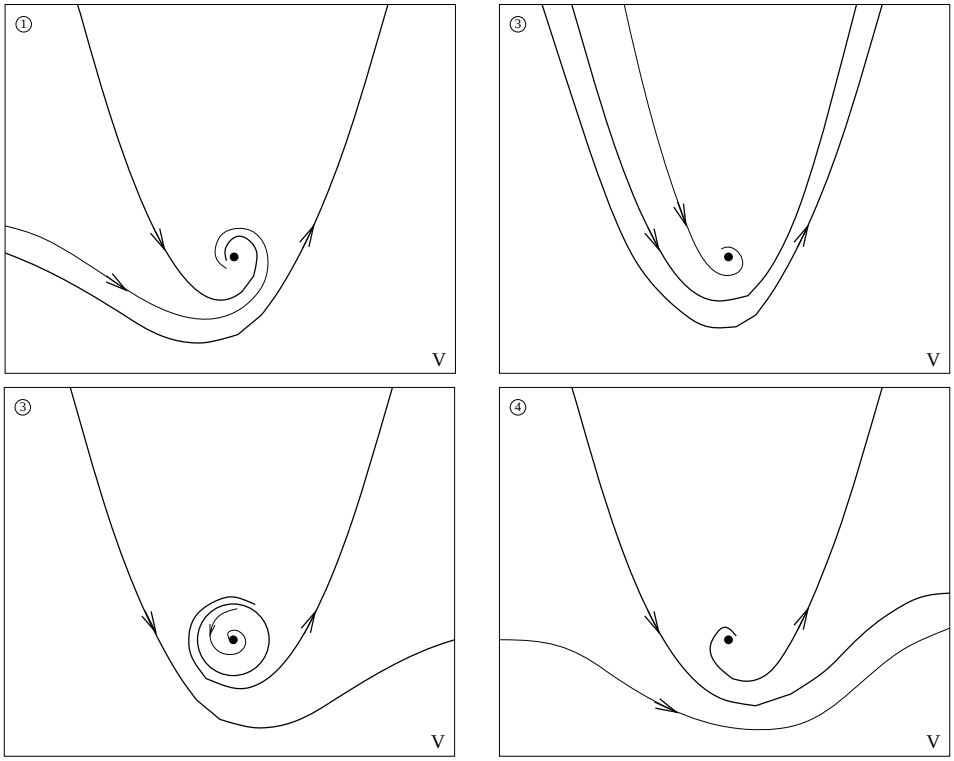

Figure 4.5: Phase portraits for $A > 0$ in the regions 1 to 4.

which yields

$$\begin{aligned}
\dot{\xi}_2 &= r_2[-\eta_2 + \xi_2^2 + r_2(-k_1\xi_2\eta_2 + k_2\xi_2^3) + O(r_2^2)],\\
\dot{\eta}_2 &= r_2[\xi_2 - \lambda_2 + r_2(k_3\xi_2^2 + k_4\eta_2) + O(r_2^2)],\\
\dot{r}_2 &= 0,\\
\dot{\lambda}_2 &= 0.
\end{aligned}$$

Desingularized according to the time transformation $t = r_2\tau$ the assertion follows. ∎

For $\varepsilon_2 = r_2 = 0$ the system reduces to

$$\begin{aligned}
\dot{\xi}_2 &= \xi_2^2 - \eta_2,\\
\dot{\eta}_2 &= \xi_2.
\end{aligned} \tag{4.13}$$

Lemma 4.10
System (4.13) is integrable with

$$H(\xi_2, \eta_2) = \tfrac{1}{2}e^{-2\eta_2}\left(\eta_2 - \xi_2^2 + \tfrac{1}{2}\right) \tag{4.14}$$

the corresponding constant of motion.

The function $H(\xi_2, \eta_2)$ has a continuous family of closed level curves

$$\Gamma_2^h \;=\; \{(\xi_2, \eta_2) : H(\xi_2, \eta_2) = h\}, \quad h \in (0, \tfrac{1}{4}),$$

contained in the interior of the parabola $\xi_2^2 - \eta_2 = \frac{1}{2}$, which corresponds to the level curve for $h = 0$. The corresponding special solution is given by

$$\gamma_{c,2} = (\xi_{c,2}(t_2), \eta_{c,2}(t_2)) = (\tfrac{1}{2}t_2, \tfrac{1}{4}t_2^2 - \tfrac{1}{2}), \quad t_2 \in \mathbb{R}. \tag{4.15}$$

The idea for proving the statements for the flow near the canard point is now to study the persistence of periodic orbits Γ_2^h for $(\tilde{\varepsilon}, \tilde{\lambda}) \neq (0, 0)$. The usual approach is to use the function H to measure the separation between forward and backward trajectories emanating from a given point. We will come back to this later.

Outline of the Proof (Theorem 4.5)
The proof of theorem 4.5 can be done entirely in system (4.12). Equation (4.12) has an equilibrium at $p_{e,2} = (\xi_{e,2}, \eta_{e,2})$ with $\xi_{e,2} = \lambda_2 + O(2)$ and $\eta_{e,2} = O(2)$, where $O(2) = O(r_2^2 + |r_2\lambda_2| + \lambda_2^2)$. The linearization at $p_{e,2}$ has purely imaginary eigenvalues for $\lambda_{H,2} = -\frac{k_4}{2}r_2 + O(r_2^2)$ and one can show, that the conditions of theorem 2.6 in chapter 3 of [8] hold. The result follows. ◇

We continue with the discussion of the dynamics in the chart K_1.

4.2.3 The Chart K_1

As in the chart K_2 we start with transforming our system to the chart K_1.

Lemma 4.11 (K_1 System)
Our system transformed to K_1 and desingularized has the form

$$\begin{aligned}
\dot{\xi}_1 &= \xi_1^2 - 1 + r_1(-k_1\xi_1 + k_2\xi_1^3) - \tfrac{1}{2}\varepsilon_1\xi_1 G_3(\xi_1, r_1, \varepsilon_1, \lambda_1),\\
\dot{r}_1 &= \tfrac{1}{2}\varepsilon_1 r_1 G_3(\xi_1, r_1, \varepsilon_1, \lambda_1),\\
\dot{\varepsilon}_1 &= -\varepsilon_1^2 G_3(\xi_1, r_1, \varepsilon_1, \lambda_1),\\
\dot{\lambda}_1 &= -\tfrac{1}{2}\varepsilon_1\lambda_1 G_3(\xi_1, r_1, \varepsilon_1, \lambda_1),
\end{aligned} \tag{4.16}$$

where

$$G_3(\xi_1, r_1, \varepsilon_1, \lambda_1) \;=\; \xi_1 - \lambda_1 + r_1(k_3\xi_1^2 + k_4) + O(r_1^2).$$

Proof.
Inserting the transformation of K_1 leads to the system

$$\begin{aligned}
\xi_1\dot{r}_1 + r_1\dot{\xi}_1 &= -r_1^2(1 + k_1 r_1\xi_1 + O(r_1^2)) + r_1^2\xi_1^2(1 + k_2 r_1\xi_1 + O(r_1^2)),\\
2r_1\dot{r}_1 &= r_1^2\varepsilon_1[r_1\xi_1(1 + k_3 r_1\xi_1 + O(r_1^2)) - r_1\lambda_1(1 + O(r_1^2)) + k_4 r_1^2],\\
2r_1\varepsilon_1\dot{r}_1 + r_1^2\dot{\varepsilon}_1 &= 0,\\
\lambda_1\dot{r}_1 + r_1\dot{\lambda}_1 &= 0,
\end{aligned}$$

which leads to

$$\begin{aligned}
\dot{\xi}_1 &= r_1(-1 + \xi_1^2 + r_1(-k_1\xi_1 + k_2\xi_1^3) + O(r_1^2)) - \tfrac{1}{r_1}\xi_1\dot{r}_1,\\
\dot{r}_1 &= \tfrac{1}{2}r_1^2\varepsilon_1[\xi_1 - \lambda_1 + r_1(k_3\xi_1^2 + k_4) + O(r_1^2)],\\
\dot{\varepsilon}_1 &= -2\tfrac{1}{r_1}\varepsilon_1\dot{r}_1,\\
\dot{\lambda}_1 &= -\tfrac{1}{r_1}\lambda_1\dot{r}_1
\end{aligned}$$

and finally we have

$$\begin{aligned}
\dot{\xi}_1 &= r_1(-1 + \xi_1^2 + r_1(-k_1\xi_1 + k_2\xi_1^3)) - \tfrac{1}{2}r_1\varepsilon_1\xi_1 G_3(\xi_1, r_1, \varepsilon_1, \lambda_1),\\
\dot{r}_1 &= \tfrac{1}{2}r_1^2\varepsilon_1 G_3(\xi_1, r_1, \varepsilon_1, \lambda_1),\\
\dot{\varepsilon}_1 &= -r_1\varepsilon_1^2 G_3(\xi_1, r_1, \varepsilon_1, \lambda_1),\\
\dot{\lambda}_1 &= -\tfrac{1}{2}r_1\varepsilon_1\lambda_1 G_3(\xi_1, r_1, \varepsilon_1, \lambda_1).
\end{aligned}$$

Desingularized according to the time transformation $t = r_1\tau$ the assertion follows. ∎

As stated above we are interested in the perturbation of the closed level curves Γ_h^2. For that reason we define the formulae for coordinate changes between the two charts K_1 and K_2.

Lemma 4.12 (Coordinate Changes)
Let κ_{12} denote the change of coordinates from K_1 to K_2. Then κ_{12} is given by

$$\xi_2 = \xi_1\varepsilon_1^{-\frac{1}{2}}, \quad \eta_2 = \varepsilon_1^{-1}, \quad r_2 = r_1\varepsilon_1^{\frac{1}{2}}, \quad \lambda_2 = \varepsilon_1^{-\frac{1}{2}}\lambda_1, \quad \text{for } \varepsilon_1 > 0, \tag{4.17}$$

and $\kappa_{21} = \kappa_{12}^{-1}$ is given by

$$\xi_1 = \xi_2\eta_2^{-\frac{1}{2}}, \quad \varepsilon_1 = \eta_2^{-1}, \quad r_1 = \eta_2^{\frac{1}{2}}r_2, \quad \lambda_1 = \eta_2^{-\frac{1}{2}}\lambda_2, \quad \text{for } \eta_2 > 0. \tag{4.18}$$

To find the corresponding closed level curves Γ_1^h we restrict system (4.16) to the invariant plane $r_1 = \lambda_1 = 0$, which leads to

$$\begin{aligned} \dot{\xi}_1 &= \xi_1^2 - 1 - \tfrac{1}{2}\varepsilon_1\xi_1^2, \\ \dot{\varepsilon}_1 &= -\varepsilon_1^2\xi_1. \end{aligned} \tag{4.19}$$

Now define $\tilde{H} = H \circ \kappa_{12}$. Then

$$\begin{aligned} \tilde{H}(\xi_1, r_1, \varepsilon_1, \lambda_1) &= \tilde{H}(\xi_1, \varepsilon_1) = H(\tfrac{\xi_1}{\sqrt{\varepsilon_1}}, \tfrac{1}{\varepsilon_1}) = \\ &= e^{-\frac{2}{\varepsilon_1}}(\tfrac{1}{4} + \tfrac{1}{2\varepsilon_1} - \tfrac{\xi_1^2}{2\varepsilon_1}) \end{aligned} \tag{4.20}$$

and system (4.19) is integrable with $\tilde{H}$ being a constant of motion. The curves

$$\Gamma_1^h = \kappa_{21}(\{(\xi_2, \eta_2) \in \Gamma_2^h : \eta_2 > 0\})$$

are level curves of $\tilde{H}$ and are invariant for system (4.19). We continue here now with the discussion of the K_1 system.

Clearly the hyperplanes $r_1 = 0$, $\varepsilon_1 = 0$ and $\lambda_1 = 0$ are invariant under the flow of system (4.16). Their intersection is the invariant line $l_1 := \{(\xi_1, 0, 0, 0) : \xi_1 \in \mathbb{R}\}$, which contains the two equilibria $p_l = (-1, 0, 0, 0)$ and $p_r = (1, 0, 0, 0)$. The dynamics in the invariant plane $\varepsilon_1 = \lambda_1 = 0$ is governed by the system

$$\begin{aligned} \dot{\xi}_1 &= \xi_1^2 - 1 + O(r_1), \\ \dot{r}_1 &= 0. \end{aligned} \tag{4.21}$$

We conclude, that p_l and p_r are endpoints of the lines of equilibria $S_{l,1}$ and $S_{r,1}$, which are the two branches of S_{2D}^0 defined in (4.11) in chart K_1. We can write system (4.21) as the layer problem in chart K_1 dropping the equation for $\dot{r}_1$.

$$\dot{\xi}_1 = \xi_1^2 - 1 + O(r_1).$$

Note, that we have gained normal hyperbolicity of the lines of equilibria $S_{l,1}$ at the point p_l and $S_{r,1}$ at the point p_r within the ξ_1 - axis due to the blow-up transformation. Indeed, p_l is stable with eigenvalue -2 and p_r is unstable with eigenvalue 2. Considered as equilibria of the whole K_1 system (4.16), both p_l and p_r have a triple eigenvalue zero. Now consider again the system (4.19) in the invariant plane $r_1 = \lambda_1 = 0$. We recover both the equilibria p_l and p_r. In this system there exists a second eigenvalue zero due to the second equation. The corresponding eigenvector at p_l is given by $(-1, 4)$ and at p_r by $(1, 4)$. We conclude that there exists a one-dimensional attracting center manifold

$N_{l,1}$ at p_l, which is unique in the half space $\varepsilon_1 > 0$ and there exists a one-dimensional repelling center manifold $N_{r,1}$ at p_r, which is also unique in the half space $\varepsilon_1 > 0$. Let

$$D_1 := \{(\xi_1, r_1, \varepsilon_1, \lambda_1) : -2 < \xi_1 < 2, 0 \leq r_1 \leq \rho, 0 \leq \varepsilon_1 \leq \delta, -\mu < \lambda_1 < \mu\},$$

where δ, ρ and μ will be chosen small. We restate proposition 3.4 in the paper of Krupa and Szmolyan [35].

Proposition 4.13 (Proposition 3.4 in [35])
Choose $q_1 < 2 < q_2$. The constants δ, ρ and μ can be chosen sufficiently small such that the following assertions hold for system:

1. *There exists an attracting three-dimensional C^k - center manifold $M_{l,1}$ at p_l that contains the line of equilibria $S_{l,1}$ and the center manifold $N_{l,1}$. In D_1 the manifold $M_{l,1}$ is given as a graph $\xi_1 = h_l(r_1, \varepsilon_1, \lambda_1)$. The branch of $N_{l,1}$ in $r_1 = \lambda_1 = 0$, $\varepsilon_1 > 0$ is unique and equal to $\gamma_{c,1} := \kappa_{21}(\gamma_{c,2})$, where $\gamma_{c,2}$ is the part of the special trajectory introduced in (4.15), corresponding to ξ_2 close to $-\infty$.*
2. *There exists a repelling three-dimensional C^k - center manifold $M_{r,1}$ at p_r which contains the line of equilibria $S_{r,1}$ and the center manifold $N_{r,1}$. In D_1 the manifold $M_{r,1}$ is given as a graph $\xi_1 = h_r(r_1, \varepsilon_1, \lambda_1)$. The branch of $N_{r,1}$ in $r_1 = \lambda_1 = 0$, $\varepsilon > 0$ is unique and equal to $\kappa_{21}(\gamma_{c,2})$ for ξ_2 close to ∞.*
3. *There exists a stable invariant foliation $\mathcal{F}^s$ with base $M_{l,1}$ and one-dimensional fibers. There exists positive constants $K_{l,1}$ and $K_{l,2}$ such that the contraction rates along $\mathcal{F}^s$ in a time interval of length T can be estimated by $K_{l,2}e^{-q_2 T}$ from below and by $K_{l,1}e^{-q_1 T}$ from above.*
4. *There exists an unstable invariant foliation $\mathcal{F}^u$ with base $M_{r,1}$ and one-dimensional fibers. There exists positive constants $K_{r,1}$ and $K_{r,2}$ such that the expansion rates along $\mathcal{F}^u$ in a time interval of length T can be estimated by $K_{r,1}e^{q_1 T}$ from below and by $K_{r,2}e^{q_2 T}$ from above.*

This proposition is a direct conclusion of center manifold theory. Now define the sections

$$\begin{aligned}
\Sigma_{l,1}^{in} &:= \{(x_1, r_1, \varepsilon_1, \lambda_1) \in V_1 : r_1 = \rho, |1 + x_1| < \vartheta\}, \\
\Sigma_{l,1}^{out} &:= \{(x_1, r_1, \varepsilon_1, \lambda_1) \in V_1 : \varepsilon_1 = \delta, |1 + x_1| < \vartheta\}, \\
\Sigma_{r,1}^{in} &:= \{(x_1, r_1, \varepsilon_1, \lambda_1) \in V_1 : \varepsilon_1 = \delta, |1 - x_1| < \vartheta\}, \\
\Sigma_{r,1}^{out} &:= \{(x_1, r_1, \varepsilon_1, \lambda_1) \in V_1 : r_1 = \rho, |1 - x_1| < \vartheta\},
\end{aligned} \tag{4.22}$$

with ϑ defined sufficiently small. For our analysis we need an estimation of the minimal time of a trajectory from a point in $\Sigma_{l,1}^{in}$ resp. $\Sigma_{r,1}^{in}$ to a point in $\Sigma_{l,1}^{out}$ resp. $\Sigma_{r,1}^{out}$. Let $\Pi_1 : \Sigma_{l,1}^{in} \to \Sigma_{l,1}^{out}$ and $\Pi_2 : \Sigma_{r,1}^{in} \to \Sigma_{r,1}^{out}$ be the transition maps defined by the flow of (4.16).

Lemma 4.14 (Transition Time)
The transition time T of a solution of the blown-up vector field in K_1 from a point $p = (x_1, \rho, \varepsilon_1, \lambda_1) \in \Sigma^{in}_{l,1}$ ($p = (x_1, \rho, \varepsilon_1, \lambda_1) \in \Sigma^{in}_{r,1}$) to the point $\Pi_1(p) \in \Sigma^{out}_{l,1}$ ($\Pi_2(p) \in \Sigma^{out}_{r,1}$) satisfies

$$T \geq \frac{1}{\mu+2+O(\rho)}\left(\frac{1}{\varepsilon_1} - \frac{1}{\delta}\right).$$

Proof.
The evolution of ε_1 determines the transition time of solutions from $\Sigma^{in}_{l,1}$ ($\Sigma^{in}_{r,1}$) to $\Sigma^{out}_{l,1}$ ($\Sigma^{out}_{r,1}$). The relevant equation is

$$\dot{\varepsilon}_1 = -\varepsilon_1^2 G_3(x_1, r_1, \varepsilon_1, \lambda_1).$$

Integration leads to

$$\varepsilon_1(t) = \frac{1}{\int_0^t G_3(x_1,r_1,\varepsilon_1,\lambda_1)ds + c}.$$

Then

$$\frac{1}{\varepsilon_1(t+T)} - \frac{1}{\varepsilon_1(t)} = \int_t^{t+T} G_3(x_1, r_1, \varepsilon_1, \lambda_1)ds.$$

Since $G_3(x_1, r_1, \varepsilon_1, \lambda_1) = x_1 - \lambda_1 + O(r_1)$ it follows, that

$$\begin{aligned} \left|\int_t^{t+T} G_3(x_1, r_1, \varepsilon_1, \lambda_1)ds\right| &\leq \int_t^{t+T} |x_1| + |\lambda_1| + |O(r_1)|ds \leq \\ &\leq \int_t^{t+T} [2 + \mu + O(\rho)]ds = \\ &= [2 + \mu + O(\rho)]T. \end{aligned}$$

Finally we get

$$\left|\frac{1}{\delta} - \frac{1}{\varepsilon_1(t)}\right| \leq [2 + \mu + O(\rho)]T.$$

The result follows. ∎

Lemma 4.14 and proposition 4.13 directly lead to the following statement. Let $I_l(\hat{\varepsilon}_1)$ be the line $\Sigma^{in}_{l,1} \cap \{\varepsilon_1 = \hat{\varepsilon}_1\}$ and $I_r(\hat{\varepsilon}_1)$ be the line $\Sigma^{out}_{r,1} \cap \{\varepsilon_1 = \hat{\varepsilon}_1\}$.

Proposition 4.15
Let ρ, δ and ϱ be sufficiently small. The transition maps $\Pi_1 : \Sigma^{in}_{l,1} \to \Sigma^{out}_{l,1}$ and $\Pi_2 : \Sigma^{in}_{r,1} \to \Sigma^{out}_{r,1}$ defined by the flow of system (4.16) have the following properties:

1. *$\Pi_1(\Sigma^{in}_{l,1})$ is a wedge-like region in $\Sigma^{out}_{l,1}$ and $\Pi_2^{-1}(\Sigma^{out}_{r,1})$ is a wedge-like region in $\Sigma^{in}_{r,1}$.*
2. *For fixed $q < 2$ there exists a constant K depending on the constants ρ, δ, ϱ and q such that for every $\varepsilon_1 \in (0, \rho]$ the map $\Pi_1|I_l(\varepsilon_1)$ and the map $\Pi_2^{-1}|I_r(\varepsilon_1)$ are contractions with contraction rate bounded by*

$$Ke^{-\frac{q}{2+\mu+O(\rho)}\left(\frac{1}{\varepsilon_1}-\frac{1}{\delta}\right)}.$$

4.2.4 Outlines Of Proofs

For the convenience of the reader we outline the proofs for theorem 4.6 and theorem 4.7. The proof of theorem 4.8 is similar to that of theorem 4.7. For details of the proofs, see [36, 35].

The idea to prove theorem 4.6 is to use a Melnikov like computation of the separation between $M_{l,2}$ and $M_{r,2}$. These are the corresponding manifolds in chart K_2 to $M_{l,1}$ and $M_{r,1}$. It is clear, that $M_{l,2}$ and $M_{r,2}$ intersect along the special trajectory $\gamma_{c,2}$ for $r_2 = \lambda_2 = 0$. Now fix $r_2 \in [0, \rho]$, ρ sufficiently small. Let $\gamma_{l,1}$ be the trajectory of system (4.16) contained in $M_{l,1}$ for which $r_1\sqrt{\varepsilon_1} = r_2$ starting at $\Sigma^{in}_{l,1}$, and let $\gamma_{l,2} = (\xi_{l,2}, \eta_{l,2})$ be the continuation of $\gamma_{l,1}$ to chart K_2. $\gamma_{l,2}$ is a solution of (4.12) being parameterized such that $\xi_{l,2}(0) = 0$. Analogously, let $\gamma_{r,1}$ be the trajectory of system (4.16) contained in $M_{r,1}$ for which $r_1\sqrt{\varepsilon_1} = r_2$ starting at $\Sigma^{in}_{r,1}$, and let $\gamma_{r,2} = (\xi_{r,2}, \eta_{r,2})$ be the corresponding backward continued solution of (4.12) parameterized such that $\xi_{r,2}(0) = 0$. Then measuring the separation of $M_{l,2}$ and $M_{r,2}$ corresponds to measuring $\eta_{l,2}(0) - \eta_{r,2}(0)$, which is equivalent to estimating the distance function

$$D_c(r_2, \lambda_2) \;=\; H(0, \eta_{l,2}(0)) - H(0, \eta_{r,2}(0)), \tag{4.23}$$

where H is defined in (4.14). Note that $\frac{\partial}{\partial \eta_2} H(0, \eta_2) \neq 0$ for $\eta_2 > 0$. We get the following proposition.

Proposition 4.16 (Proposition 3.5 in [35])
For ρ and μ small enough, the distance function $D_c(r_2, \lambda_2)$ has the expansion

$$D_c(r_2, \lambda_2) \;=\; d_{r_2} r_2 + d_{\lambda_2} \lambda_2 + O(2),$$

where

$$d_{r_2} \;=\; \int_{-\infty}^{\infty} \nabla H(\gamma_{c,2}(t)) \cdot G(\gamma_{c,2}(t)) dt$$

and

$$d_{\lambda_2} \;=\; \int_{-\infty}^{\infty} \nabla H(\gamma_{c,2}(t)) \cdot \begin{pmatrix} 0 \\ -1 \end{pmatrix} dt.$$

Now we are able to outline the proof of theorem 4.6.

Outline of the Proof (Theorem 4.6)
The function $D_c(r_2, \lambda_2) = 0$ can be solved for λ_2 by the implicit function theorem given that $d_{\lambda_2} \neq 0$. The two parameters can be computed by repeated integration, which leads to the desired statement. Indeed, we get

$$d_{\lambda_2} \;=\; -\tfrac{e}{2} \textstyle\int_{-\infty}^{\infty} e^{-\frac{t^2}{2}} dt \quad \text{and} \quad d_{r_2} \;=\; -\tfrac{e}{4}(k_4 + \tfrac{1}{4}A) \textstyle\int_{-\infty}^{\infty} e^{-\frac{t^2}{2}} dt. \qquad \diamond$$

As we have stated earlier, we now deal with finding periodic orbits as perturbations of the family Γ_2^h, $h \in (0, \frac{1}{4})$. For h close to $\frac{1}{4}$ the existence of periodic orbits are a direct conclusion of theorem 4.5. Let $h_0 \in (0, \frac{1}{4})$ and consider $h \in (0, h_0)$. Then let $\gamma_2^h(t) = (\xi_2^h(t), \eta_2^h(t))$ be a solution corresponding to Γ_2^h such that $\xi_2^h(0) = 0$ and $\eta_2^h(0) > 0$. Let γ_{r_2,λ_2}^h and $\hat{\gamma}_{r_2,\lambda_2}^h$ be the forward and backward solution of (4.12) for each $(r_2, \lambda_2) \in [0, \sqrt{\varepsilon_0}) \times (-\mu, \mu)$ satisfying $\gamma_{r_2,\lambda_2}^h(0) = \hat{\gamma}_{r_2,\lambda_2}^h(0) = \gamma_2^h(0)$. Let $(0, \eta_{r_2,\lambda_2}^h)$ (resp. $(0, \hat{\eta}_{r_2,\lambda_2}^h)$) be the intersection points of γ_{r_2,λ_2}^h (resp. $\hat{\gamma}_{r_2,\lambda_2}^h$) with the negative part of the η_2 - axis, respectively. We define the distance function

$$D_s(h, r_2, \lambda_2) \;=\; H(0, \eta_{r_2,\lambda_2}^h) - H(0, \hat{\eta}_{r_2,\lambda_2}^h).$$

Since $\frac{\partial}{\partial \eta_2} H(0, \eta_2) \neq 0$ it follows that periodic orbits of (4.12) correspond to solutions of

$$D_s(h, r_2, \lambda_2) \;=\; 0.$$

Let $\sigma(h) = (\eta_2^h(0))^{-1}$ and define

$$U_0 \;=\; (0, h_0) \times [0, \rho\sqrt{\sigma(h)}) \times (-\mu, \mu).$$

We have the following proposition.

Proposition 4.17 (Proposition 4.1 in [36])
Let ρ be sufficiently small. Then for $r_2 \leq \rho\sqrt{\sigma(h)}$, $\lambda_2 \in (-\mu, \mu)$ and $h \in (0, h_0)$ the function D_s has the expansion

$$D_s(h, r_2, \lambda_2) \;=\; d_{r_2}^h r_2 + d_{\lambda_2}^h \lambda_2 + \hat{Q}(h, r_2, \lambda_2),$$

where, with T_h being the half period of Γ^h,

$$d_{r_2}^h \;=\; \int_{-T^h}^{T^h} \nabla H(\gamma_2^h(t)) \cdot G(\gamma_2^h(t)) dt,$$

$$d_{\lambda_2}^h \;=\; \int_{-T^h}^{T^h} \nabla H(\gamma_2^h(t)) \cdot \begin{pmatrix} 0 \\ -1 \end{pmatrix} dt$$

and $\hat{Q}$ satisfies for some constant $K > 0$

$$|\hat{Q}(h, r_2, \lambda_2)| \;\leq\; K(r_2 + |\lambda_2|)^2,$$

$$|\frac{\partial}{\partial h} \hat{Q}(h, r_2, \lambda_2)| \;\leq\; K\rho(r_2 + |\lambda_2|)\sigma(h)^{-\frac{3}{2}}.$$

Moreover, the partial derivatives $|\frac{\partial}{\partial r_2} D_s(h, r_2, \lambda_2)|$, $|\frac{\partial}{\partial \lambda_2} D_s(h, r_2, \lambda_2)|$, $|\frac{\partial^2}{\partial r_2^2} D_s(h, r_2, \lambda_2)|$, $|\frac{\partial^2}{\partial \lambda_2^2} D_s(h, r_2, \lambda_2)|$ and $|\frac{\partial^2}{\partial r_2 \partial \lambda_2} D_s(h, r_2, \lambda_2)|$ are uniformly bounded.

And we outline the proof of theorem 4.7.

Outline of the Proof (Theorem 4.7)
We drop the proof for statements (i) and (iii) here. For details see [36].

For (ii) first let $h_0 \in (0, \frac{1}{4})$ arbitrary, fixed. One concludes the existence of a curve $\lambda_2(r_2, h_0)$ such that there is a unique attracting periodic orbit for the flow of (4.12) restricted to a large disc centered at the origin for any $r_2 \in (0, \rho)$ and $\lambda_H(r_2) < \tilde{\lambda} < \lambda_2(r_2, h_0)$ using theorem 4.5 and the relative position of $S_{l,\tilde{\varepsilon}}$ and $S_{r,\tilde{\varepsilon}}$.

Now let $h \in (0, h_0)$. With the help of proposition 4.17 one obtains

$$\frac{\partial}{\partial \lambda_2} D_s(h, r_2, \lambda_2) \neq 0 \quad \text{for } (h, r_2, \lambda_2) \in U_0.$$

Hence a solution $\lambda_2(h, r_2)$ of $D_s(h, r_2, \lambda_2) = 0$ can be obtained by repeated application of the implicit function theorem. Uniqueness can be shown by a direct argumentation.

It can directly be shown that the curve λ_{sc} can be written as

$$\lambda_{sc}(r_2) = r_2 \lambda_2(h_{sc}(r_2), r_2),$$

where for all $h \geq h_{sc}$ the constructed periodic orbit lies entirely in V and for all $h < h_{sc}$ the constructed periodic orbit leaves V.

The orbit $\Gamma_{1,sc}$ in chart K_1 corresponding to $\lambda_2(h_{sc}(r_2), r_2)$ passes $O(e^{-\frac{K}{\tilde{\varepsilon}}})$ close to both $M_{l,1}$ and $M_{r,1}$, where $K > 0$ is some constant. We get

$$D_c(r_2, \lambda_2(h_{sc}, r_2)) = O(e^{-\frac{K}{\tilde{\varepsilon}}})$$

and finally , since $\frac{\partial}{\partial \lambda_2} D_c(0, 0) \neq 0$,

$$|\lambda_2(h_{sc}, r_2) - \lambda_{c,2}(r_2)| = O(e^{-\frac{K}{\tilde{\varepsilon}}}). \qquad \diamond$$

Remark 4.18
We note, that we have not yet proved the statement of stabilities of the periodic orbits in V. However, we address this issue in the context of the analysis of the global flow.

We continue with the local flow near the homoclinic point (x_s, y_s).

4.3 The Homoclinic Point

This section is dedicated to the local flow near the homoclinic point (x_s, y_s). The homoclinic point (x_s, y_s) is a stationary point of system (4.2) for $\lambda = 0$, i.e. the following equations hold.

$$\begin{aligned} 0 &= f_2(\tfrac{1}{c_1} f_1(x_s)) - (c_2 + h(y_s))x_s = F(x_s, y_s), \\ 0 &= g(\tfrac{1}{c_1} f_1(x_s)) - c_3 y_s = G(x_s, y_s, 0). \end{aligned}$$

Taylor expansion of the functions F with respect to (x_s, y_s) and G with respect to $(x_s, y_s, 0)$ leads to the following system in some neighborhood of the homoclinic point.

$$\begin{aligned} \dot{\xi} &= \hat{a}_1\xi + \hat{a}_2\eta + \hat{a}_3\xi^2 + \hat{a}_4\xi\eta + \hat{a}_5\eta^2 + O(\xi^3 + |\xi^2\eta| + |\xi\eta^2| + \eta^3), \\ \dot{\eta} &= \varepsilon[\hat{b}_1\xi + \hat{b}_2\eta + \hat{b}_3\lambda + O(\xi^2)], \end{aligned} \tag{4.24}$$

where

$$\begin{gathered} \hat{a}_1 = \tfrac{\partial}{\partial x}F(x_s, y_s), \quad \hat{a}_2 = \tfrac{\partial}{\partial y}F(x_s, y_s), \\ \hat{a}_3 = \tfrac{1}{2}\tfrac{\partial^2}{\partial x^2}F(x_s, y_s), \quad \hat{a}_4 = \tfrac{1}{2}\tfrac{\partial^2}{\partial x \partial y}F(x_s, y_s), \quad \hat{a}_5 = \tfrac{1}{2}\tfrac{\partial^2}{\partial y^2}F(x_s, y_s), \end{gathered}$$

and

$$\hat{b}_1 = \tfrac{\partial}{\partial x}G(x_s, y_s, 0), \quad \hat{b}_2 = \tfrac{\partial}{\partial y}G(x_s, y_s, 0), \quad \hat{b}_3 = \tfrac{\partial}{\partial \lambda}G(x_s, y_s, 0).$$

We have the following lemma.

Lemma 4.19
Define a sufficiently small neighborhood U_s of (x_s, y_s). Then there exists an $\varepsilon_0 > 0$ and a $\lambda_0 > 0$ such that for each $0 < \varepsilon < \varepsilon_0$, $|\lambda| < \lambda_0$ equation (4.24) has precisely one equilibrium $p_s \in U_s$ which converges to (x_s, y_s) as $(\varepsilon, \lambda) \to 0$. Moreover, p_s is an equilibrium of saddle type with a slow stable manifold and a fast unstable manifold.

Proof.
We first note that since (x_s, y_s) is a stationary point of the layer problem of system (4.2) lying on the unstable part of the critical manifold, i.e. it is the middle zero of the three ordered zeros of $F(x, y_s)$, the constant $\hat{a}_1$ is positive. A simple calculation shows, that additionally $\hat{b}_1 > 0$ and $\hat{a}_2$, $\hat{b}_2$, $\hat{b}_3 < 0$.

Further note that $\frac{-\hat{a}_1}{\hat{a}_2}$ is the slope of the critical manifold and $\frac{-\hat{b}_1}{\hat{b}_2}$ is the slope of Z^0_{2D}, both evaluated at the homoclinic point (x_s, y_s). This leads to the following inequalities.

$$\tfrac{-\hat{a}_1}{\hat{a}_2} > \tfrac{-\hat{b}_1}{\hat{b}_2} \quad \Leftrightarrow \quad \hat{a}_1\hat{b}_2 - \hat{a}_2\hat{b}_1 < 0 \quad \Leftrightarrow \quad \hat{b}_2 - \tfrac{\hat{a}_2\hat{b}_1}{\hat{a}_1} < 0. \tag{4.25}$$

The only stationary point in U_s takes the form $p_{s,\lambda} = (\xi_{s,\lambda}, \eta_{s,\lambda})$ with $\xi_{s,\lambda} = \hat{k}_1\lambda + O(\lambda^2)$ and $\eta_{s,\lambda} = \hat{k}_2\lambda + O(\lambda^2)$, where $\hat{k}_1 = \frac{\hat{a}_2\hat{b}_3}{\hat{a}_1\hat{b}_2 - \hat{a}_2\hat{b}_1}$ and $\hat{k}_2 = -\frac{\hat{a}_1\hat{b}_3}{\hat{a}_1\hat{b}_2 - \hat{a}_2\hat{b}_1}$. The Jacobian at the equilibrium $p_{s,\lambda}$ reads

$$J_{s,\varepsilon,\lambda} = \begin{pmatrix} \hat{a}_1 + (2\hat{a}_3\hat{k}_1 + \hat{a}_4\hat{k}_2)\lambda + O(\lambda^2) & \hat{a}_2 + (\hat{a}_4\hat{k}_1 + 2\hat{a}_5\hat{k}_2)\lambda + O(\lambda^2) \\ \varepsilon\hat{b}_1 + O(\varepsilon\lambda) & \varepsilon\hat{b}_2 + O(\varepsilon\lambda) \end{pmatrix}.$$

And the eigenvalues are

$$\hat{a}_1 + \frac{\hat{a}_2\hat{b}_1}{\hat{a}_1}\varepsilon + (2\hat{a}_3\hat{k}_1 + \hat{a}_4\hat{k}_2)\lambda + O(\varepsilon^2 + |\varepsilon\lambda| + \lambda^2)$$

and

$$(\hat{b}_2 - \frac{\hat{a}_2\hat{b}_1}{\hat{a}_1})\varepsilon + O(\varepsilon^2 + |\varepsilon\lambda| + \lambda^2).$$

The result follows with (4.25). ∎

We further note that the eigenvectors of the Jacobian have the expressions $(1 + O(\varepsilon, \lambda), \frac{\hat{b}_1}{\hat{a}_1}\varepsilon + O((\varepsilon + \lambda)^2))^T$ and $(-\hat{a}_2 + O(\varepsilon, \lambda), \hat{a}_1 + O(\varepsilon, \lambda))^T$ for their respective eigenvalues, so that the flow in U_s is as shown in figure 4.6.

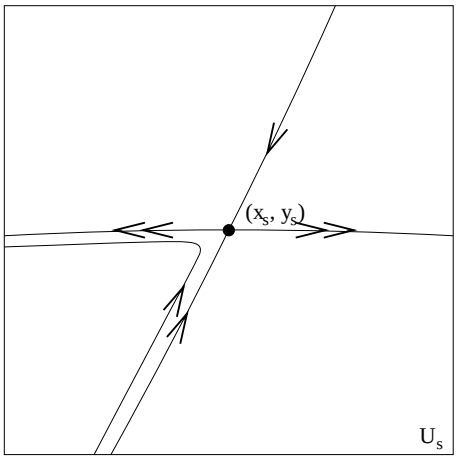

Figure 4.6: A picture for the flow near the homoclinic point.

Analyzing the global aspects of the flow, we will be interested in backward trajectories reaching a neighborhood of p_s. Here we investigate the local behavior of such trajectories. For this reason we rescale time according to the transformation $\tau = -t$. The resulting system can locally be written in Fenichel coordinates, since we are in a neighborhood

of a normally hyperbolic subset of the critical manifold. In this new coordinates, the system of the local flow near the homoclinic point reads (see (2.9))

$$\begin{aligned} \dot{\tilde{w}} &= \Lambda(\tilde{w}, \tilde{z}, \varepsilon, \lambda)\tilde{w}, \\ \dot{\tilde{z}} &= \varepsilon h(\tilde{z}, \varepsilon) = \varepsilon \tilde{h}(\tilde{z}, \varepsilon)\tilde{z}, \end{aligned} \tag{4.26}$$

where $\Lambda(0, 0, \tilde{z}, 0) < 0$ and $\tilde{h}(0, 0) > 0$. The last equality in the second equation is due to the fact, that the origin as the homoclinic point remains stationary. After a simple time transformation we obtain

$$\begin{aligned} \dot{w} &= \tilde{\Lambda}(w, z, \varepsilon, \lambda)w, \\ \dot{z} &= \varepsilon z. \end{aligned} \tag{4.27}$$

Let $\varrho > 0$ be fixed and sufficiently small and define the section Δ by

$$\Delta = \{(w, z) : 0 \leq w \leq \varrho, 0 \leq z \leq \varrho\}.$$

Theorem 4.20 (Trajectories near p_s)
There exist $\varrho > 0$, $\varepsilon_0 > 0$ and $\lambda_0 > 0$ small enough, such that for every $\varepsilon \in (0, \varepsilon_0]$ and $|\lambda| < \lambda_0$ the following statement holds. Every trajectory $(w(t), z(t))$ entering Δ parameterized such that $(w(0), z(0)) = (\varrho, \delta)$ with $0 < \delta < \varrho$ leaves Δ after time $T = \frac{1}{\varepsilon} \ln(\frac{\varrho}{\delta})$. For $\delta \to 0$ it holds that

$$|w(T)| \to 0, \quad |\tfrac{\partial}{\partial \delta} w(T)| \to 0.$$

Proof.
The first step is to compute the time T, for which the trajectory $(w(t), z(t))$ with the initial conditions $(w(0), z(0)) = (\varrho, \delta)$ stays in Δ. The evolution of z determines this transition time. We obtain

$$\delta e^{\varepsilon T} = \varrho.$$

Solving this equation for T leads to

$$T = \tfrac{1}{\varepsilon} \ln(\tfrac{\varrho}{\delta}).$$

The second step now estimates $|w(T)|$. First note, that for $(w, z) \in \Delta$ the following estimate holds if ϱ, ε_0 and λ_0 are small enough.

$$\tilde{\Lambda}(w, z, \varepsilon, \lambda) \leq -q,$$

for some $q > 0$. Then applying the method of variation of parameters yields

$$|w(T)| = w(0) e^{\int_0^T \tilde{\Lambda}(w,z,\varepsilon,\lambda) dt} \leq \varrho e^{-qT} = \varrho (\tfrac{\delta}{\varrho})^{\frac{q}{\varepsilon}}. \tag{4.28}$$

For the third step we differentiate our system with respect to the initial value δ. We obtain the system

$$\begin{array}{rcl} \dot{w}_\delta & = & \frac{\partial}{\partial w}\tilde{\Lambda}(w,z,\varepsilon,\lambda)ww_\delta + \frac{\partial}{\partial z}\tilde{\Lambda}(w,z,\varepsilon,\lambda)wz_\delta + \tilde{\Lambda}(w,z,\varepsilon,\lambda)w_\delta, \\ \dot{z}_\delta & = & \varepsilon z_\delta, \end{array} \tag{4.29}$$

with the initial conditions $w_\delta(0) = 0$ and $z_\delta(0) = 1$. For $t \geq 0$ it holds that $|w(t) \leq \varrho e^{-qt}|$, analogously to (4.28). Now note that for $(w,z) \in \Delta$ the following inequalities hold if ϱ, ε_0 and λ_0 are small enough.

$$\begin{aligned} &\tilde{\Lambda}(w,z,\varepsilon,\lambda) + \tfrac{\partial}{\partial w}\tilde{\Lambda}(w,z,\varepsilon,\lambda)w \leq -\mu, \\ &|\tfrac{\partial}{\partial z}\tilde{\Lambda}(w,z,\varepsilon,\lambda)w| \leq \tilde{q}e^{-\hat{\mu}t}, \end{aligned}$$

where $\tilde{q} > 0$, $\mu > 0$ and $\hat{\mu} > 0$ are constants. Using the method of variation of parameters for the second equation now yields

$$\begin{array}{rcl} |w_\delta(T)| & = & |\int_0^T e^{\int_t^T \tilde{\Lambda} + \frac{\partial}{\partial w}\tilde{\Lambda}w d\tau}\frac{\partial}{\partial z}\tilde{\Lambda}we^{\varepsilon t}dt| \leq \\ & \leq & \int_0^T e^{-\int_t^T \mu d\tau}\tilde{q}e^{-\tilde{\mu}t}e^{\varepsilon t}dt = \\ & = & \tilde{q}e^{-\mu T}\int_0^T e^{(\mu+\varepsilon-\tilde{\mu})t}dt = \\ & = & \frac{\tilde{q}}{\mu+\varepsilon-\tilde{\mu}}(e^{(\varepsilon-\tilde{\mu})T} - e^{-\mu T}) \leq \\ & \leq & Le^{-CT} \leq L(\frac{\delta}{\varrho})^{\frac{C}{\varepsilon}} \end{array} \tag{4.30}$$

for $\mu + \varepsilon - \tilde{\mu} \neq 0$ and otherwise

$$|w_\varrho(T)| \leq \tilde{q}Te^{-\mu T} = \tfrac{\tilde{q}}{\varepsilon}(\ln\tfrac{\varrho}{\delta})(\tfrac{\delta}{\varrho})^{\frac{\mu}{\varepsilon}}. \tag{4.31}$$

This proves the statement. ∎

This theorem now allows us to describe properties of the global flow of system (4.2). We will see that local Hopf cycles near the canard point will grow to canard cycles, finally reaching a homoclinic orbit and afterwards vanishing as λ varies.

4.4 Global Aspects Of The Flow

For easier notation and description we scale our two-dimensional system (4.2) according to the same transformations used in the local analysis of the canard point. More precisely recall the parameters θ_i, $i = 1,...,4$ in (4.6) and define

$$\begin{array}{rcl} \tilde{F}(\xi,\eta) & := & \theta_1 F(\frac{1}{\theta_1}\xi + x_c, \frac{1}{\theta_2}\eta + y_c), \\ \tilde{G}(\xi,\eta,\tilde{\lambda}) & := & \frac{\theta_2}{\theta_3}G(\frac{1}{\theta_1}\xi + x_c, \frac{1}{\theta_2}\eta + y_c, \frac{1}{\theta_4}\tilde{\lambda}). \end{array}$$

Then system (4.2) can be written in new coordinates according to the transformation $\xi = \theta_1(x - x_c)$, $\eta = \theta_2(y - y_c)$, $\tilde{\varepsilon} = \theta_3\varepsilon$ and $\tilde{\lambda} = \theta_4\lambda$ as

$$\begin{aligned} \dot{\xi} &= \tilde{F}(\xi, \eta), \\ \dot{\eta} &= \tilde{\varepsilon}\tilde{G}(\xi, \eta, \tilde{\lambda}). \end{aligned} \tag{4.32}$$

Also note, that system (4.5) is the local linearization of system (4.32) in a neighborhood of the canard point.

For the description of the global flow of (4.32) we patch forward and backward trajectories emanating from points $(0, s)$ on the positive η-axis. The analysis of the local flow near the canard point guarantees the existence of "small" periodic orbits for small values of s. We have the following proposition, compare proposition 4.3 in [36].

Proposition 4.21 (Proposition 4.3 in [36])
Assume that $A \neq 0$ and that ρ and ε_0 are sufficiently small. Then, for $\tilde{\varepsilon} \in (0, \varepsilon_0)$, there exists a continuous family of periodic orbits

$$s \;\rightarrow\; (\lambda(s, \sqrt{\tilde{\varepsilon}}), \Gamma(s, \sqrt{\tilde{\varepsilon}})), \quad s \in (0, \rho^2), \quad \Gamma(s, \sqrt{\tilde{\varepsilon}}) \subset V,$$

where $\lambda(s, \sqrt{\varepsilon})$ is C^k in $(s, \sqrt{\tilde{\varepsilon}})$ and $\Gamma(s, \sqrt{\tilde{\varepsilon}}))$ passes through the point $(0, s)$. If $A < 0$ then $\frac{\partial}{\partial s}\lambda(s, \sqrt{\tilde{\varepsilon}}) > 0$ and the periodic orbit is stable. If $A > 0$ then $\frac{\partial}{\partial s}\lambda(s, \sqrt{\tilde{\varepsilon}}) < 0$ and the periodic orbit is unstable. Any periodic orbit in V is a member of the family $\Gamma(s, \sqrt{\tilde{\varepsilon}}))$.

Outline of the Proof
The existence of a family of periodic orbits

$$h \;\rightarrow\; (\lambda(h, r_2), \Gamma(h, r_2))$$

is guaranteed by the proof of theorem 4.7. After a parametrization change this proof shows the statements on the sign of $\frac{\partial}{\partial s}\lambda(s, \sqrt{\tilde{\varepsilon}})$ as well as the uniqueness of periodic orbits in V. Again, see [36] for details. The statement about the stability, which was skipped earlier, now follows from considering the return map of Δ_s to itself, where

$$\Delta_s \;:=\; \{(0, s, \tilde{\lambda}, \tilde{\varepsilon}) : s \in (0, s_0), \tilde{\varepsilon} \in (0, \varepsilon_0), \tilde{\lambda} \in (-\lambda_0, \lambda_0)\}.$$

Let $\Pi_s : \Delta_s \rightarrow \Delta_s$ be this return map. Differentiating the identity $\Pi_s(s, \lambda(s, r_2), r_2) = s$ with respect to s yields

$$1 - \tfrac{\partial \Pi_s}{\partial s} \;=\; \tfrac{\partial \Pi_s}{\partial \tilde{\lambda}}(s, \lambda(s, r_2), r_2)\tfrac{\partial \lambda}{\partial s}(s, r_2).$$

Note that $\frac{\partial \Pi_s}{\partial s} > 0$ due to the order preserving property of the flow. Furthermore, if $A < 0$ the right hand side is positive and $\frac{\partial \Pi_s}{\partial s} < 1$ and if $A > 0$ the right hand side is negative and $\frac{\partial \Pi_s}{\partial s} > 1$. The statements on the right hand side are direct conclusions of the relative positions of λ_H, λ_{sc} and λ_c. This concludes the statement. $\diamond$

As $\tilde{\lambda}$ varies the periodic orbits will grow and limit in an homoclinic orbit with respect to the homoclinic point. The existence and uniqueness of the homoclinic orbit is stated in the next theorem.

Theorem 4.22
Suppose ε_0 is sufficiently small and fix $\tilde{\varepsilon} \in (0, \varepsilon_0]$. There exists a smooth function $\lambda_{Ho}(\sqrt{\tilde{\varepsilon}})$ and a constant $K > 0$, with

$$|\lambda_{Ho}(\sqrt{\tilde{\varepsilon}}) - \lambda_c(\sqrt{\tilde{\varepsilon}})| < O(e^{-\frac{K}{\tilde{\varepsilon}}}),$$

such that equation (4.32) has a unique, unstable homoclinic orbit with respect to the homoclinic point $(\xi_{s,\lambda_{Ho}(\sqrt{\tilde{\varepsilon}})}, \eta_{s,\lambda_{Ho}(\sqrt{\tilde{\varepsilon}})})$.

Proof.
We consider the forward trajectory $\gamma_u(t)$ emanating from a point on the fast unstable manifold of the homoclinic point $(\xi_{s,\tilde{\lambda}}, \eta_{s,\tilde{\lambda}})$ in dependence of $\tilde{\lambda}$. This trajectory is exponentially attracted by $S_{l,\tilde{\varepsilon}}$ and we have $\gamma_u(t) \in V$ in some interval $I_u \subset [0, \infty)$. So $\gamma_u(t)$ gives rise to a trajectory in the blow-up system and therefore to associated trajectories $\gamma_{u,j}$, $j = 1, 2$, in charts K_1 and K_2. Let $(0, \eta_{u,2})$ be the point, where $\gamma_{u,2}(t)$ crosses the ξ_2 - axis. The backward trajectory $\hat{\gamma}_u(t)$ emanating from a point on the stable manifold of the homoclinic point gives rise to a point $(0, \hat{\eta}_{u,2})$ in the same way.

Furthermore remember the solutions $\gamma_{l,2}(t) = (\xi_{l,2}(t), \eta_{l,2}(t))$ and $\gamma_{r,2}(t) = (\xi_{r,2}(t), \eta_{r,2}(t))$ contained in $M_{l,2}$ and $M_{r,2}$, respectively, with $\xi_{l,2}(0) = \xi_{r,2}(0) = 0$. We consider $\eta_{l,2}(0)$ and $\eta_{r,2}(0)$ defined analogously as for equation (4.23).

Since $\gamma_{u,1}(t)$ and $\hat{\gamma}_{u,1}(t)$ pass through $\Sigma_{l,1}^{out}$ and $\Sigma_{r,1}^{in}$, respectively, we obtain for $\tilde{\varepsilon} = r_2^2$ and some constant $K > 0$

$$\begin{aligned} |\eta_{u,2} - \eta_{l,2}(0)| &= O(e^{-\frac{K}{\tilde{\varepsilon}}}), \\ |\hat{\eta}_{pu,2} - \eta_{r,2}(0)| &= O(e^{-\frac{K}{\tilde{\varepsilon}}}) \end{aligned}$$

and analogous estimates for the partial derivatives of $\eta_{u,2} - \eta_{l,2}(0)$ and $\hat{\eta}_{u,2} - \eta_{r,2}(0)$ with respect to r_2 and λ_2 according to Fenichel theory and proposition 4.15. We define

$$D_u(r_2, \lambda_2) = \eta_{u,2} - \hat{\eta}_{u,2}$$

and consider $D_u(r_2, \lambda_2) - D_c(r_2, \lambda_2)$, where D_c has been introduced in (4.23). The above estimates implies that $D_u(r_2, \lambda_2) - D_c(r_2, \lambda_2)$ and its partial derivatives are $O(e^{-\frac{K}{\tilde{\varepsilon}}})$ - small. Hence $D_u(r_2, \lambda_2)$ can be solved for λ_2 as a function of r_2, called $\lambda_{Ho}(r_2)$. Furthermore for this $\lambda_{Ho}(r_2)$ the above estimates hold, so that the separation of $M_{l,2}$ and $M_{r,2}$ is bounded by $O(e^{-\frac{K}{\tilde{\varepsilon}}})$, i.e $D_c(r_2, \lambda_{Ho}(r_2)) = O(e^{-\frac{K}{\tilde{\varepsilon}}})$. Hence, since $\frac{\partial}{\partial \lambda_2} D_c(0, 0) \neq 0$

$$|\lambda_{Ho}(\sqrt{\tilde{\varepsilon}}) - \lambda_c(\sqrt{\tilde{\varepsilon}})| < O(e^{-\frac{K}{\tilde{\varepsilon}}}).$$

The instability of the homoclinic orbit is a direct consequence of the time scales. The positive eigenvalue of the Jacobian at the homoclinic point is independent of $\tilde{\varepsilon}$, whereas the negative eigenvalue is multiplied with $\tilde{\varepsilon}$, see proof of lemma 4.19. This proves the statement. ∎

Now consider the intersection of the fast stable manifold of the homoclinic point with the positive η - axis for $\tilde{\varepsilon} \in (0, \varepsilon_0)$. Let $s^*(\tilde{\lambda})$ be this intersection. This function has an infimum and a supremum for $\tilde{\lambda} \in (-\lambda_0, \lambda_0)$ on the positive η - axis. We denote the infimum with s^*_- and the supremum with s^*_+. Define the section Δ_m by

$$\Delta_m \;:=\; \{(0, s, \tilde{\lambda}, \tilde{\varepsilon}) : s \in (\tilde{s}_0, s^*_- - \tilde{s}_0), \tilde{\varepsilon} \in (0, \varepsilon_0), \tilde{\lambda} \in (-\lambda_0, \lambda_0)\},$$

where $\tilde{s}_0 > 0$ is sufficiently small and fixed. We consider forward and backward trajectories emanating from points in Δ_m under the flow of (4.32). For $p \in \Delta_m$ let $\gamma_p(t)$ be the forward trajectory of p and $\hat{\gamma}_p(t)$ be the backward trajectory of p. Then $\gamma_p(t)$ is exponentially attracted by $S_{l,\tilde{\varepsilon}}$ and $\hat{\gamma}_p(t)$ is exponentially attracted by $S_{r,\tilde{\varepsilon}}$. Both trajectories enter V and give rise to trajectories in the blow-up system and therefore to associated trajectories $\gamma_{p,j}$ and $\hat{\gamma}_{p,j}$, $j = 1, 2$, in the charts K_1 and K_2. As in the proof of theorem 4.22 let $(0, \eta_{p,2})$ be the point, where $\gamma_{p,2}$ crosses the ξ_2 - axis and let $(0, \hat{\eta}_{p,2})$ be the point, where $\hat{\gamma}_{p,2}$ crosses the ξ_2 - axis.

Lemma 4.23
There exists $K > 0$ such that, for any $p \in \Delta_m$,

$$\begin{aligned} |\eta_{p,2} - \eta_{l,2}(0)| &= O(e^{-\frac{K}{\tilde{\varepsilon}}}), \\ |\hat{\eta}_{p,2} - \eta_{r,2}(0)| &= O(e^{-\frac{K}{\tilde{\varepsilon}}}), \end{aligned}$$

where $\tilde{\varepsilon} = r_2^2$. Analogous estimates hold for the partial derivatives of $\eta_{p,2} - \eta_{l,2}(0)$ and $\hat{\eta}_{p,2} - \eta_{r,2}(0)$ with respect to r_2 and λ_2.

Proof.
The trajectories $\gamma_{p,1}$ and $\hat{\gamma}_{p,1}$ pass through $\Sigma^{out}_{l,1}$ and $\Sigma^{in}_{r,1}$, respectively. The estimate follows from proposition 4.15. ∎

By the following proposition we construct "medium" periodic orbits.

Proposition 4.24
Consider $s \in (\tilde{s}_0, s^*_- - \tilde{s}_0)$ and $\tilde{\varepsilon} \in (0, \varepsilon_0)$. There exists a C^k smooth function $\lambda(s, \sqrt{\tilde{\varepsilon}})$ such that the orbit of (4.12) passing through $(0, s)$ is periodic if and only if $\tilde{\lambda} = \lambda(s, \sqrt{\tilde{\varepsilon}})$.

Proof.
Let $r_2 = \sqrt{\tilde{\varepsilon}}$ and $\tilde{\lambda} = r_2\lambda_2$. Define

$$D(s, r_2, \lambda_2) \;:=\; \eta_{p,2} - \hat{\eta}_{p,2}.$$

Lemma 4.23 implies that the expression $D(s, r_2, \lambda_2) - D_c(r_2, \lambda_2)$ and its partial derivatives with respect to r_2 and λ_2 are $O(e^{-\frac{K}{\tilde{\varepsilon}}})$ small, where D_c is again the function defined in (4.23). Hence the equation $D(s, r_2, \lambda_2) = 0$ can be solved for λ_2 as a function of s and r_2. The result follows. ∎

We note that Δ_s and Δ_m have overlapping domains. The families of periodic orbits constructed in proposition 4.21 and in proposition 4.24 can be combined to one family

$$(\lambda(s, \sqrt{\tilde{\varepsilon}}), \Gamma(s, \sqrt{\tilde{\varepsilon}})), \quad s \in (0, s_-^* - \tilde{s}_0),$$

with $\tilde{s}_0$ fixed, but arbitrary small, since both families satisfy an uniqueness property. For every $s \in (0, s_0)$, respectively $s \in (\tilde{s}_0, s_-^* - \tilde{s}_0)$, there exists an unique $\tilde{\lambda}$ and a corresponding periodic orbit, unique with respect to the property, that it passes through $(0, s)$. Now define

$$\Delta_l \;:=\; \{(0, s, \tilde{\lambda}, \tilde{\varepsilon}) : s \in (s_-^* - \hat{s}_0, s_+^* + \hat{s}_0), \tilde{\varepsilon} \in (0, \varepsilon_0), \tilde{\lambda} \in (-\lambda_0, \lambda_)\}.$$

The approach is the same as for Δ_m. However, the backward trajectory for $p \in \Delta_l$ may not reach V. For the forward trajectory emanating from a given point $p \in \Delta_l$ define $\gamma_p(t)$ as before. Clearly this defines a point $(0, \eta_{p,2})$ as before.

We change the definition of $\hat{\gamma}_p(t)$ for a given point $p = (0, s_p, \tilde{\lambda}_p, \tilde{\varepsilon}_p) \in \Delta_l$ slightly. For $s_p < s^*(\tilde{\lambda})$ let $\hat{\gamma}_p(t)$ be the backward trajectory of p just as before. For $s_p \geq s^*(\tilde{\lambda})$ let $\hat{\gamma}_p(t)$ be the backward trajectory emanating from a given point (ξ_{s_p}, η_{s_p}) on the slow stable manifold of the homoclinic point $(\xi_{h,\tilde{\lambda}}, \eta_{h,\tilde{\lambda}})$ with $d_\eta = \eta_{h,\tilde{\lambda}}) - \eta_{s_p} > 0$, d_η sufficiently small. Then the construction of $\hat{\gamma}_p(t)$ gives rise to a point $(0, \hat{\eta}_{p,2})$ the same way as before. $\hat{\eta}_{p,2}$ is a C^1 - function of its arguments, which is guaranteed by theorem (4.20).

Lemma 4.25
There exists a $K > 0$ such that, for any $p \in \Delta_l$,

$$\begin{aligned} |\eta_{p,2} - \eta_{l,2}(0)| &= O(e^{-\frac{K}{\tilde{\varepsilon}}}), \\ |\hat{\eta}_{p,2} - \eta_{r,2}(0)| &= O(e^{-\frac{K}{\tilde{\varepsilon}}}), \end{aligned}$$

where $\tilde{\varepsilon} = r_2^2$. Analogous estimates hold for the partial derivatives of $\eta_{p,2} - \eta_{l,2}(0)$ and $\hat{\eta}_{p,2} - \eta_{r,2}(0)$ with respect to r_2 and λ_2.

Proof.
Analogously to the proof of lemma 4.23.

In the next step, we construct "large" periodic orbits.

Proposition 4.26
Consider $\tilde{\varepsilon} \in (0, \varepsilon_0)$ and $s \in (s^*_- - \hat{s}_0, s^*(\lambda_{Ho}(\sqrt{\tilde{\varepsilon}})))$. There exists a C^k smooth function $\lambda(s, \sqrt{\tilde{\varepsilon}})$ such that the orbit of (4.12) passing through $(0, s)$ is periodic if and only if $\tilde{\lambda} = \lambda(s, \sqrt{\tilde{\varepsilon}})$. For $s \in (s^*(\lambda_{Ho}(\sqrt{\tilde{\varepsilon}})), s^*_+ + \hat{s}_0)$ there is no periodic orbit passing through $(0, s)$.

Proof.
As in the proof of proposition 4.24 define

$$D(s, r_2, \lambda_2) \;\; := \;\; \eta_{p,2} - \hat{\eta}_{p,2}.$$

With the same arguments we conclude, that $D(s, r_2, \lambda_2)$ can be solved for λ_2 as a function of s and r_2. The homoclinic orbit is unique, i.e. there is exactly one $\lambda_2 = \lambda_{Ho}(\sqrt{\tilde{\varepsilon}})$ for which there exists a homoclinic orbit with respect to the homoclinic point, and the right hand side of equation (4.32) is continuous in $\tilde{\lambda}$. Assume that there exists a $s \in (s^*_- - \hat{s}_0, s^*(\lambda_{Ho}(\sqrt{\tilde{\varepsilon}})))$ for which there exists no $\tilde{\lambda}$ such that the orbit passing through $(0, s)$ is periodic, then there would be a $\hat{s} \leq s$ and a corresponding $\tilde{\lambda}$, such that the orbit passing through $(0, \hat{s})$ is a homoclinic orbit. This is a contradiction to the uniqueness property of the homoclinic orbit. With the same reasoning one excludes the existence of periodic orbits passing through $(0, s)$ for $s \in (s^*(\lambda_{Ho}(\sqrt{\tilde{\varepsilon}})), s^*_+ + \hat{s}_0)$. This concludes the statement. ∎

Our observations can be combined to prove the existence of a family of periodic orbits.

Theorem 4.27 (Family Of Periodic Orbits)
Suppose ε_0 is sufficiently small. Then there exists a smooth family of periodic solutions

$$(\lambda(s, \sqrt{\tilde{\varepsilon}}), \Gamma(s, \sqrt{\tilde{\varepsilon}})), \quad \tilde{\varepsilon} \in (0, \varepsilon_0), s \in (0, s^*(\lambda_{Ho}(\sqrt{\tilde{\varepsilon}})).$$

Proof.
Note, that we have overlapping domains of Δ_m and Δ_l and the uniqueness property of the periodic solutions holds as before. This concludes the statement. ∎

We close this chapter with a remark on stability.

Remark 4.28 (Stability)

- Krupa and Szmolyan [36] have introduced the so-called "way in-way out" function $R(s)$, see also [6]. Since the homoclinic orbit is always unstable due to the different time scales, we obtain similar statements to theorem 3.4 and theorem 3.6 in [36].
- Under the assumptions of theorem 4.8 assume additionally $R(s) > 0$ for all $s \in (0, s^*(\lambda_{Ho}(\sqrt{\tilde{\varepsilon}}))$. Then all periodic orbits are unstable and the functions $\lambda(s, \sqrt{\tilde{\varepsilon}})$ are monotonic in s.

- Under the assumptions of theorem 4.7 assume that $R(s)$ has exactly one simple zero s_{lp} in $(0, s^*(\lambda_{Ho}(\sqrt{\tilde{\varepsilon}}))$. Then there exists a C^1 function $s_{lp}(\sqrt{\tilde{\varepsilon}})$ such that, for each $\tilde{\varepsilon} \in (0, \varepsilon_0)$, the curve $(s, \lambda(s, \sqrt{\tilde{\varepsilon}}))$ has a unique, non-degenerated limit point for $s = s_{lp}(\sqrt{\tilde{\varepsilon}}))$. The cycles $\Gamma(s, \sqrt{\tilde{\varepsilon}})$ are attracting for $s \in (0, s_{lp}(\sqrt{\tilde{\varepsilon}}))$ and repelling for $s \in (s_{lp}(\sqrt{\tilde{\varepsilon}}), s^*(\lambda_{Ho}(\sqrt{\tilde{\varepsilon}}))$.
- The bifurcation diagram for fixed $\tilde{\varepsilon}$ is as shown in figure 4.7.

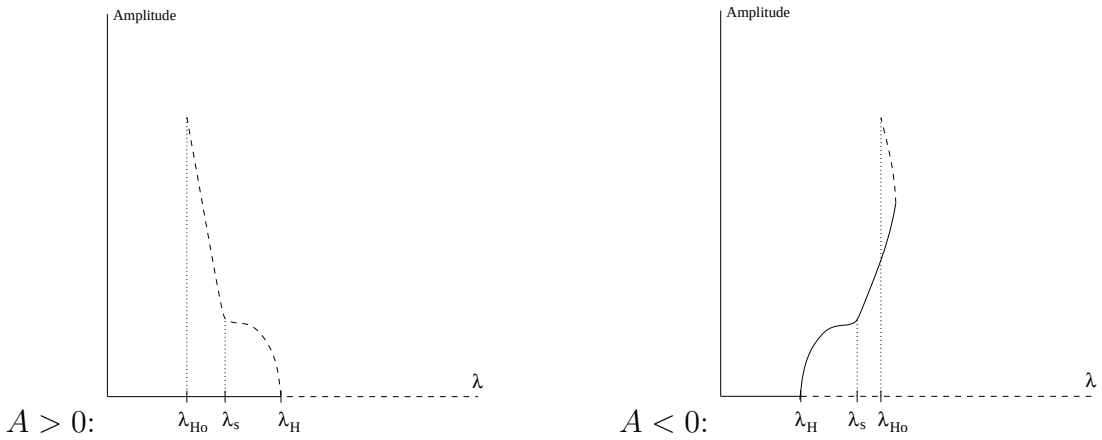

Figure 4.7: Bifurcation diagram for fixed $\tilde{\varepsilon}$ and $A > 0$ (left panel) resp. $A < 0$ (right panel).

5 Three-dimensional Approach

After analyzing properties of the flow of the two-dimensional system in the last chapter we return to the discussion of the three-dimensional one introduced in the third chapter. With the help of center manifold theory we reduce the discussion of the local flow in a neighborhood of the canard point to two dimensions, so that we are able to apply the results of the last chapter. The construction principles for "small" and "medium" periodic orbits as well as for the homoclinic orbit carry over; we only need to control one additional degree of freedom corresponding to the third dimension. The proof of "large" homoclinic orbits and the transition of the periodic orbits into the homoclinic one are only discussed under an additional mathematical hypothesis.

5.1 Local Flow Near The Canard Point

We start by recalling the three-dimensional system. The system we discuss in this chapter reads

$$\begin{aligned} \dot{x}_1 &= f_1(x_2) - c_1 x_1; \\ \dot{x}_2 &= f_2(x_1) - (c_2 + h(y))x_2; \\ \dot{y} &= \varepsilon[g(x_1) - (c_3 + \lambda)y]. \end{aligned} \tag{5.1}$$

Since we are interested in transferring the results of the last chapter, we reduce our three-dimensional system locally to the canard point using center manifold theory, see for instance [23]. As usual we extend the system by the two equations $\dot{\varepsilon} = 0$ and $\dot{\lambda} = 0$ to obtain the five-dimensional system

$$\begin{aligned} \dot{x}_1 &= f_1(x_2) - c_1 x_1; \\ \dot{x}_2 &= f_2(x_1) - (c_2 + h(y))x_2; \\ \dot{y} &= \varepsilon[g(x_1) - (c_3 + \lambda)y], \\ \dot{\varepsilon} &= 0, \\ \dot{\lambda} &= 0. \end{aligned} \tag{5.2}$$

Let $F(x, y) = f_2(\frac{1}{c_1} f_1(x)) - (c_2 + h(y))x$ be defined as before and let $G_\lambda(x_1, x_2, y) = g(x_1) - (c_3 + \lambda)y$.

Proposition 5.1
Consider system (5.2). Then there exists a four-dimensional C^r center manifold CM, $r < \infty$, corresponding to the canard point $(x_1, x_2, y, \varepsilon, \lambda) = (\frac{1}{c_1} f_1(x_c), x_c, y_c, 0, 0)$ such that the flow on CM is locally topologically equivalent to the system

$$\begin{aligned}
\dot{\xi} &= -\eta h_1(\xi, \eta, \tilde{\lambda}, \tilde{\varepsilon}) + \xi^2 h_2(\xi, \eta, \tilde{\lambda}, \tilde{\varepsilon}) + \tilde{\varepsilon} h_3(\xi, \eta, \tilde{\lambda}, \tilde{\varepsilon}), \\
\dot{\eta} &= \tilde{\varepsilon}(\xi h_4(\xi, \eta, \tilde{\lambda}, \tilde{\varepsilon}) - \tilde{\lambda} h_5(\xi, \eta, \tilde{\lambda}, \tilde{\varepsilon}) + \eta h_6(\xi, \eta, \tilde{\lambda}, \tilde{\varepsilon})), \\
\dot{\tilde{\varepsilon}} &= 0, \\
\dot{\tilde{\lambda}} &= 0,
\end{aligned} \tag{5.3}$$

where

$$\begin{aligned}
h_3(\xi, \eta, \tilde{\lambda}, \tilde{\varepsilon}) &= O(\xi, \eta, \tilde{\lambda}, \tilde{\varepsilon}), \\
h_{\tilde{k}}(\xi, \eta, \tilde{\lambda}, \tilde{\varepsilon}) &= 1 + O(\xi, \eta, \tilde{\lambda}, \tilde{\varepsilon}), \qquad \tilde{k} = 1, 2, 4, 5.
\end{aligned}$$

Proof.
We apply the method of center manifold reduction as described in [23]. As the computations are straight and standard but lengthy and tedious, they have been performed using Mathematica [53] and have been checked by hand. We only present the result. Since we expand our system in a neighborhood of the canard point, define $\tilde{x}_1 = x_1 - \frac{1}{c_1} f_1(x_c)$, $\tilde{x}_2 = x_2 - x_c$ and $\tilde{y} = y - y_c$. The Jacobian of (5.2) at the canard point has one negative eigenvalue and four zero eigenvalues, so that the desired center manifold is four-dimensional. The geometric multiplicity of the zero eigenvalues is three, so that we have to chose a basis of generalized eigenvectors, such that the linear part of the bifurcating system is in block diagonal form. For the variables on the center manifold we obtain

$$\begin{aligned}
v &= \frac{c_1 f_2'(\frac{1}{c_1} f_1(x_c))}{f_1'(x_c) f_2'(\frac{1}{c_1} f_1(x_c)) + c_1^2} \quad \tilde{x}_1 + \frac{c_1^2}{f_1'(x_c) f_2'(\frac{1}{c_1} f_1(x_c)) + c_1^2} \quad \tilde{x}_2 + \\
&\quad + \frac{c_1^2 x_c h'(y_c)}{(f_1'(x_c) f_2'(\frac{1}{c_1} f_1(x_c)) + c_1^2)^2} (f_1'(x_c) f_2'(\frac{1}{c_1} f_1(x_c)) + c_1^2 + c_1) \quad \tilde{y}, \\
w &= -\frac{c_1^2 x_c h'(y_c)}{f_1'(x_c) f_2'(\frac{1}{c_1} f_1(x_c)) + c_1^2} \quad \tilde{y}.
\end{aligned} \tag{5.4}$$

After applying the center manifold reduction the resulting system on the center manifold reads

$$\begin{aligned}
\dot{v} &= w\ (1 + O(v, w, \varepsilon, \lambda)) + \\
&\quad + v^2\ (\tfrac{1}{2} \tfrac{c_1^2}{f_1'(x_c) f_2'(\frac{1}{c_1} f_1(x_c)) + c_1^2} \tfrac{\partial^2}{\partial x^2} F(x_c, 0) + O(v, w, \varepsilon, \lambda)) + \\
&\quad + \varepsilon\ O(v, w, \varepsilon, \lambda), \\
\dot{w} &= \tfrac{c_1^2 h'(y_c) x_c}{f_1'(x_c) f_2'(\frac{1}{c_1} f_1(x_c)) + c_1^2}\ \varepsilon\ [\ - v\ (\tfrac{1}{c_1} f_1'(x_c) g'(\tfrac{1}{c_1} f_1(x_c)) + O(v, w, \varepsilon, \lambda)) + \\
&\quad + \lambda\ (y_c + O(v, w, \varepsilon, \lambda)) - \\
&\quad - w\ (\hat{h}_6(v, w, \varepsilon, \lambda))], \\
\dot{\varepsilon} &= 0, \qquad \dot{\lambda} = 0.
\end{aligned}$$

Now we apply a coordinate change according to

$$\begin{aligned} v &= \frac{2[f_1'(x_c)f_2'(\frac{1}{c_1}f_1(x_c))+c_1^2]}{c_1^2\frac{\partial^2}{\partial x^2}F(x_c,0)} \quad \xi, & w &= -\frac{2[f_1'(x_c)f_2'(\frac{1}{c_1}f_1(x_c))+c_1^2]}{c_1^2\frac{\partial^2}{\partial x^2}F(x_c,0)} \quad \eta, \\ \varepsilon &= \frac{f_1'(x_c)f_2'(\frac{1}{c_1}f_1(x_c))+c_1^2}{c_1h'(y_c)x_cf_1'(x_c)g'(\frac{1}{c_1}f_1(x_c))} \quad \tilde{\varepsilon}, & \lambda &= \frac{2[f_1'(x_c)f_2'(\frac{1}{c_1}f_1(x_c))+c_1^2][f_1'(x_c)g'(\frac{1}{c_1}f_1(x_c))]}{c_1^3\frac{\partial^2}{\partial x^2}F(x_c,0)y_c} \quad \tilde{\lambda}. \end{aligned} \tag{5.5}$$

The result follows. ∎

We drop the two equations $\dot{\tilde{\varepsilon}} = 0$ and $\dot{\tilde{\lambda}} = 0$ again and obtain the normal form of [36] for the local flow near the canard point. The last proposition guarantees that the flow local to the canard point on the center manifold is equivalent to the flow local to the canard point in the last chapter, respectively to the local flow in [36]. The existence of small periodic orbits is thus guaranteed like before by a Hopf bifurcation. As $\tilde{\lambda}$ varies these periodic orbits will grow, eventually leaving the neighborhood of the canard point and not lying entirely in the center manifold CM anymore.

For every fixed pair $(\hat{\varepsilon}, \hat{\lambda})$ denote the plane $\{(v, w, \varepsilon, \lambda) : \tilde{\varepsilon} = \hat{\varepsilon}, \tilde{\lambda} = \hat{\lambda}\} \cap CM$ by $CM_{\hat{\varepsilon},\hat{\lambda}}$. Every $CM_{\hat{\varepsilon},\hat{\lambda}}$ defines a two-dimensional invariant manifold, which can be written in (x_1, x_2, y) - coordinates and thus lying in the three-dimensional (x_1, x_2, y) - space.

5.2 Periodic Orbits I

Since we are interested in carrying over the findings of the last chapter we construct a two-dimensional manifold transversal to the flow of (5.1). Remember the layer problem (3.12) in chapter 3. We need the definition of monotone systems here.

Definition 5.2 (Type $\mathbb{R}^n_+$ monotone systems)
The solution operator Φ_t of an autonomous ordinary differential equation preserves the partial ordering $\leq$ and is type $\mathbb{R}^n_+$ monotone, if whenever $x \leq y$ then $\Phi_t(x) \leq \Phi_t(y)$ for all $t \geq 0$ (wherever defined).

After the definition we state a lemma from Smith [48].

Lemma 5.3
Consider $\dot{x} = f(x)$, where $f \in C^1(U)$, U open and convex in $\mathbb{R}^n$. Then Φ_t preserves the partial ordering $\leq$ for $t \geq 0$ if and only if $Df(x)$ has nonnegative off-diagonal elements for every $x \in U$.

As a direct consequence we state the following lemma.

Lemma 5.4
System (3.12) is type $\mathbb{R}^2_+$ monotone.

Proof.
Consider the Jacobian (3.6) and apply lemma 5.3. ∎

In order to parameterize the periodic orbits in a similar way like that in the two-dimensional setting we construct a two-dimensional manifold, which we use in a similar way like a Poincarè section. For every $y \in (h^{-1}(-c_2), \infty)$ there exists a positive invariant rectangle due to theorem 3.6 with vertices $(0,0)$ and $(\frac{\tilde{C}}{\tilde{c}_1}, \frac{\tilde{C}}{\tilde{c}_2})$. Furthermore

$$\frac{\partial}{\partial x_1}[f_1(x_2) - c_1 x_1] \frac{\partial}{\partial x_2}[f_2(x_1) - (c_2 + h(y))x_2] \;\; = \;\; (-c_1)(-c_2 - h(y)) > 0$$

and we conclude, that there exists no periodic orbit for the layer problem due to the negative Bendixson criterion. The theorem of Poincarè-Bendixson together with the monotonicity of solutions now guarantees the existence of a monotone heteroclinic orbit connecting the saddle point with the positive stable node for every $y \in (y_{tr}, y_c)$. For fixed $y \in (y_{tr}, y_c)$ this heteroclinic orbit can be parameterized by its length. Let L denote its complete length. The central point p_y of the heteroclinic orbit is defined as the point corresponding to $\frac{L}{2}$ and we consider the associated straight line orthogonal to that heteroclinic orbit at p_y. The conjunction of these lines for every $y \in (y_{tr}, y_c)$ defines a two-dimensional C^∞ manifold in the three-dimensional (x_1, x_2, y)-space. Denote the so constructed manifold by M_{ft}. The manifold M_{ft} is by construction orthogonal to $CM_{0,\hat{\lambda}}$ for every $|\hat{\lambda}| < \lambda_0$, λ_0 sufficiently small. Additionally define the one-dimensional smooth manifold $\tilde{P}$ consisting of the conjunction of points p_y, $y \in (y_{tr}, y_c)$. A sketch of this construction is shown in figure 5.1. On the left hand side we see the (x_1, x_2) space for fixed $y \in (y_{tr}, y_c)$, the point p_y and the straight line orthogonal to the heteroclinic orbit. The right hand side shows M_{ft} in the three-dimensional setting.

Lemma 5.5 (Transversality)
There exists a band B of uniform width larger zero on M_{ft} symmetric around $\tilde{P}$ such that the flow of (5.1) is transversal to M_{ft} at every point of B for every $\tilde{\varepsilon} \in (0, \varepsilon_0]$, ε_0 sufficiently small.

Proof.
We first construct a band $\tilde{B}$ such that the flow of the layer problem is transversal to M_{ft} at every point of $\tilde{B}$ for every $y \in (y_{tr}, y_c)$.

Fix $y \in (y_{tr}, y_c)$ and consider the point p_y. By construction the flow of the layer problem is orthogonal to M_{ft} at p_y. Let the associated straight line be written as $p_y + \imath_y \cdot v_y$, $\|v_y\| = 1$. Then there exists a $\imath_{y,max}$ such that the flow of the layer problem is transversal to M_{ft} at every point $p_y + \imath_y \cdot v_y$ for $|\imath_y| < \imath_{y,max}$. Let $\tilde{\imath} = \frac{1}{2}(\min_{y \in (y_{tr}, y_c)} \imath_{y,max})$. Define the conjunction of $p_y + \imath_y \cdot v_y$ for all $y \in (y_{tr}, y_c)$ and $|\imath_y| < \tilde{\imath}$ as $\tilde{B}$.

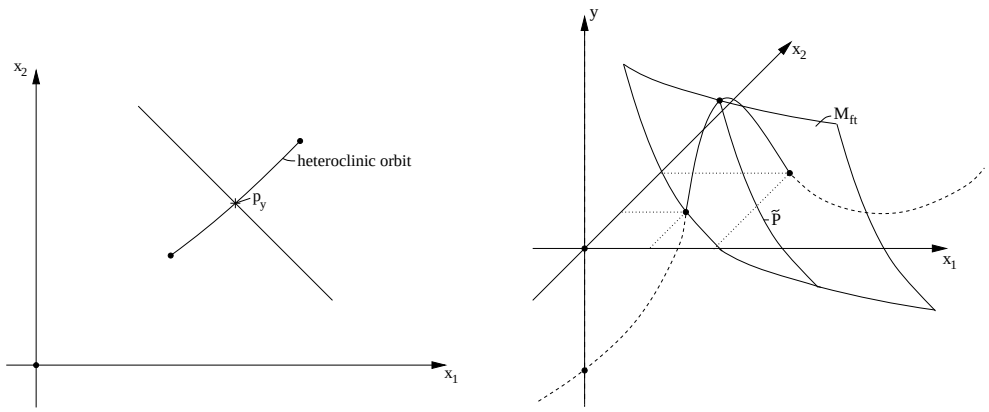

Figure 5.1: Left hand side: The heteroclinic orbit for fixed $y \in (y_{tr}, y_c)$, the point p_y and the orthogonal straight line. Right hand side: The manifold M_{ft}.

Since the vector field is changed only by $O(\varepsilon)$ for $\varepsilon > 0$ there exists a band B, which fulfills the statements of the lemma. ∎

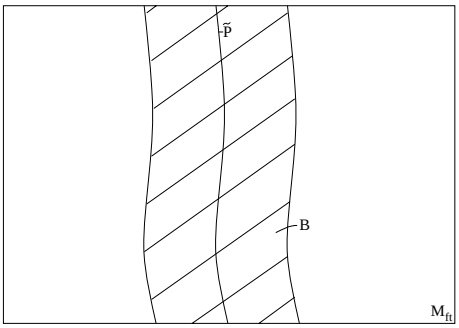

Figure 5.2: A sketch of B on M_{ft}.

A sketch of B is shown in figure 5.2. In the following the parameter A is meant to be the parameter defined according to [36] for system (5.3) on the center manifold, (see also (4.8)). As a consequence of the analysis of the flow local to the canard point we obtain the following statement.

Proposition 5.6 ("Small" Periodic Orbits)
Assume that $A \neq 0$ and that ρ and ε_0 are sufficiently small. Consider $s \in (y_c, y_c - \rho)$ and $\varepsilon \in (0, \varepsilon_0)$. There exists a C^k smooth function $\lambda(s, \sqrt{\varepsilon})$ and a point $(x_{1,o}, x_{2,o}, s) \in B$ such that the orbit passing through $(x_{1,o}, x_{2,o}, s)$ is periodic if and only if $\lambda = \lambda(s, \sqrt{\varepsilon})$.

Proof.
Consider the system on the center manifold (5.3). Proposition 4.3 in [36] (see also proposition 4.21 in chapter 4) guarantees, that there exists a C^k smooth function $\tilde{\lambda}(\tilde{s}, \sqrt{\tilde{\varepsilon}})$ and a $\tilde{\rho} > 0$ sufficiently small, such that there exists a periodic orbit passing

through $(0, \tilde{s})$ for $\tilde{s} \in (0, \tilde{\rho})$ on the center manifold if and only if $\tilde{\lambda} = \tilde{\lambda}(\tilde{s}, \sqrt{\tilde{\varepsilon}})$.

The interval $(0, \tilde{\rho})$ on the center manifold corresponds to the interval $(y_c, y_c - \rho)$ for a suitable $\rho > 0$, since we can express y by η. Equating the two equations for w in (5.4) and (5.5) we obtain

$$-\frac{c_1^2 x_c h'(y_c)}{f_1'(x_c) f_2'(\frac{1}{c_1} f_1(x_c)) + c_1^2} \quad (y - y_c) \quad = \quad -\frac{2[f_1'(x_c) f_2'(\frac{1}{c_1} f_1(x_c)) + c_1^2]}{c_1^2 \frac{\partial^2}{\partial x^2} F(x_c, 0)} \quad \eta,$$

and therefore

$$y \quad = \quad \frac{2[f_1'(x_c) f_2'(\frac{1}{c_1} f_1(x_c)) + c_1^2]^2}{c_1^4 x_c h'(y_c) \frac{\partial^2}{\partial x^2} F(x_c, 0)} \quad \eta + y_c.$$

Note that the coefficient in front of η is negative, since $\frac{\partial^2}{\partial x^2} F(x_c, 0)$ is negative as x_c is a maximum of $F(x, 0)$ considered as a function of x.

The interval $(0, \tilde{\varepsilon}_0]$ corresponds to the interval $(0, \varepsilon_0]$ for a suitable ε_0, since $\tilde{\varepsilon}$ relates to ε as given by equation (5.5).

Now fix $\varepsilon \in (0, \varepsilon_0]$ and thus also the associated $\tilde{\varepsilon} \in (0, \tilde{\varepsilon}_0]$. Then there exists an associated $CM_{\tilde{\varepsilon}, \tilde{\lambda}(\tilde{s}, \sqrt{\tilde{\varepsilon}})}$ which contains the periodic orbit and is transversal to M_{ft}. Therefore the periodic orbit will intersect M_{ft} at one point $(x_{1,o}, x_{2,o}, s) \in B$. This proves the statement. ∎

The last proposition guarantees the existence of "small" periodic orbits for s near y_c due to the center manifold reduction. Like in the two-dimensional case we continue with the proof of the existence of an homoclinic orbit with respect to the homoclinic point.

5.3 Homoclinic Orbit

The general idea for the construction of the homoclinic orbit is to follow the forward trajectory in the fast unstable manifold of the homoclinic point. Since this trajectory is exponentially attracted by the opposite branch of the slow manifold it will arrive in a neighborhood of the canard point. In accordance to the last chapter we denote the branch of $S_{3D}^{(2)}$ (for definition see chapter 3) between the canard point and the transcritical bifurcation point by $S_{r,0}$ an its perturbed equivalence by $S_{r,\varepsilon}$. Equivalently denote the stable branch of $S_{3D}^{(2)}$ on the other side of the canard point by $S_{l,0}$ an its perturbed equivalence by $S_{l,\varepsilon}$. In the two-dimensional case in the last chapter we followed the backward trajectory emanating from the homoclinic point. Here we substitute this backward trajectory by the stable manifold $W^s(S_{r,\varepsilon})$, whose existence is guaranteed by Fenichel's second theorem, see theorem 2.8. The idea is to use the information of the flow on the center manifold to patch the forward trajectory with the stable manifold $W^s(S_{r,\varepsilon})$.

Preliminary Constructions

We construct another manifold, which is used in a similar way like a Poincarè section, on which we can control the distance of $S_{l,\varepsilon}$ and $S_{r,\varepsilon}$. Let ε_0 and λ_0 be sufficiently small and fix $\varepsilon \in (0, \varepsilon_0]$ and $\lambda \in (-\lambda_0, \lambda_0)$. The associated $\tilde{\varepsilon}$ and $\tilde{\lambda}$ are thus also fixed with equation (5.5) and we consider $CM_{\tilde{\varepsilon},\tilde{\lambda}}$. Now define the two-dimensional manifold M_{ps} containing the η-axis of $CM_{\tilde{\varepsilon},\tilde{\lambda}}$ and orthogonal to $CM_{\tilde{\varepsilon},\tilde{\lambda}}$ defined for every y, where $CM_{\tilde{\varepsilon},\tilde{\lambda}}$ is defined. Both $S_{l,\varepsilon}$ and $S_{r,\varepsilon}$ enter $CM_{\tilde{\varepsilon},\tilde{\lambda}}$ and intersect $M_{ps} \cap CM_{\tilde{\varepsilon},\tilde{\lambda}}$, which we know from the two-dimensional case. Note, that there are some technical difficulties in following the forward trajectory as well as $W^s(S_{r,\varepsilon})$ near the canard point, since Fenichel theory is no longer valid. However, the center manifold reduction gives a description of the flow near $CM_{\tilde{\varepsilon},\tilde{\lambda}}$.

Theorem 5.7 (Homoclinic Orbit)
Suppose ε_0 is sufficiently small and fix $\varepsilon \in (0, \varepsilon_0]$. Then there exists a smooth function $\lambda_{Ho}(\sqrt{\varepsilon})$ such that equation (5.1) has an unique homoclinic orbit with respect to the homoclinic point.

Proof.
The center manifold reduction above (proposition 5.1) implies that system (5.1) is locally topologically equivalent to

$$\begin{aligned} \dot{u} &= -\frac{f_1'(x_c) f_2'(\frac{1}{c_1} f_1(x_c)) + c_1^2}{c_1}\, u, \\ \dot{\xi} &= -\eta h_1(\xi, \eta, \tilde{\lambda}, \tilde{\varepsilon}) + \xi^2 h_2(\xi, \eta, \tilde{\lambda}, \tilde{\varepsilon}) + \tilde{\varepsilon} h_3(\xi, \eta, \tilde{\lambda}, \tilde{\varepsilon}), \\ \dot{\eta} &= \tilde{\varepsilon}(\xi h_4(\xi, \eta, \tilde{\lambda}, \tilde{\varepsilon}) - \tilde{\lambda} h_5(\xi, \eta, \tilde{\lambda}, \tilde{\varepsilon}) + \eta h_6(\xi, \eta, \tilde{\lambda}, \tilde{\varepsilon})). \end{aligned} \tag{5.6}$$

As already mentioned, we follow the forward trajectory emanating from a point of the fast unstable manifold of the homoclinic point in dependence of λ. This trajectory is exponentially attracted by $S_{l,\varepsilon}$ and therefore arrives in a neighborhood of the canard point $O(e^{-\frac{K}{\varepsilon}})$ close to $CM_{\tilde{\varepsilon},\tilde{\lambda}}$, giving rise to a trajectory in (u, ξ, η)-coordinates. The projection along u onto $CM_{\tilde{\varepsilon},\tilde{\lambda}}$ defines a trajectory γ_π entering V, the blow-up region in $CM_{\tilde{\varepsilon},\tilde{\lambda}}$, close to $S_{l,\varepsilon}$. With the same arguments as in the two-dimensional case we retrieve trajectories $\gamma_{\pi,1}$ resp. $\gamma_{\pi,2}$ in the charts K_1 and K_2 and finally a point $(0, \eta_{\pi,2})$, where $\gamma_{\pi,2}$ crosses the η_2-axis. Let $(0, \eta_{p,2})$ be the intersection point of the trajectory in K_2 associated with $S_{l,\varepsilon}$ and the η_2-axis. Since $\gamma_{\pi,1}$ pass through $\Sigma_{l,1}^{out}$, there exists a $K > 0$ such that $|\eta_{p,2} - \eta_{\pi,2}| = O(e^{-\frac{K}{\varepsilon}})$ as well as $|\frac{\partial}{\partial \lambda_2}(\eta_{p,2} - \eta_{\pi,2})| = O(e^{-\frac{K}{\varepsilon}})$.

Now consider $S_{r,\varepsilon}$ and the associated stable manifold $W^s(S_{r,\varepsilon})$. As $S_{r,\varepsilon}$ reaches a neighborhood of $CM_{\tilde{\varepsilon},\tilde{\lambda}}$, so does $W^s(S_{r,\varepsilon})$ and we can express $W^s(S_{r,\varepsilon})$ in (u, ξ, η)-coordinates. For $\varepsilon = 0$ the stable manifold $W^s(S_{r,\varepsilon})$ intersects $CM_{\tilde{\varepsilon},\tilde{\lambda}}$ orthogonally. Now note, that Fenichel theory is valid until $S_{r,\varepsilon}$ reaches V at some point $(0, \hat{\xi}, \hat{\eta})$. On the plain $\{(u, \xi, \eta) : \xi = \hat{\xi}\}$ the stable manifold $W^s(S_{r,\varepsilon})$ is given as a graph

$O(\varepsilon)$ close to that of $W^s(S_{r,0})$. Now we take the projection of every point $\tilde{p}_{W^s}$ in $W^s(S_{r,\varepsilon}) \cap \{(u,\xi,\eta) : \xi = \hat{\xi}\}$ with $|\tilde{p}_{W^s} - (u,\xi,\eta)^T| = O(e^{-\frac{K}{\varepsilon}})$ along u onto $CM_{\tilde{\varepsilon},\tilde{\lambda}}$. This projection can be expressed by the points $(0,\hat{\xi},\tilde{\eta})$ with $\tilde{\eta} \in (\hat{\eta} - O(e^{-\frac{K}{\varepsilon}}), \hat{\eta} + O(e^{-\frac{K}{\varepsilon}}))$.

Consider the backward flow of every point $(0,\hat{\xi},\tilde{\eta})$. This gives rise to trajectories in K_1 and K_2 again with every trajectory in K_1 passing through $\Sigma_{l,1}^{in}$. Let $(0,\eta_{\hat{\pi},2})$ be the intersection point of such a trajectory in K_2 with the η_2-axis and let $(0,\eta_{\hat{p},2})$ be the intersection point of the trajectory in K_2 associated with the backward trajectory on $S_{r,\varepsilon}$. Then again we get $|\eta_{\hat{p},2} - \eta_{\hat{\pi},2}| = O(e^{-\frac{K}{\varepsilon}})$ as well as $|\frac{\partial}{\partial\lambda_2}(\eta_{\hat{p},2} - \eta_{\hat{\pi},2})| = O(e^{-\frac{K}{\varepsilon}})$.

The original forward trajectory passes $O(e^{-\frac{K}{\varepsilon}})$ close to $S_{l,\varepsilon}$, eventually intersecting M_{ps}. On the other hand we take the backward flow of $\tilde{p}_{W^s}$ in $W^s(S_{r,\varepsilon}) \cap \{(u,\xi,\eta) : \xi = \hat{\xi}\}$ with $|\tilde{p}_{W^s} - (u,\xi,\eta)^T| = O(e^{-\frac{K}{\varepsilon}})$, and its intersection with M_{ps}. Since this backward flow is repelled by the center manifold in u direction and remains close to $S_{r,\varepsilon}$ in η direction, the intersection of this backward flow with M_{ps} is a two-dimensional manifold, which can be represented by a graph in u and is defined for all u with $|u| = O(e^{-\frac{K}{\varepsilon}})$. We denote this intersection by p_{W^s}. Figure 5.3 shows a sketch of the construction.

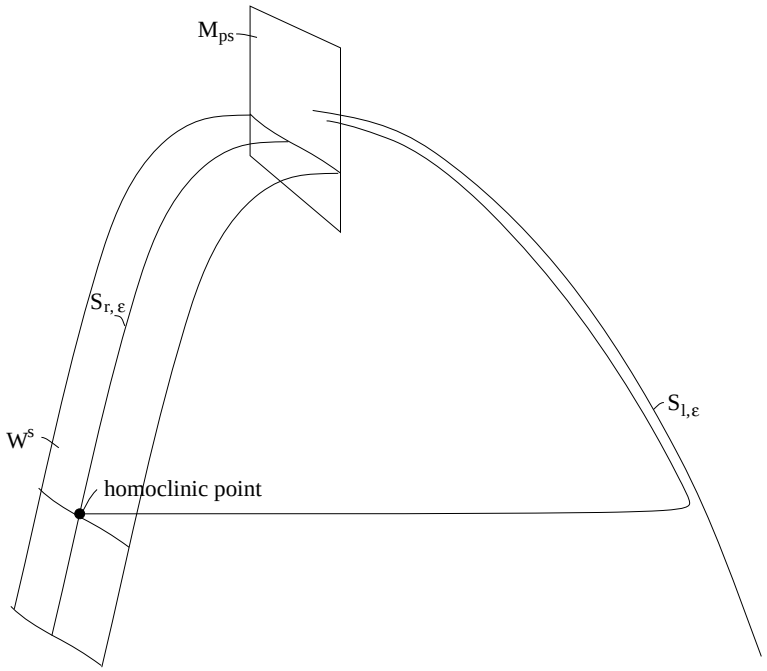

Figure 5.3: A three-dimensional sketch of the forward trajectory of the homoclinic point and of the stable manifold of $S_{r,\varepsilon}$.

Furthermore denote the intersection of $S_{l,\varepsilon}$ with M_{ps} by p_{S_l} and the intersection of $S_{r,\varepsilon}$ with M_{ps} by p_{S_r}. For a sketch of the situation on M_{ps} see figure 5.4. Denote the η component of p_{tr}, p_{S_l} and p_{S_r} by $p_{tr,\eta}$, $p_{S_l,\eta}$ and $p_{S_r,\eta}$. For all ε, λ fixed pick $p_{bt} \in p_{W^s}$ by the condition $p_{bt,u} = p_{tr,u}$, where $p_{bt,u}$, resp. $p_{tr,u}$, is the u component of p_{bt}, resp. p_{tr}.

Accordingly denote the η component of p_{bt} by $p_{bt,\eta}$. Then

$$\begin{aligned} |p_{tr} - p_{bt}| &= |p_{tr,\eta} - p_{bt,\eta}| \leq \\ &\leq |p_{tr,\eta} - p_{S_l,\eta}| + |p_{S_l,\eta} - p_{S_r,\eta}| + |p_{S_r,\eta} - p_{W^s,\eta}|. \end{aligned}$$

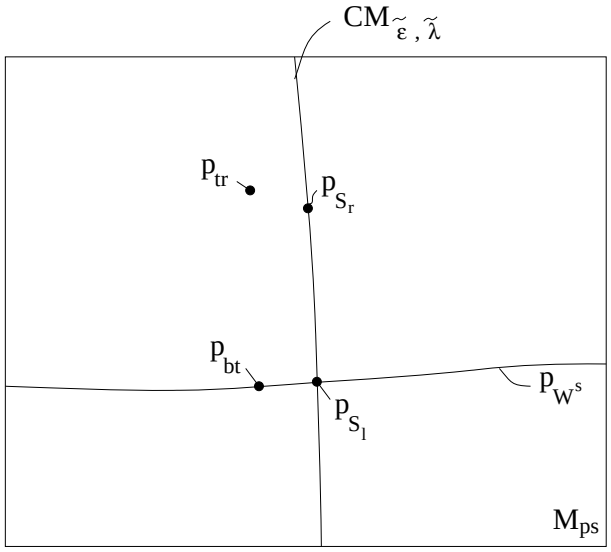

Figure 5.4: The manifold M_{ps} with the points p_{tr}, p_{bt}, p_{S_l} and p_{S_r}.

The right hand side can be completely translated into the blow-up space, since the η-axis corresponds to the η_2-axis in chart K_2. We obtain

$$|\eta_{p,2} - \eta_{\pi,2}| + |\eta_{p,2} - \eta_{\hat{p},2}| + |\eta_{\hat{p},2} - \eta_{\hat{\pi},2}| = |\eta_{p,2} - \eta_{\hat{p},2}| + O(e^{-\frac{K}{\varepsilon}})$$

and

$$|\tfrac{\partial}{\partial\lambda_2}(\eta_{p,2} - \eta_{\pi,2})| + |\tfrac{\partial}{\partial\lambda_2}(\eta_{p,2} - \eta_{\hat{p},2})| + |\tfrac{\partial}{\partial\lambda_2}(\eta_{\hat{p},2} - \eta_{\hat{\pi},2})| = |\tfrac{\partial}{\partial\lambda_2}(\eta_{p,2} - \eta_{\hat{p},2})| + O(e^{-\frac{K}{\varepsilon}})$$

as well as

$$|\tfrac{\partial}{\partial r_2}(\eta_{p,2} - \eta_{\pi,2})| + |\tfrac{\partial}{\partial r_2}(\eta_{p,2} - \eta_{\hat{p},2})| + |\tfrac{\partial}{\partial r_2}(\eta_{\hat{p},2} - \eta_{\hat{\pi},2})| = |\tfrac{\partial}{\partial r_2}(\eta_{p,2} - \eta_{\hat{p},2})| + O(e^{-\frac{K}{\varepsilon}}).$$

Thus $|\eta_{\pi,2} - \eta_{\hat{\pi},2}| = 0$ can be solved by the implicit function theorem for λ_2 as a function of r_2, called $\lambda_{Ho}(r_2)$. Furthermore we retrieve $|\lambda_{Ho}(\sqrt{\varepsilon}) - \lambda_c(\sqrt{\varepsilon})| < O(e^{-\frac{K}{\varepsilon}})$ as in the two-dimensional setting (see proof of theorem 4.22). Here $\lambda_c(\sqrt{\varepsilon})$ is the function defined as in the two-dimensional case for the system on the center manifold as a function of $\sqrt{\varepsilon}$. This proves the statement. ∎

5.4 Periodic Orbits II

We return to the construction of periodic orbits. Since we transfer the approach from the two-dimensional setting, we take points in B, whose forward and backward trajectories arrive in a neighborhood of the canard point. The line $\tilde{P}$ in B is the intersection of the unstable manifold $W^u(S_{r,0})$ of the critical manifold $S_{r,0}$ with M_{ft}. Therefore there exists a one-dimensional manifold $\tilde{P}_\varepsilon$ lying in B which is $O(\varepsilon)$ close to $\tilde{P}$ for every $\varepsilon \in (0, \varepsilon_0]$, which has the property that backward trajectories of points in $\tilde{P}_\varepsilon$ are lying on the unstable manifold $W^u(S_{r,\varepsilon})$ and thus are exponentially attracted by $S_{r,\varepsilon}$. The forward trajectory emanating from a point of the fast unstable manifold of the homoclinic point intersects $\tilde{P}_\varepsilon$ at some point. Let $s^*(\lambda)$ be the y component of this intersection point. As in the two-dimensional setting, this function has an infimum s^*_- and a supremum s^*_+ on $\tilde{P}_\varepsilon$ for $\lambda \in (-\lambda_0, \lambda_0)$. We note, that backward trajectories of points in B for a given y component lying in $(s^*_+ + \tilde{s}_0, y_c - \tilde{s}_0)$ do not reach a neighborhood of the canard point, if their distance to $\tilde{P}_\varepsilon$ is not sufficiently small. For given ε, λ let $B_{\varepsilon,\lambda}$ be a band in B symmetric with respect to $\tilde{P}_\varepsilon$ and $O(\varepsilon)$ close to $\tilde{P}_\varepsilon$. Define the section Δ_m by

$$\begin{aligned}\Delta_m \;:=\; &\{(x_1, x_2, s, \lambda, \varepsilon) : \varepsilon \in (0, \varepsilon_0], \lambda \in (-\lambda_0, \lambda_0),\\ &s \in (s^*_+ + \tilde{s}_0, y_c - \tilde{s}_0), (x_1, x_2, s) \in B_{\varepsilon,\lambda}\},\end{aligned}$$

where $\tilde{s}_0 > 0$ is sufficiently small and fixed. Again we consider forward and backward trajectories emanating from points in Δ_m. We construct periodic orbits of "medium" size.

Proposition 5.8 ("Medium" Periodic Orbits)
Consider $s \in (s^*_+ + \tilde{s}_0, y_c - \tilde{s}_0)$ and $\varepsilon \in (0, \varepsilon_0]$. There exists a C^k smooth function $\lambda(s, \sqrt{\varepsilon})$ and a unique point $(x_{1,o}, x_{2,o}, s) \in B_{\varepsilon,\lambda}$, unique with respect to its x_1 and x_2 component, such that the orbit of (5.1) passing through $(x_{1,o}, x_{2,o}, s)$ is periodic if and only if $\lambda = \lambda(s, \sqrt{\varepsilon})$.

Proof.
Fix $s \in (s^*_+ + \tilde{s}_0, y_c - \tilde{s}_0)$, $\varepsilon \in (0, \varepsilon_0]$ and $\lambda \in (-\lambda_0, \lambda_0)$, the corresponding $\tilde{\varepsilon}$ and $\tilde{\lambda}$ are also fixed. We consider the forward and backward trajectories emanating from points on the straight line $L_m = \{(x_1, x_2, s) : (x_1, x_2, s) \in B_{\varepsilon,\lambda}\}$.

The forward trajectories of each of those points are exponentially attracted by $S_{l,\varepsilon}$, thus reaching a neighborhood of the canard point $O(e^{-\frac{K}{\varepsilon}})$ close to $CM_{\tilde{\varepsilon},\tilde{\lambda}}$ and eventually intersect M_{ps}. Let the conjunction of the u components of those intersection points be the interval $(\hat{u_-}, \hat{u_+})$.

Not all of the backward trajectories of points in L_m reach a neighborhood of the canard point. However, close to $\tilde{P}_\varepsilon \cap L_m$ they do, since the backward trajectory of $\tilde{P}_\varepsilon \cap L_m$ lies in the unstable manifold of $S_{r,\varepsilon}$, thus is exponentially attracted by $S_{r,\varepsilon}$ and reaches the neighborhood of the canard point. Continuity arguments now

guarantee, that there is an interval in L_m, which is $O(e^{-\frac{K}{\varepsilon}})$ close around $\tilde{P}_\varepsilon \cap L_m$, such that the backward trajectory of each of the points in this interval reaches a neighborhood of the canard point. On the plain $\{(u, \xi, \eta) : \xi = \hat{\xi}\}$ defined in the proof of theorem 5.7 the conjunction of the intersection points of these backward trajectories with $\{(u, \xi, \eta) : \xi = \hat{\xi}\}$ can be written as a graph $O(\varepsilon)$ close to that of that of $W^s(S_{r,0})$, since every trajectory is exponentially attracted by $W^s(S_{r,\varepsilon})$. As for $W^s(S_{r,\varepsilon})$ in the proof of theorem 5.7 we continue this graph to M_{ps}. Figure 5.5 shows a sketch of the construction. This intersection can be written as a graph in u and is defined for all u with $|u| = O(e^{-\frac{K}{\varepsilon}})$. Denote this intersection by p_{L_m}. Now define the map, which maps the interval $|u| = O(e^{-\frac{K}{\varepsilon}})$ to itself according to the forward trajectory emanating from the points in p_{L_m} to the u component of the intersection of this trajectory with M_{ps} again. This map is C^∞ and a contraction. Therefore we get an unique fixed point u_{fix}. There is an unique trajectory emanating from the point in p_{L_m}, whose u component is u_{fix}, defining also an unique point $p_{u_{fix}}$ in L_m.

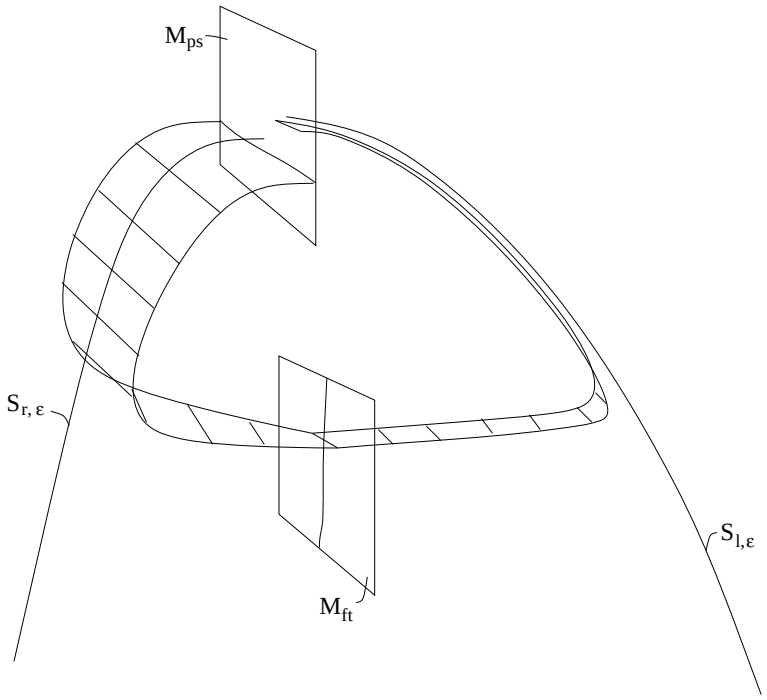

Figure 5.5: A three-dimensional sketch of the forward and backward trajectories of points in L_m.

Fix $\varepsilon \in (0, \varepsilon_0]$. For $\lambda \in (-\lambda_0, \lambda_0)$ we patch the forward and backward trajectories emanating from $p_{u_{fix}}$ in dependence of s and λ. The forward trajectory reaches a neighborhood of the canard point and can be expressed in (u, ξ, η) coordinates. The projection along u onto $CM_{\tilde{\varepsilon},\tilde{\lambda}}$ defines a trajectory γ_{p_u} entering V, the blow-up region in $CM_{\tilde{\varepsilon},\tilde{\lambda}}$, close to $S_{l,\varepsilon}$. This gives rise to trajectories in charts K_1 and K_2 and as always we obtain $(0, \eta_{p_u,2})$ as the intersection of the trajectory in K_2 with the negative η_2-axis. The backward trajectory also reaches a neighborhood of the canard point and

can be expressed in (u, ξ, η) coordinates. The projection along u onto $CM_{\tilde{\varepsilon},\tilde{\lambda}}$ defines a trajectory $\gamma_{\hat{p}_u}$ entering V, the blow-up region in $CM_{\tilde{\varepsilon},\tilde{\lambda}}$, close to $S_{r,\varepsilon}$. We obtain $(0, \eta_{\hat{p}_u,2})$ as the intersection of the associated trajectory in chart K_2 with the negative η_2-axis.

Let p_f be the intersection point of the forward trajectory emanating from $p_{u_{fix}}$ with M_{ps} and let $p_{\hat{f}}$ be the intersection point of the backward trajectory emanating from $p_{u_{fix}}$ with M_{ps}. As before p_{S_l} is the intersection point of $S_{l,\varepsilon}$ with M_{ps} and p_{S_r} is the intersection point of $S_{r,\varepsilon}$ with M_{ps}. A sketch of the situation on M_{ps} is shown in figure 5.6. Denote the η, component of p_f, $p_{\hat{f}}$, p_{S_l} and p_{S_r} by $p_{f,\eta}$, $p_{\hat{f},\eta}$, $p_{S_l,\eta}$ and $p_{S_r,\eta}$. We obtain

$$\begin{aligned} |p_f - p_{\hat{f}}| &= |p_{f,\eta} - p_{\hat{f},\eta}| \leq \\ &\leq |p_{f,\eta} - p_{S_l,\eta}| + |p_{S_l,\eta} - p_{S_r,\eta}| + |p_{S_r,\eta} - p_{\hat{f},\eta}|. \end{aligned}$$

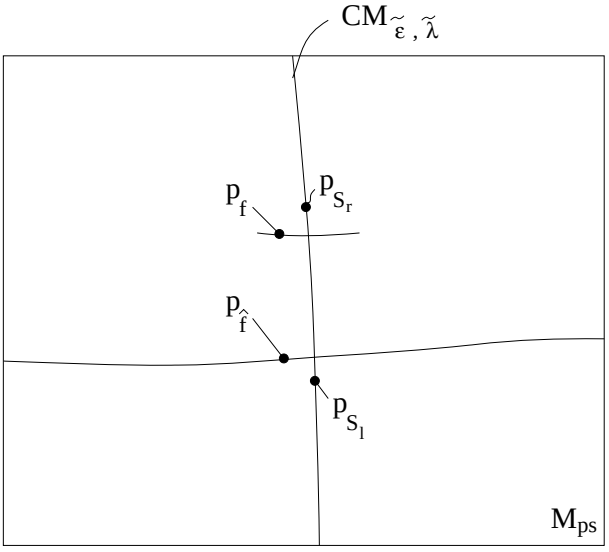

Figure 5.6: The manifold M_{ps} with the points p_f, $p_{\hat{f}}$, p_{S_l} and p_{S_r}.

The right hand side can be completely translated into the blow-up space, since the η-axis corresponds to the η_2-axis in chart K_2. We obtain

$$|\eta_{p,2} - \eta_{p_u,2}| + |\eta_{p,2} - \eta_{\hat{p},2}| + |\eta_{\hat{p},2} - \eta_{\hat{p}_u,2}| = |\eta_{p,2} - \eta_{\hat{p},2}| + O(e^{-\frac{K}{\varepsilon}}).$$

and

$$|\tfrac{\partial}{\partial\lambda_2}(\eta_{p,2} - \eta_{p_u,2})| + |\tfrac{\partial}{\partial\lambda_2}(\eta_{p,2} - \eta_{\hat{p},2})| + |\tfrac{\partial}{\partial\lambda_2}(\eta_{\hat{p},2} - \eta_{\hat{p}_u,2})| = |\tfrac{\partial}{\partial\lambda_2}(\eta_{p,2} - \eta_{\hat{p},2})| + O(e^{-\frac{K}{\varepsilon}})$$

as well as

$$|\tfrac{\partial}{\partial r_2}(\eta_{p,2} - \eta_{p_u,2})| + |\tfrac{\partial}{\partial r_2}(\eta_{p,2} - \eta_{\hat{p},2})| + |\tfrac{\partial}{\partial r_2}(\eta_{\hat{p},2} - \eta_{\hat{p}_u,2})| = |\tfrac{\partial}{\partial r_2}(\eta_{p,2} - \eta_{\hat{p},2})| + O(e^{-\frac{K}{\varepsilon}}).$$

Thus $|\eta_{p_u,2} - \eta_{\hat{p}_u,2}| = 0$ can be solved by the implicit function theorem for λ_2 as a function of s and r_2. The result follows. ∎

For the construction of "large" periodic orbits, we would have to adapt theorem 4.20 from the two-dimensional case into the three-dimensional setting, i.e. we investigate properties of trajectories entering a neighborhood of the homoclinic point. As in the two-dimensional case we consider a neighborhood of a normally hyperbolic subset of the slow manifold near the homoclinic point. There we write our system in Fenichel coordinates. The resulting equations are

$$\begin{aligned}\dot{\tilde{v}} &= \Lambda(\tilde{v},\tilde{w},\tilde{z},\varepsilon,\lambda)\tilde{v},\\ \dot{\tilde{w}} &= \Theta(\tilde{v},\tilde{w},\tilde{z},\varepsilon,\lambda)\tilde{w},\\ \dot{\tilde{z}} &= \varepsilon(\tilde{h}(\tilde{z},\varepsilon)\tilde{z}+\Xi(\tilde{v},\tilde{w},\tilde{z},\varepsilon,\lambda)(\tilde{v},\tilde{w})),\end{aligned}$$

where $\Lambda(\tilde{v},0,0,0,0) < 0$, $\Theta(0,\tilde{w},0,0,0) > 0$ and $\tilde{h}(0,0) < 0$. After a simple time transformation we obtain

$$\begin{aligned}\dot{v} &= \tilde{\Lambda}(v,w,z,\varepsilon,\lambda)v,\\ \dot{w} &= \tilde{\Theta}(v,w,z,\varepsilon,\lambda)w,\\ \dot{z} &= \varepsilon(-z+\tilde{\Xi}(v,w,z,\varepsilon,\lambda)(v,w)),\end{aligned}$$

Now define the section Δ by

$$\Delta = \{(v,w,z) : 0 \le v \le \varrho, 0 \le w \le \varrho, 0 \le z \le \varrho\}.$$

Theorem 5.9 (Trajectories Near The Homoclinic Point)
There exist $\varrho > 0$, $\varepsilon_0 > 0$ and $\lambda_0 > 0$ sufficiently small, such that for every $\varepsilon \in (0,\varepsilon_0]$ and $|\lambda| < \lambda_0$ the following statement holds. Every trajectory entering Δ parameterized such that $(v(0),w(0),z(0)) = (\delta_1,\delta_2,\varrho)$ leaves Δ after time $T \ge \frac{1}{\hat{\mu}}\ln(\frac{\varrho}{\delta_2})$. For $\delta_2 \to 0$ it holds that

$$|v(T)| \to 0, \quad |z(T)| \to 0.$$

Proof.
We start by estimating the time, for which the trajectory $(v(t),w(t),z(t))$ with initial condition $(v(0),w(0),z(0)) = (\delta_1,\delta_2,\varrho)$ stays in Δ. This time is given here by the evolution of $w(t)$. Note that in Δ we obtain the following estimates for $0 < \mu < \infty$, $0 < \hat{\mu} < \infty$.

$$|\tilde{\Lambda}(v,w,z,\varepsilon,\lambda)| \le -\mu, \quad |\tilde{\Theta}(v,w,z,\varepsilon,\lambda)| \le \hat{\mu}.$$

Therefore we have

$$|w(T)| = \varrho = |\delta_2 e^{\int_0^T \tilde{\Theta}(v,w,z,\varepsilon,\lambda)dt}| \le \delta_2 e^{\hat{\mu}T}$$

The estimation for T then reads

$$T \ge \tfrac{1}{\hat{\mu}}\ln(\tfrac{\varrho}{\delta_2}).$$

For $v(T)$ we get

$$|v(T)| = |\delta_1 e^{\int_0^T \tilde{\Lambda}(v,w,z,\varepsilon,\lambda)dt}| \leq \delta_1 (\tfrac{\delta_2}{\varrho})^{\frac{\mu}{\tilde{\mu}}}.$$

In Δ we have (see [27]) for some $q > 0$

$$|\tilde{\Xi}(v(t), w(t), z(t), \varepsilon, \lambda)(v(t), w(t))| \leq c|v(t)||w(t)| \leq q\varrho\delta_1 e^{-\mu t}.$$

And finally we obtain for $|z(T)|$ for some $\tilde{q} > 0$

$$|z(T)| = |\varrho e^{-\varepsilon T} + \int_0^T e^{-\varepsilon(T-t)}\varepsilon\tilde{\Xi}(v(t), w(t), z(t), \varepsilon, \lambda)(v(t), w(t))dt| \leq \varrho(e^{-\varepsilon T} + \tilde{q}e^{-\mu T}).$$

Therefore

$$|z(T)| \leq \varrho[(\tfrac{\delta_2}{\varrho})^{\frac{\varepsilon}{\tilde{\mu}}} + \tilde{q}(\tfrac{\delta_2}{\varrho})^{\frac{\mu}{\tilde{\mu}}}]$$

This proves the statement. ∎

The last theorem can be seen as the C^0 version of theorem 4.20 for the three-dimensional setting. A picture of the situation is shown in figure 5.7.

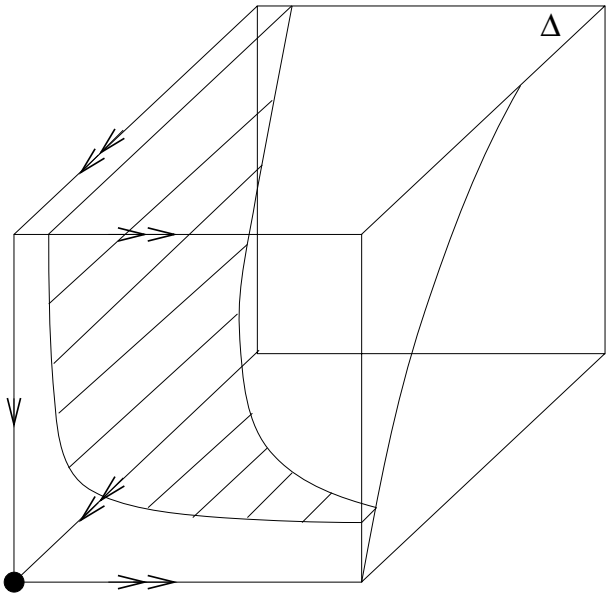

Figure 5.7: A sketch of the flow in Δ.

Parenthesis: On the C^1 version of theorem 5.9

Theorem 5.9 shows, that for $s \in (s^*(\lambda_{Ho}(\sqrt{\varepsilon})), s_+^* + \hat{s}_0)$ the intervals around P_ε in B for which the backward trajectories reach a neighborhood of the canard point become smaller and smaller as $s \to s^*(\lambda_{Ho}(\sqrt{\varepsilon}))$. The backward flow of such an interval passes through Δ, leaving Δ as a two-dimensional manifold near $W^s(S_{r,\varepsilon})$. A C^1 version of theorem 5.9 would allow to take $W^s(S_{r,\varepsilon})$ as the limiting exit manifold of backward trajectories as s passes through $s^*(\lambda_{Ho}(\sqrt{\varepsilon}))$. The proof of such a C^1 version would involve the same ingredients as the proof of the Exchange Lemma (see [27, 30]) and is omitted in the context of this work. For the reason of completeness in transferring the results of the two-dimensional setting, we formulate the hypothesis:

(H) A C^1 version of theorem 5.9 holds.

Under the assumption of (H) the proof of "large" periodic solutions limiting in the homoclinic orbit is possible.

End Parenthesis

Now follow the forward flow of every such trajectory passing through Δ in the way as described in proposition 5.9 and take its intersection with M_{ft} For $s \in (s^*(\lambda_{Ho}(\sqrt{\varepsilon})), s_+^* + \hat{s}_0)$ define $B_{\varepsilon,\lambda}$ as the conjunction of this intersection points. For $s \in (s_-^* - \hat{s}_0, s^*(\lambda_{Ho}(\sqrt{\varepsilon})))$ define $B_{\varepsilon,\lambda}$ as only the line P_ε. Then we obtain the following statement under the hypothesis (H).

Proposition 5.10 ("Large" Periodic Orbits)
Assume that (H) holds. Consider $\varepsilon \in (0, \varepsilon_0]$ and $s \in (s^*(\lambda_{Ho}(\sqrt{\varepsilon})), s_+^* + \hat{s}_0)$. There exists a C^k smooth function $\lambda(s, \sqrt{\varepsilon})$ and a unique point $(x_{1,o}, x_{2,o}, s) \in B_{\varepsilon,\lambda}$, unique with respect to its x_1 and x_2 component, such that the orbit of (5.1) passing through $(x_{1,o}, x_{2,o}, s)$ is periodic if and only if $\lambda = \lambda(s, \sqrt{\varepsilon})$. Furthermore

$$\lim_{s \to s^*(\lambda_{Ho}(\sqrt{\varepsilon}))} (x_{1,o}, x_{2,o}, s) = (x_{1,Ho}, x_{2,Ho}, s^*(\lambda_{Ho}(\sqrt{\varepsilon}))).$$

Proof.
Fix $s \in (s_-^* - \hat{s}_0, s_+^* + \hat{s}_0)$, $\varepsilon \in (0, \varepsilon_0]$ and $\lambda \in (-\lambda_0, \lambda_0)$. Again consider the forward flow of the straight line $L_m = \{(x_1, x_2, s) : (x_1, x_2, s) \in B_{\varepsilon,\lambda}\}$ (L_m reduces to a point for $s > s^*(\lambda_{Ho}(\sqrt{\varepsilon}))$). For $s \in (s^*(\lambda_{Ho}(\sqrt{\varepsilon})), s_+^* + \hat{s}_0)$ take the backward flow of $L_m = \{(x_1, x_2, s) : (x_1, x_2, s) \in B_{\varepsilon,\lambda}\}$ and for $s \in (s_-^* - \hat{s}_0, s^*(\lambda_{Ho}(\sqrt{\varepsilon})))$ substitute this backward flow by the backward flow on $W^s(S_{r,\varepsilon})$. Then the proof continues exactly like the proof of theorem 5.8. The result follows. ∎

We combine our observations in the following theorem.

Theorem 5.11 (Family Of Periodic Orbits)
Assume that (H) holds. Suppose ε_0 is sufficiently small. Then there exists a smooth family of periodic solutions

$$(\lambda(s,\sqrt{\varepsilon}),\Gamma(s,\sqrt{\varepsilon})), \quad \varepsilon \in (0,\varepsilon_0), s \in (s^*(\lambda_{Ho}(\sqrt{\varepsilon})), y_c).$$

Proof.
As in the two-dimensional case, we have overlapping domains for the small, medium and large periodic solutions as well as the analogously defined uniqueness property for every $s \in (s^*(\lambda_{Ho}(\sqrt{\varepsilon})), y_c)$. The result follows. ∎

6 Global Behavior Of Prototypical Examples

In this chapter we return to the canonical form (4.5) of the two-dimensional system. The aim is to sketch some aspects of the global behavior. First we investigate properties that lead to a Takens-Bogdanov bifurcation in some point (ε, λ) of the parameter space. We find that the appearance of the Takens - Bogdanov bifurcation is rather generic in the sense that the genericity conditions form manifolds with higher co-dimensions in the parameter space. Afterwards, we consider four different examples which correspond to the four cases defined by either $A > 0$ or $A < 0$ near the canard point and either stable or unstable closed orbits near the Takens - Bogdanov point. We show that the line of Hopf points, i.e. the curve in the parameter space at which the canard point has two purely imaginary eigenvalues, connects the origin, where the canard bifurcation takes place, with the Takens - Bogdanov bifurcation point. Numerical analysis reveals that also the homoclinic line starting at the Takens - Bogdanov bifurcation point connects to the origin. Thus, if the stability of the lines do not match, a global bifurcation is to expect. The detailed analysis of these systems is by far out of the scope of the present work. We give a detailed picture of the global behavior in every case using numerical simulations. All simulations within this chapter are performed with XPPAUT, [10].

6.1 Takens - Bogdanov Bifurcation

Recall the canonical form (4.5) introduced in chapter 3. For simplicity reasons we use here x, y as variables and ε, λ as parameters. We consider

$$\begin{aligned} \dot{x} &= -y(1+\tilde{h}_1(x,y)) + x^2(1+\tilde{h}_2(x)), \\ \dot{y} &= \varepsilon[x(1+\tilde{h}_3(x)) - \lambda - \kappa y], \end{aligned} \tag{6.1}$$

where $\tilde{h}_1(x,y) = O(x,y)$, $\tilde{h}_2(x) = O(x)$ and $\tilde{h}_3 = O(x)$ in accordance to the functions h_i, $i = 1, ..., 5$ given by (4.7). Now assume that there exists a λ_{TB} such that for every $\varepsilon > 0$ the isoclines are tangent to each other at the point (x_{TB}, y_{TB}). Then the determinant of the Jacobian

$$J = \begin{pmatrix} 2x(1+\tilde{h}_2(x)) + x^2\tilde{h}_2'(x) - y\partial_1\tilde{h}_1(x,y) & -(1+\tilde{h}_1(x,y)) - y\partial_2\tilde{h}_1(x,y) \\ \varepsilon(1+\tilde{h}_3(x) + x\tilde{h}_3'(x)) & -\kappa\varepsilon \end{pmatrix}$$

vanishes at (x_{TB}, y_{TB}). Furthermore assume, that $2x_{TB}(1+\tilde{h}_2(x_{TB})) + x_{TB}^2\tilde{h}_2'(x_{TB}) - y_{TB}\partial_1\tilde{h}_1(x_{TB}, y_{TB}) > 0$ and $\kappa > 0$. Then there exists a $\varepsilon_{TB} = \frac{1}{\kappa}[2x_{TB}(1+\tilde{h}_2(x_{TB})) + x_{TB}^2\tilde{h}_2'(x_{TB}) - y_{TB}\partial_1\tilde{h}_1(x_{TB}, y_{TB})] > 0$ such that the trace of the Jacobian vanishes at $(x_{TB}, y_{TB}, \varepsilon_{TB}, \lambda_{TB})$ as well. Define $W(x) = 1 + \tilde{h}_3(x) + x\tilde{h}_3'(x)$ and $W = W(x_{TB})$ and note that $W \neq 0$. With these definitions the Jacobian at $(x_{TB}, y_{TB}, \varepsilon_{TB}, \lambda_{TB})$ reads

$$J_{TB} = \begin{pmatrix} \kappa\varepsilon_{TB} & -\frac{\kappa^2}{W}\varepsilon_{TB} \\ W\varepsilon_{TB} & -\kappa\varepsilon_{TB} \end{pmatrix}.$$

We transform our system such that the point $(x_{TB}, y_{TB}, \varepsilon_{TB}, \lambda_{TB})$ is shifted to the origin. Then the system reads

$$\begin{aligned} \dot{\tilde{x}} &= -(\tilde{y}+y_{TB})(1+\tilde{h}_1(\tilde{x}+x_{TB}, \tilde{y}+y_{TB})) + (\tilde{x}+x_{TB})^2(1+\tilde{h}_2(\tilde{x}+x_{TB})), \\ \dot{\tilde{y}} &= (\tilde{\varepsilon}+\varepsilon_{TB})[(\tilde{x}+x_{TB})(1+\tilde{h}_3(\tilde{x}+x_{TB})) - (\tilde{\lambda}+\lambda_{TB}) - \kappa(y+y_{TB})]. \end{aligned} \tag{6.2}$$

We follow here Kuznetsov theorem 8.4 [37] and give requirements for (BT.0) - (BT.3) defined there. Under the assumption that there exists such a λ_{TB} as described above we have already that

$$2x_{TB}(1+\tilde{h}_2(x_{TB})) + x_{TB}^2\tilde{h}_2'(x_{TB}) - y_{TB}\partial_1\tilde{h}_1(x_{TB}, y_{TB}) > 0 \text{ and } \kappa > 0 \;\Rightarrow\; (BT.0). \tag{6.3}$$

The generalized eigenvectors of the Jacobian at the critical point are given by

$$\begin{pmatrix} \kappa \\ W \end{pmatrix}, \quad \begin{pmatrix} \frac{1}{2\varepsilon_{TB}} \\ -\frac{W}{2\kappa\varepsilon_{TB}} \end{pmatrix}.$$

We define M as the matrix with the eigenvectors as columns and we obtain

$$M = \begin{pmatrix} \kappa & \frac{1}{2\varepsilon_{TB}} \\ W & -\frac{W}{2\kappa\varepsilon_{TB}} \end{pmatrix}, \quad M^{-1} = \begin{pmatrix} \frac{1}{2\kappa} & \frac{1}{2W} \\ \varepsilon_{TB} & -\frac{\kappa}{W}\varepsilon_{TB} \end{pmatrix}.$$

Transforming our system according to the transformation $(u, v)^T = M(\tilde{x}, \tilde{y})^T$ results in a system of the form (8.37) in [37]. We are only interested in the non-degeneracy conditions. After a tedious computation using the transformation above we obtain with the notation of [37]

$$\begin{aligned} a_{20}(0) + b_{11}(0) &= \kappa(2 + 2\tilde{h}_2(x_{TB}) + 4x_{TB}\tilde{h}_2'(x_{TB}) + x_{TB}^2\tilde{h}_2''(x_{TB}) - y_{TB}\partial_1^2\tilde{h}_1(x_{TB}, y_{TB})) \\ &\quad -W(\partial_1\tilde{h}_1(x_{TB}, y_{TB}) + y_{TB}\partial_1\partial_2\tilde{h}_1(x_{TB}, y_{TB})) \end{aligned} \tag{6.4}$$

and

$$\begin{aligned} b_{20}(0) &= \varepsilon_{TB}[\kappa^2(2 + 2\tilde{h}_2(x_{TB}) + 4x_{TB}\tilde{h}_2'(x_{TB}) + x_{TB}^2\tilde{h}_2''(x_{TB}) - y_{TB}\partial_1^2\tilde{h}_1(x_{TB}, y_{TB})) \\ &\quad -W^2(2\partial_1\tilde{h}_1(x_{TB}, y_{TB}) + y_{TB}\partial_2^2\tilde{h}_1(x_{TB}, y_{TB})) \\ &\quad -\kappa W(2\partial_1\tilde{h}_1(x_{TB}, y_{TB}) + 2y_{TB}\partial_1\partial_2\tilde{h}_1(x_{TB}, y_{TB})) \\ &\quad -\tfrac{\kappa^3}{W}\varepsilon_{TB}\tilde{h}_3'(x_{TB})]. \end{aligned} \tag{6.5}$$

Another tedious computation yields for the non-degeneracy condition (BT.3), that it is equivalent to

$$\begin{aligned}\tfrac{\kappa^2}{W^2}\varepsilon_{TB} \quad & [W^2(1+\tilde{h}_3(x_{TB}))(2\partial_1\tilde{h}_1(x_{TB},y_{TB})+y_{TB}\partial_2^2\tilde{h}_1(x_{TB},y_{TB}))\\ & +\kappa W^2(2\partial_1\tilde{h}_1(x_{TB},y_{TB})+2y_{TB}\partial_1\partial_2\tilde{h}_1(x_{TB},y_{TB})))\\ & -\kappa^2(W+x_{TB}\tilde{h}_3'(x_{TB}))\\ & (2+2\tilde{h}_2(x_{TB})+4x_{TB}\tilde{h}_2'(x_{TB})+x_{TB}^2\tilde{h}_2''(x_{TB})-y_{TB}\partial_1^2\tilde{h}_1(x_{TB},y_{TB}))\\ & -2\kappa^3\varepsilon_{TB}\tilde{h}_3'(x_{TB})]\neq 0.\end{aligned} \tag{6.6}$$

We recapitulate our findings in the following proposition.

Lemma 6.1
Consider system (6.1) and assume that there exists a λ_{TB} such that for every $\varepsilon > 0$ the isoclines are tangent to each other at the point (x_{TB}, y_{TB}). Additionally assume that $2x_{TB}(1+\tilde{h}_2(x_{TB}))+x_{TB}^2\tilde{h}_2'(x_{TB})-y_{TB}\partial_1\tilde{h}_1(x_{TB},y_{TB})>0$ and $\kappa>0$. Then there exists an $\varepsilon_{TB}=\frac{1}{\kappa}[2x_{TB}(1+\tilde{h}_2(x_{TB}))+x_{TB}^2\tilde{h}_2'(x_{TB})-y_{TB}\partial_1\tilde{h}_1(x_{TB},y_{TB})]>0$ such that the point $(x_{TB},y_{TB},\varepsilon_{TB},\lambda_{TB})$ exhibits a Takens - Bogdanov bifurcation if and only if the terms in (6.4), (6.5) and (6.6) are non-zero.

In our following examples we always chose $\tilde{h}_1(x,y)=0$ and $\kappa>0$. Therefore our conditions for the Takens - Bogdanov bifurcation reduce to

$$\begin{aligned}& 2x_{TB}(1+\tilde{h}_2(x_{TB}))+x_{TB}^2\tilde{h}_2'(x_{TB})>0\\ & a_{20}(0)+b_{11}(0)=\kappa[2+2\tilde{h}_2(x_{TB})+4x_{TB}\tilde{h}_2'(x_{TB})+x_{TB}^2\tilde{h}_2''(x_{TB})]\neq 0\\ & b_{20}(0)=\varepsilon_{TB}[\kappa^2(2+2\tilde{h}_2(x_{TB})+4x_{TB}\tilde{h}_2'(x_{TB})+x_{TB}^2\tilde{h}_2''(x_{TB}))\\ & \quad -\tfrac{\kappa^3}{W}\varepsilon_{TB}\tilde{h}_3'(x_{TB})]\neq 0\\ & \tfrac{\kappa^2}{W^2}\varepsilon_{TB}[-\kappa^2(W+x_{TB}\tilde{h}_3'(x_{TB}))(2+2\tilde{h}_2(x_{TB})+4x_{TB}\tilde{h}_2'(x_{TB})+x_{TB}^2\tilde{h}_2''(x_{TB}))\\ & \quad -2\kappa^3\varepsilon_{TB}\tilde{h}_3'(x_{TB})]\neq 0\end{aligned} \tag{6.7}$$

The stability of the periodic orbits near the Takens - Bogdanov bifurcation is determined by the sign of the product of $a_{20}(0)+b_{11}(0)$ and $b_{20}(0)$. We have unstable periodic orbits if $b_{20}(0)(a_{20}(0)+b_{11}(0))>0$ and stable periodic orbits if $b_{20}(0)(a_{20}(0)+b_{11}(0))<0$. The parameter A, which indicates the local stability of periodic orbits near the canard point is given by

$$A \;=\; 3\tilde{h}_2'(0)-2\tilde{h}_3'(0)+2\kappa. \tag{6.8}$$

6.2 Unstable TB Orbits, A > 0

In this first section we consider the following system.

$$\begin{aligned} \dot{x} &= x^2 - y; \\ \dot{y} &= \varepsilon[x - \lambda - 2y], \end{aligned} \tag{6.9}$$

which means that $\tilde{h}_2(x) = 0$, $\tilde{h}_3(x) = 0$ and $\kappa = 2$. Thus $A = 4 > 0$ and the periodic orbits near the canard point are unstable as well as the homoclinic orbit. The stationary states of this system are the canard point $(\frac{1}{4}(1 - \sqrt{1 - 8\lambda}), \frac{1}{8}(1 - \sqrt{1 - 8\lambda}) - \frac{1}{2}\lambda)$ and the homoclinic point reads $(\frac{1}{4}(1 + \sqrt{1 - 8\lambda}), \frac{1}{8}(1 + \sqrt{1 - 8\lambda}) - \frac{1}{2}\lambda)$. For $\lambda = \frac{1}{8}$ the two isoclines are tangent to each other at the point $(x, y) = (\frac{1}{4}, \frac{1}{16})$ and we have a Takens - Bogdanov bifurcation at $\varepsilon = \frac{1}{4}$. Indeed, $a_{20}(0) + b_{11}(0) = 4$, $b_{20}(0) = 2$ and (BT.3) reduces to $-8 \neq 0$. Since $a_{20}(0) + b_{11}(0)$ and $b_{20}(0)$ are both positive, we have unstable periodic orbits and unstable homoclinic orbits near the Takens - Bogdanov bifurcation point.

Lemma 6.2 (Line Of Hopf Points)
For every $\varepsilon \in (0, \frac{1}{4})$ there exists a $\lambda = \lambda(\varepsilon) \in (0, \frac{1}{8})$ so that the Jacobian of the right hand side of (6.9) at the canard point has a pair of purely imaginary eigenvalues.

Proof.
The Jacobian at the canard point reads

$$J_c = \begin{pmatrix} \frac{1}{2}(1 - \sqrt{1 - 8\lambda}) & -1 \\ \varepsilon & -2\varepsilon \end{pmatrix}.$$

The requirements for a pair of purely imaginary eigenvalues are that the trace vanishes and that the determinant is positive. The trace vanishes for $\lambda = \lambda(\varepsilon) = \frac{1}{8} - \frac{1}{8}(1 - 4\varepsilon)^2$. The determinant reads $\varepsilon(\sqrt{1 - 8\lambda})$, which is positive for all $\lambda \in (0, \frac{1}{8})$. ∎

We note that $\lambda(\varepsilon)$ is strictly increasing for $\varepsilon \in (0, \frac{1}{4})$ and connects the canard point with the Takens - Bogdanov point in the parameter space. Further note that the line of Hopf points corresponds to $\lambda_H(\sqrt{\varepsilon})$ local to the origin in the parameter space. Indeed, theorem 4.5 tells that $\lambda_H(\sqrt{\varepsilon}) = \varepsilon + O(\varepsilon^{\frac{3}{2}})$, which corresponds to $\lambda(\varepsilon) = \varepsilon - 2\varepsilon^2$.

We conjecture that the homoclinic line emanating from the canard point $(\varepsilon, \lambda) = (0, 0)$ in the parameter space connects as well to the Takens - Bogdanov point $(\varepsilon, \lambda) = (\frac{1}{4}, \frac{1}{8})$ as shown in figure 6.1, where the homoclinic line is determined by numerical simulations.

Note that this sketch of the parameter space, as well as all following ones, is the result of numerical simulations. In this example, every periodic orbit is unstable and limits in an unstable homoclinic orbit. We have four different regions in the parameter space.

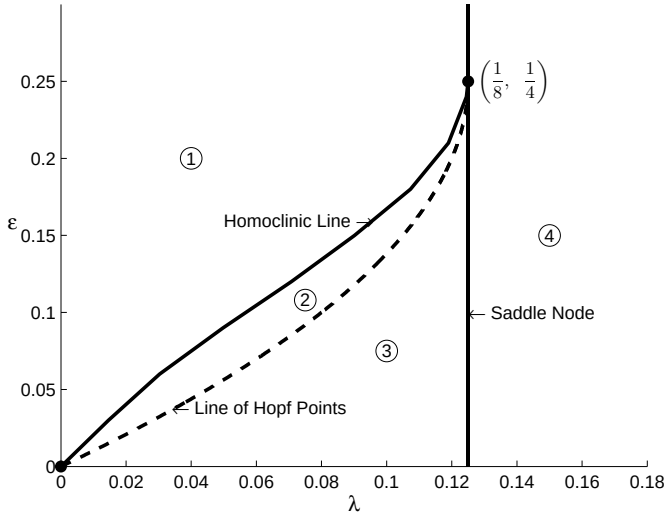

Figure 6.1: The parameter space for system (6.9)

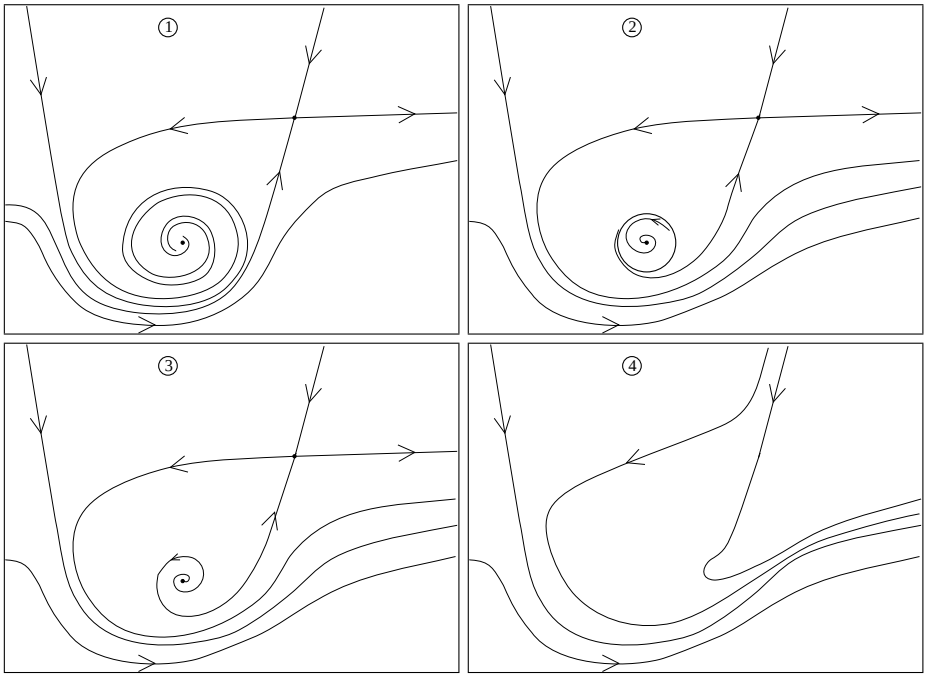

Figure 6.2: The flow for system (6.9) for regions 1 (top left) to 4 (bottom right)

The pictures in figure 6.2 show the behavior in each of these regions.

These sketches display the flow for $\varepsilon = 0.1$ and different values of λ. In the picture for region 1 (top left) we see, that the canard point is stable. The picture for region 2 (top right) shows an unstable periodic orbit, while in the picture for region 3

(bottom left) the canard point has lost its stability through the Hopf bifurcation. In the last picture for region 4 there is no equilibrium anymore. A sketch for the flow on the homoclinic line is given in figure 6.3.

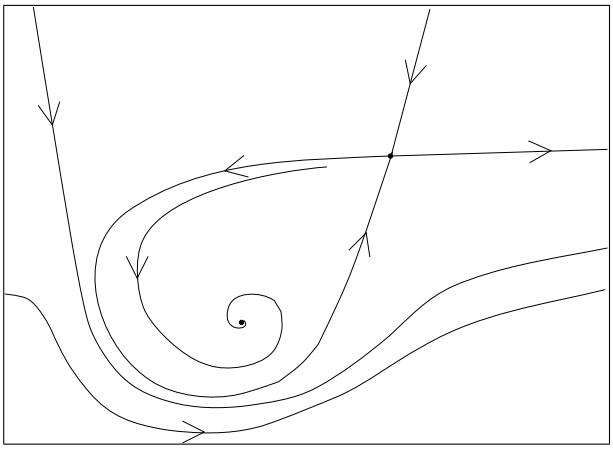

Figure 6.3: The flow for system (6.9) on the homoclinic line

This example is the easiest case that arises in systems like (6.1). Since every closed orbit, i.e. every periodic and homoclinic orbit, is unstable, there is no further bifurcation to see. This will change, when we change the sign of A.

6.3 Unstable TB Orbits, A $<$ 0

Our second example reads

$$\begin{aligned} \dot{x} &= x^2 - y; \\ \dot{y} &= \varepsilon[x(1 + \tfrac{6}{5}x - \tfrac{7}{2}x^2 - \tfrac{16}{5}x^3 - x^4) - \lambda - y]. \end{aligned} \tag{6.10}$$

In this case it is $\tilde{h}_2(x) = 0$, $\tilde{h}_3(x) = \frac{6}{5}x - \frac{7}{2}x^2 - \frac{16}{5}x^3 - x^4$ and $\kappa = 1$. The parameter A is now negative, since $A = 2(\kappa - \tilde{h}_3'(0)) = -\frac{2}{5} < 0$, which means that the periodic orbits emanating from the canard point are stable for small ε. Numerically we obtain a Takens - Bogdanov bifurcation at the point $(x, y, \varepsilon, \lambda) \approx (0.26, 0.06, 0.52, 0.18)$. The conditions (BT.0) - (BT.3) approximately read in that order 0.52, 2, 2.83 and 3.35, which implies that $(a_{20}(0) + b_{11}(0))b_{20}(0) > 0$. The periodic orbits as well as the homoclinic ones near the Takens - Bogdanov bifurcation remain unstable as in our first example. Again we conjecture that the line of Hopf points and the homoclinic line both emanating at the origin in the parameter space connect to the point in the parameter space, where the Takens Bogdanov bifurcation takes place. Numerical simulations lead to the following figure for the parameter space, see figure 6.4 (top left). We see that the picture has not changed much. We have the same four regions and the flow in these regions looks the

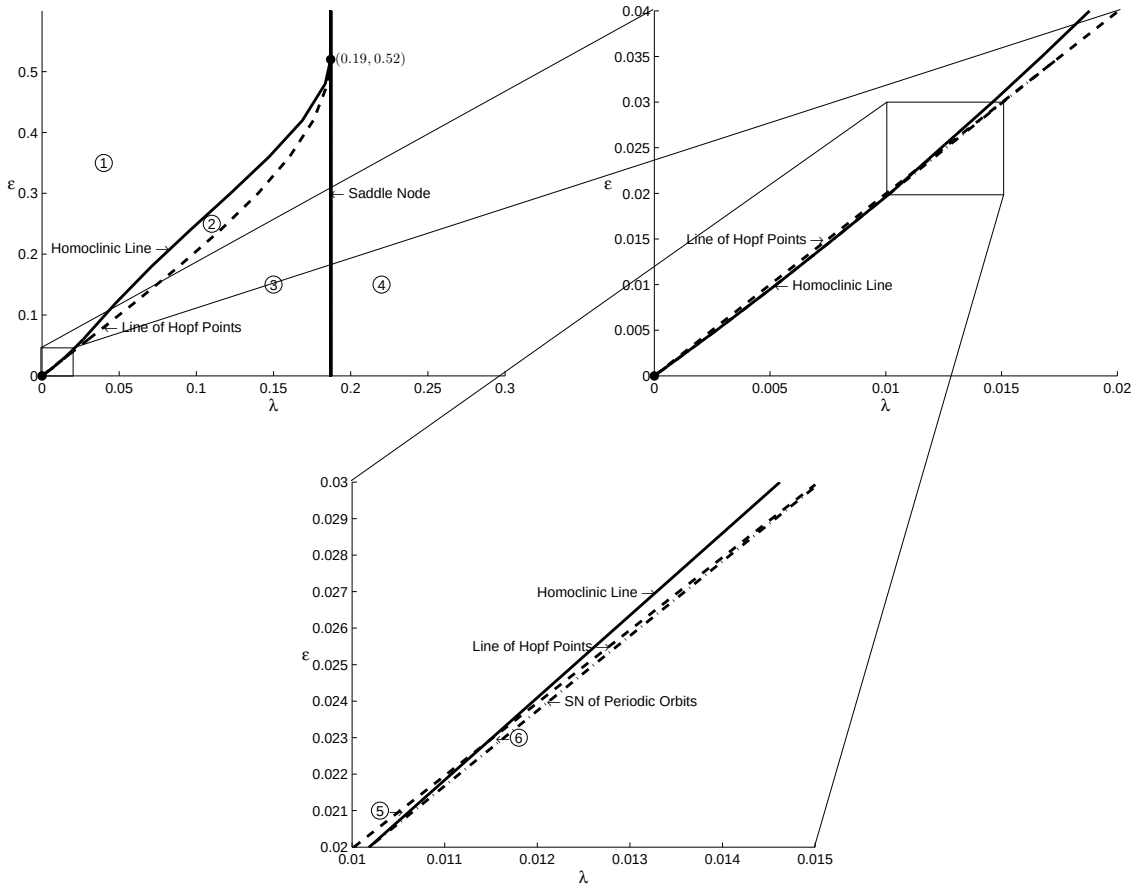

Figure 6.4: The parameter space for system (6.10)

same as in our first example, see figure 6.5. However, the local analysis of the canard point tells us that the relative position of the homoclinic line and the line of Hopf points has changed near the origin in the parameter space in comparison to our previous example. If we zoom near the origin, we get the following picture, figure 6.4 (top right). We see that the homoclinic line crosses the line of Hopf points. At the origin there emanates another line, a line of a saddle - node bifurcation of periodic orbits. Since this line is exponentially close to the homoclinic line, we have to zoom in one more time. In figure 6.4 (bottom) we see the parameter space in a neighborhood of the intersection of the homoclinic line and the line of Hopf points.

This results are in accordance to our findings for the flow local to the canard point, see also [36] Fig. 7. After the homoclinic line crosses the line of Hopf points, the line of saddle - node bifurcations of periodic orbits eventually hits the line of Hopf points changing the Hopf - bifurcation from supercritical to subcritical. Thus we conjecture the existence of a Bautin bifurcation at this branching point. In the next figure we see the flow in the two different regions 5 and 6 of the parameter space, marked in figure 6.4 (bottom). The homoclinic orbit is always unstable, but we have two different sketches of the flow on

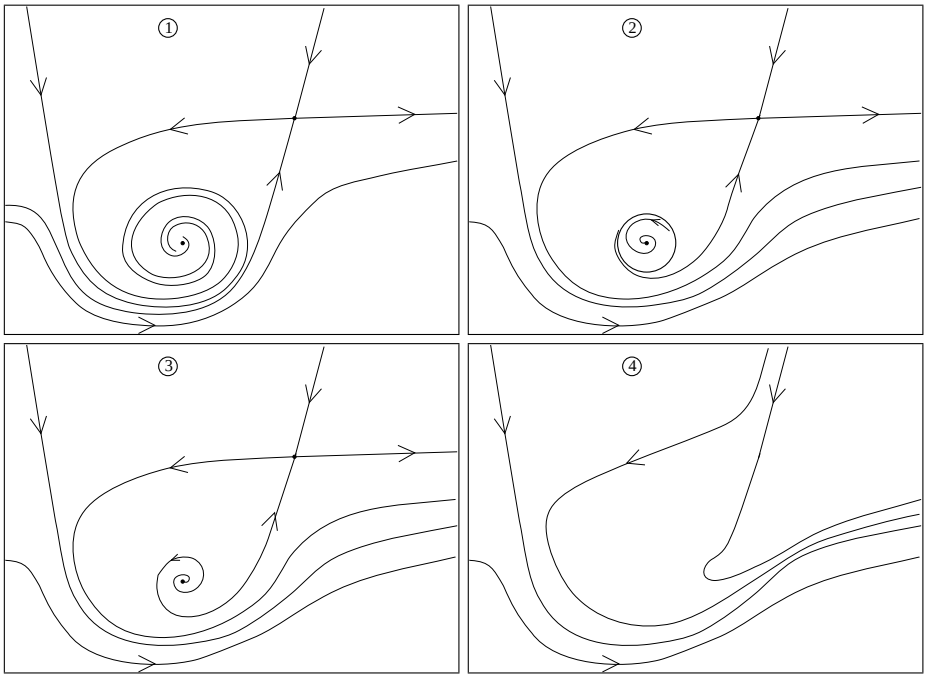

Figure 6.5: The flow for system (6.10) for regions 1 (top left) to 4 (bottom right)

the homoclinic line for ε small, i.e. smaller than the value of ε at the Bautin bifurcation point, and ε large, see figure 6.7. The last two examples have in common that the closed orbits near the Takens - Bogdanov bifurcation are unstable, which means, that the sign of $(a_{20}(0)+b_{11}(0))b_{20}(0)$ is positive. The next two examples will show the behavior of the global flow when the closed orbits near the Takens - Bogdanov bifurcation are stable.

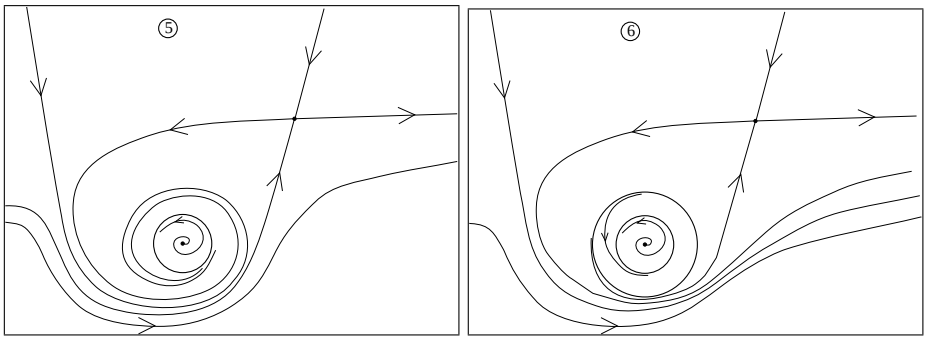

Figure 6.6: The flow for system (6.10) for regions 5 (left) and 6 (right)

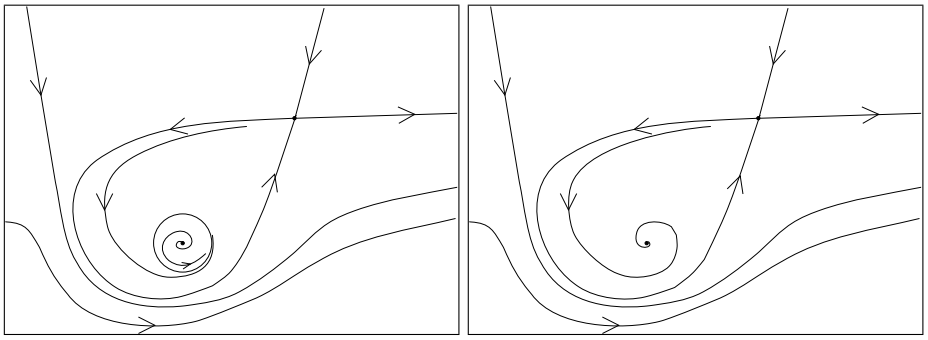

Figure 6.7: The flow for system (6.10) on the homoclinic line for small ε (left) and large ε (right)

6.4 Stable TB Orbits, A < 0

Our third example system reads

$$\begin{aligned} \dot{x} &= x^2(1-2x+\tfrac{4}{3}x^2)-y; \\ \dot{y} &= \varepsilon[x(1-x)-\lambda-y], \end{aligned} \tag{6.11}$$

so that $\tilde{h}_2(x) = -2x + \frac{4}{3}x^2$, $\tilde{h}_3(x) = -x$ and $\kappa = 1$. Again numerical simulations suggest a Takens - Bogdanov bifurcation, here located at the point $(x, y, \varepsilon, \lambda) \approx (0.41, 0.07, 0.18, 0.17)$. The conditions (BT.0) - (BT.3) read in that order 0.21, -0.23, 0.95 and 1.68. The parameter A in this case takes the value -2, meaning that again we have stable periodic orbits emanating from the canard point for small ε. However, we have changed the stability of closed orbits near the Takens - Bogdanov bifurcation, meaning that there has to be a change in the stability of the homoclinic orbit. As in the last example, locally to the canard point there is a line of saddle - node bifurcations of periodic orbits. Since the homoclinic line does not intersect the line of Hopf points and the homoclinic orbit changes its stability, we conjecture that the line of saddle - node bifurcation hits the homoclinic line forming a point of a Bautin - like bifurcation for homoclinic orbits. In figure 6.8 (left) we see exactly this situation for our example, where the lines again are numerically determined.

Again the line of saddle - node bifurcations is exponentially close to the homoclinic line. Enlarging the sketch near the origin yields figure 6.8 (right). The lines distinguish five different regions 1 - 5. In the next figure we see sketches of the flow in each of this regions inspired by numerical results, figure 6.9. The flow on the homoclinic line is again divided into two different regions, one for small ε, i.e. smaller than the value of ε at the Bautin-like bifurcation point, and one for large ε, figure 6.10.

Another interesting peculiarity is the behavior of the flow for $\varepsilon > 0.18$. Here we see that the line of Hopf points continues above the value of ε_{TB}, then turn around and finally reach the Takens - Bogdanov bifurcation point from above. Thus there exists a

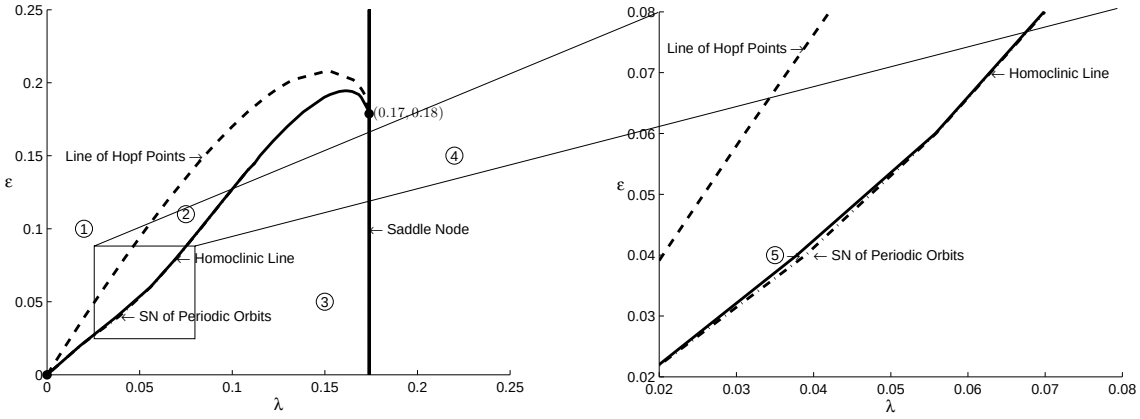

Figure 6.8: The parameter space for system 6.11

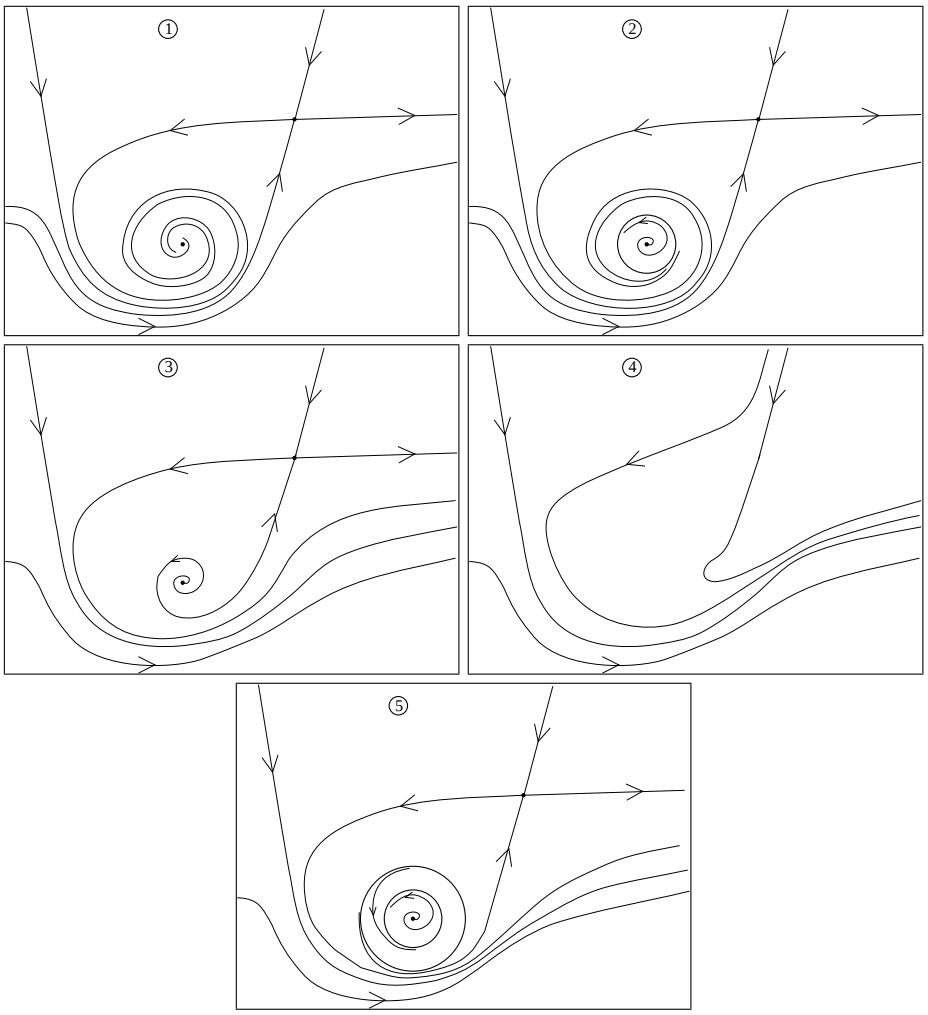

Figure 6.9: The flow for system (6.11) for regions 1 (top left) to 5 (bottom)

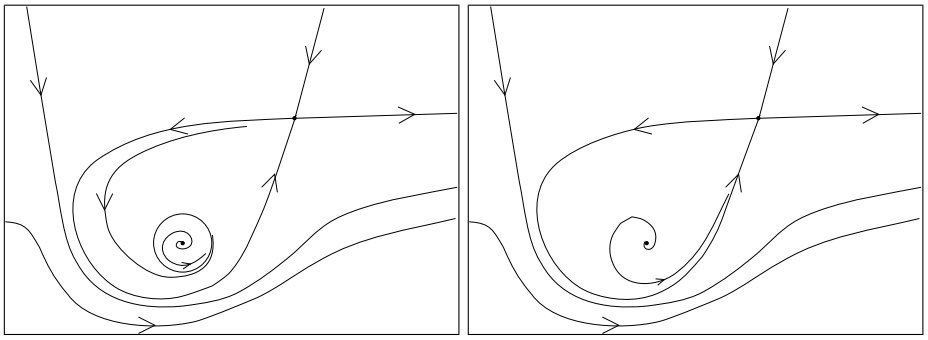

Figure 6.10: The flow for system (6.11) on the homoclinic line for small ε (left) and large ε (right)

region for which there are two different Hopf bifurcation points for different values of λ. The homoclinic line shows the same behavior. This behavior appears naturally since the change of the stability changed the relative position of both the line of Hopf points and the homoclinic line. However, we are not able to exclude the existence of global bifurcations here. We see the same behavior local to the Takens - Bogdanov bifurcation point also in the last example. There we again change the sign of A.

6.5 Stable TB Orbits, A > 0

Our last example system reads

$$\begin{aligned} \dot{x} &= x^2(1 - 2x + \tfrac{4}{3}x^2) - y; \\ \dot{y} &= \varepsilon[x(1 - \tfrac{1}{2}x) - \lambda - \tfrac{7}{2}y]. \end{aligned} \tag{6.12}$$

Again we have $\tilde{h}_2(x) = -2x + \frac{4}{3}x^2$. Furthermore we obtain $\tilde{h}_3(x) = -\frac{1}{2}x$ and $\kappa = \frac{7}{2}$. The numerical Takens - Bogdanov bifurcation point is located at $(x, y, \varepsilon, \lambda) \approx (0.27, 0.04, 0.06, 0.09)$. (BT.0) - (BT.3) take the numerical values 0.25, -0.31, 0.08 and 4.38, the parameter A the value 2. The closed orbits near the Takens - Bogdanov bifurcation point are stable while the closed orbits near the canard bifurcation point are unstable. This means that the Hopf bifurcation has to change from subcritical to supercritical along the line of Hopf points and also the homoclinic orbit has to change its stability along the homoclinic line. The conjecture now is a combination of example 2 and 3. The change of the Hopf bifurcation is achieved through a Bautin bifurcation, which gives rise to a line of saddle - node bifurcations of periodic orbits. This line will then connect to the homoclinic line where we again have a Bautin - like bifurcation of homoclinic orbits. This will then change the stability of the homoclinic orbit. Figure 6.11 (left) shows the numerical results in the parameter space of this behavior.

The flow in regions 1 to 3 is shown in figure 6.12. We enlarge the sketch of the parameter

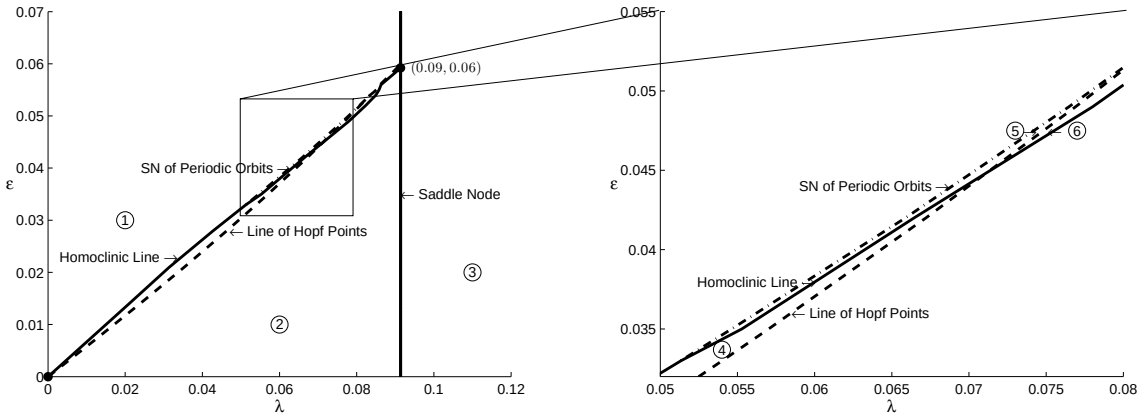

Figure 6.11: The parameter space for system 6.12

space at the intersection of the homoclinic line with the line of Hopf points, figure 6.11 (right). As one can see there are three additional regions in the parameter space. The flow for region 4 to 6 is shown in figure 6.13. As stated before, the behavior of the flow near the Takens - Bogdanov bifurcation point is as in Example 3. The flow on the homoclinic line in this example splits into three different regions.

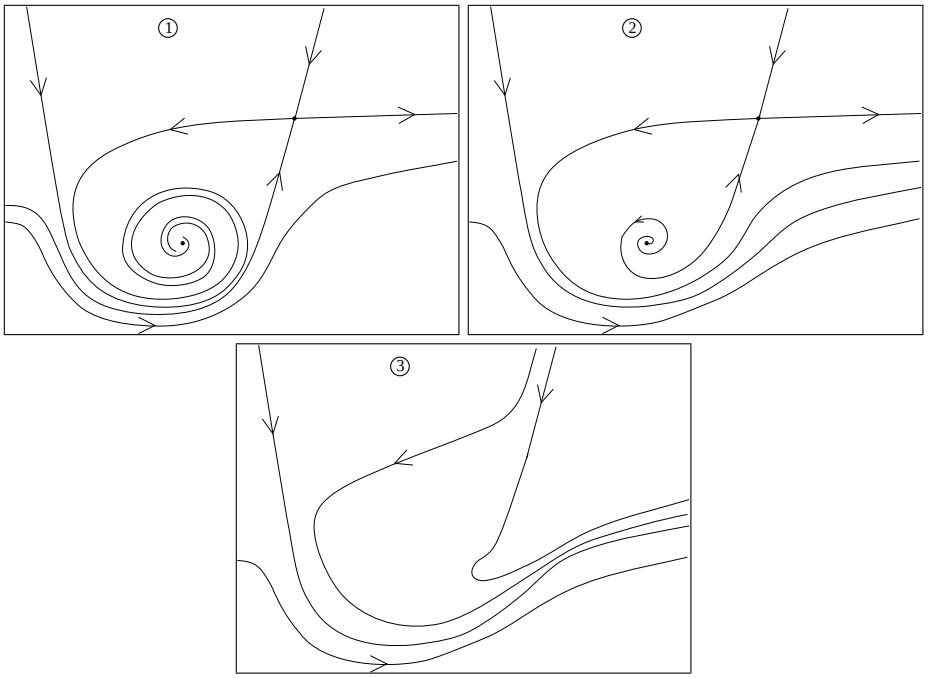

Figure 6.12: The flow for system (6.12) for regions 1 (top left) to 3 (bottom)

For small ε, i.e. smaller than the value of ε at the Bautin-like bifurcation point, we have an unstable homoclinic orbit with the canard point being stable. For ε taking values between the Bautin-like bifurcation point and the Bautin bifurcation point there exists

a stable homoclinic orbit having an unstable periodic orbit in its interior. And for ε large, i.e. larger than the value of ε at the Bautin bifurcation point, the homoclinic orbit is stable and the canard point is unstable. These situations are shown in figure 6.14.

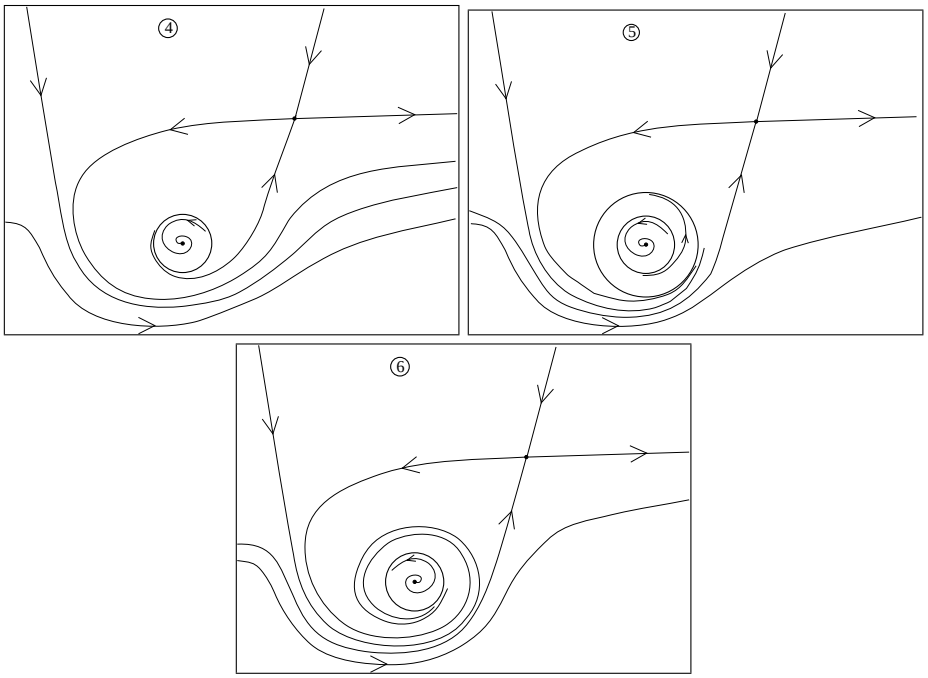

Figure 6.13: The flow for system (6.12) for regions 4 (top left) to 6 (bottom)

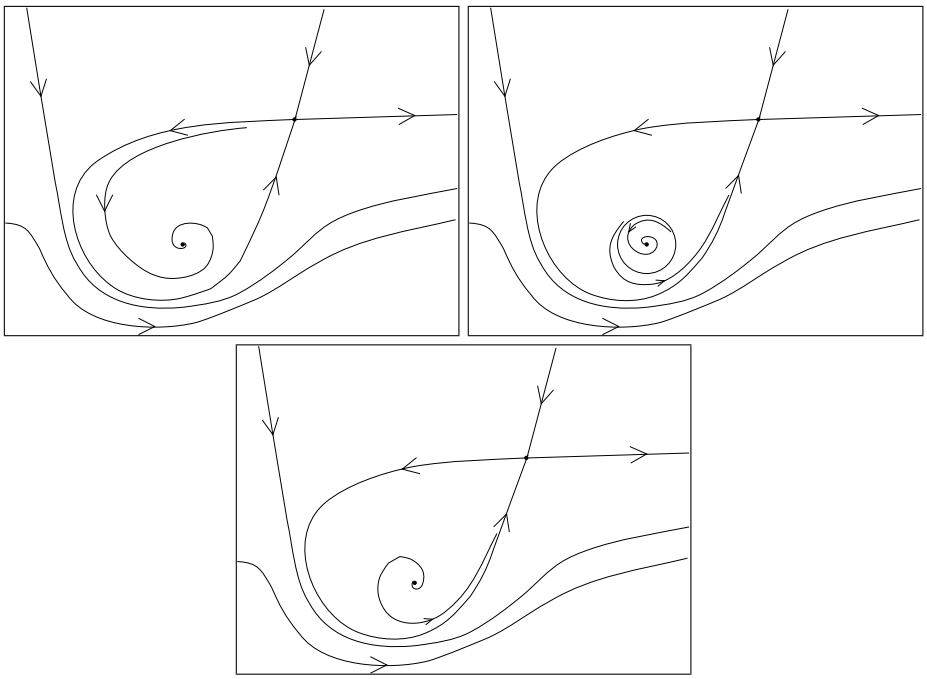

Figure 6.14: The flow for system (6.12) on the homoclinic line for small (top left), middle (top right) and large (bottom) ε

7 Application: The Extrinsic Coagulation System

This chapter focuses on the quest for mechanisms that are able to create tolerance and an activation threshold in the extrinsic coagulation cascade. We propose that the interplay of coagulation inhibitor and blood flow creates threshold behavior. First we test this hypothesis in a minimal, four dimensional model. This model can be analyzed by means of time scale analysis. We find indeed that only the interplay of blood flow and inhibition together are able to produce threshold behavior. The mechanism relies on a combination of raw substance supply and wash-out effect by the blood flow and a stabilization of the resting state by the inhibition. We use the insight into this minimal model to interpret the simulation results of a large model. Here, we find that the initiating steps (TF that produces together with VII(a) factor Xa) does not exhibit threshold behavior, but the overall system does. Hence, the threshold behavior appears via the feedback loop (in that IIa produces indirectly Xa that in turn produces IIa again) by ATIII and blood flow.

Our aim here is to describe a biological application for systems of coupled feedback loops. The main interest is in the outcome of the biological interpretation. Hence the mathematical aspect in this chapter is short and for some parts hand waving arguments are used. The full analysis in terms of time scale analysis is out of the scope of this chapter. However, it turns out that the general concept of modelling coupled feedback loops can give useful insight into biological applications.

7.1 Motivation

Physiologic signalling systems are typically tolerant towards very small signal levels; this tolerance protects against noise, rendering them robust against arbitrary yet physiologically subcritical events. Only a distinct signal induces a reaction. An excellent and prototypic example is the activation of neurons: they will fire only if a distinct stimulus is present. There are several sources of noise in the neuronal system: a noisy input signal, a noisy transport of the signal in the ganglion, and the processing system in the neuron itself has some intrinsic noise. The neuronal system handles these noise sources on two levels. The basic level is the threshold behavior of the single neuron. The second level concerns the network structure; e.g. feedback loops and redundant elements in the network topology are able to provide reliable responses on noisy signals. The

neuronal system is able to filter input signals in standard situations. Small amplitudes and fluctuations of high frequency are likely to be discarded as noise. It is to expect that such an essential system like the coagulation cascade exhibits similar mechanisms that provide stability against noise, e.g. caused by the expression of tissue factor by endothelial cells in case of localized inflammatory events. The intrinsic noise of the cascade due to small molecule numbers is less likely to play a role, as due to the powerful amplification mechanisms most parts of the signaling cascade are based on high molecule numbers.

Quite often, mechanisms of tolerance are connected with separation of two time scales, a fast and a slow one. The fast time scale corresponds to the natural time scale of the input signal, while the slow one is used to process the input signal, to act like a low pass filter that averages out fluctuations and to generate an output signal: nonlinear feedback yields bistability of the slow system with respect to the fast time scale; the two stable branches of (with respect to the fast time scale) stationary states correspond to two different output signals. Hysteresis will generically prevent the system to jump arbitrarily fast between these two states if the input signal is perturbed by noise. This feedback mechanism is able to realize switches with different properties. For an overview see eg. [51] or [43, Chapter 6]. Here we investigate mechanisms in the coagulation system that may lead to tolerance.

The historical model of the coagulation system assumed two different starting points of the coagulation process. The intrinsic pathway is activated by contact of plasma with charged surfaces and aims to handle very small lesions. The extrinsic pathway was thought to target on larger lesions and was thus considered the faster and more effective pathway. Both pathways enter a common final pathway leading to fibrin formation. However, this concept has been revised as tissue factor (TF) has been identified as the universal initiator of all clinically relevant coagulation events (subendothelial TF initiates coagulation following vascular damage, TF on plaque surfaces initiates coagulation e.g. in coronary heart disease, TF on monocyte surface initiates coagulation in inflammatory states ultimately resulting in disseminated intravascular coagulation (DIC)).

The omnipresence of TF and its enormous biological potency warrant a regulation mechanism that exerts sufficient tolerance against minor events, e.g. a localized inflammatory reaction or minor vascular damage while providing a fast and complete activation of the coagulation cascade in case of a major event. Thus bistable feedback mechanisms should be a key component of the regulatory mechanisms of the coagulation system.

Coagulation disorders are a common problem in trauma patients. The trauma induced tissue damage results in an exposure of large amounts of TF, i.e. consumption of coagulation factors, while trauma induced haemorrhage also reduces the concentrations of coagulation factors. The therapeutic approach is based mainly on substitution of coagulation factors and control of haemorrhage (i.e. surgery). However, while surgical

control of haemorrhage is usually successful and prevents acute exsanguination, the coagulation disorder often persists and transfusion even of large amounts of coagulation factors cannot stabilize the coagulation system. Coagulation physiology in trauma patients is only incompletely understood. It is unclear when the coagulation disorder actually starts, how the progress of the coagulation disorder is affected by medical interventions (e.g. drug application, infusion of fluids etc.) to name but a few.

Most experiments seem to hint that the coagulation cascade is basically unstable, i.e. a small activating challenge finally leads to clot formation [7]. Once initiated (TF, fVIIa), the coagulation process consists of two major steps: first, small amounts of factor X are cleaved to its activated form fXa. This small amount of fXa is able to cleave factor II to its activated form fIIa. The second step comprises a powerful positive feedback loop of fIIa enhanced fIIa production by a factor around 10^5 to 10^9 [7], resulting in a fIIa burst. This large amount of IIa is able to cleave factor fI to fIa - Ia being the substance that organizes the clot (for details see e.g. the review articles [7, 41, 42] and below). Experiments *in vitro* seem to hint that even smallest amount of fTF are able to initiate the coagulation cascade [5]. Due to the self-amplifying positive feedback loops, namely the fIIa burst, the coagulation process is then completely activated [38]. As minor amounts of either TF or soluble tissue factor (sTF) are ubiquitously present (e.g. localized tissue damage or locally contained inflammatory reaction), the coagulation cascade is challenged stochastically. However, spontaneous thromboembolic events are extremely rare *in vivo*. Consequently, a certain tolerance against arbitrary stimuli within the regulatory system can be expected. For a deeper understanding of trauma associated coagulopathy it is necessary to understand the regulatory mechanisms within the coagulation cascade. Due to methodological and ethical considerations the regulatory and activating mechanisms of the coagulation system can hardly be investigated in a clinical context.

The modelling approach is quite accepted in the coagulation community. We find the whole spectrum of models, from small toy models that focus on the understanding of special mechanisms to large simulation models that quantitatively reproduce experiments. The large simulation models mostly address the behavior of “artificial plasma” in a closed reactor [7]. The advantage of these models is the connection to experimental data - a lot of work is done to develop an experimental model system where different aspects like the lack of certain factors can be manipulated in a controlled way. The models are able to reproduce and to predict these experimental data quite satisfyingly [32]. However, the coagulation system is also influenced by cells like platelets or endothelial cells, which are not present in the “artificial plasma”. Furthermore, biophysical processes e.g. blood flow, which is severely impaired in trauma patients suffering from haemorrhagic shock, mostly are not taken into account. Only recently the effect of blood flow attracted attention [2, 16, 39, 9].

Some work is done with respect to threshold behavior of the former extrinsic pathway. One of the first investigations in this field was conducted by Khanin and

Semenov [33]. Their model basically assumes Michaelis Menten kinetics with one positive feedback loop. The network topology of this model is sufficient to produce threshold behavior in the sense that a minimal stimulus is necessary to induce a reaction. If this stimulus is above the threshold, the effect will grow linearly with this stimulus. There is no bistability or hysteresis. Experiments show that the system tends to complete activation. This finding indicates that there are other relevant mechanisms that need to be implemented into the model. From the mathematical point of view more nonlinear terms are necessary to obtain a model that adequately reproduces the expected behavior. One approach might be to add mechanisms that are related to the surface of cellular components involved in the coagulation process. Activated platelets provide high concentrations of phospholipids. The expression of phospholipids can be induced by activated zymogenes, i.e. coagulation factors [3]. Thus, if there are enough coagulation factors to stimulate the platelets, the cascade is able to work much more efficient than in states of low coagulation activation. This process creates bistable behavior [54]. Fogelson and Tania [16] found evidence that blood flow may be a crucial control mechanism as their simulation model exhibited threshold behavior of the extrinsic pathway after blood flow was integrated into the model. These results are in accordance with experimental evidence presented by Gemmell et al. in 1988 [18].

As our clinical focus is set on trauma patients with hemodynamic alterations due to haemorrhagic shock, i.e. impaired tissue blood flow, we aim at a deeper understanding of the interplay of biochemistry with biophysics. The rest of the chapter is organized as follows. First, we describe briefly the coagulation system with respect to its clinically relevant components. We then introduce a minimal model of this system, taking into account blood flow in a very simple manner: the substances may flow into resp. out of the system at a certain rate. For this model we are able to perform a bifurcation analysis and find bistable behavior. As a second step we then focus on experimental findings respectively on models validated by experiments. We equip one of these models with our concept of blood flow and investigate the change of behavior due to this biophysical process by means of numerical simulations. This is first done for a submodel that focuses on the very first step of the coagulation cascade, and then for a large simulation model that takes into account most physiological relevant parts of the whole system.

7.2 Key Players

The most prominent molecules of the extrinsic pathway are TF (tissue factor), factor fVII and fVIIa, TFPI (tissue factor pathway inhibitor), fX and fXa, fV and fVa, XIII and fXIIIa, fIX and fXIa, fII (prothrombin) and fIIa (thrombin), fATIII (antithrombin III) and protein C (PC) resp. activated protein C (APC) (see Fig. 7.1). Most of these substances are present in the plasma in their non-active form. Activation is achieved by enzymatic reactions.

The cascade is induced by contact of TF with factor fVII resp. fVIIa. They form a membrane-bound complex. TF is expressed constitutionally on the surface of tissue cells, but not on endothelial cells. Until recently, it has been common sense that sufficient amounts of TF and blood (i.e. factor fVII resp. fVIIa) are in contact only in case of a major lesion to the vessel wall. However, experimental evidence clearly shows that sTF, a soluble form of TF, is constitutively present in the blood. sTF seems to play an important role for the growth of thrombi. If the activation process of the coagulation cascade is determined by an "all-or-none" mechanism, the coagulation cascade needs to distinguish between blood borne and tissue related TF to avoid permanent, uncontrolled coagulation. Alternatively a concentration dependent activation mechanism might regulate this pathway.

In the complex TF/fVII, the ligand fVII is transformed into its active form fVIIa. The complex TF/fVIIa is the first key player of the coagulation cascade: this complex is able to enhance its own production due to its ability to activate free fVII. The resulting fVIIa binds even faster to free TF. Beyond this positive feedback loop TF/fVIIa is able to activate the second key player of the coagulation cascade, i.e. fX is converted to fXa, which in turn is controlled by TFPI and ATIII.

The positive feedback is regulated by several inhibitory molecules, the most prominent of which are TFPI (tissue factor pathway inhibitor) and ATIII (antithrombin III). TFPI forms a complex with fXa, and this complex as well as ATIII react with TF/fVIIa and TF/fVII; the resulting complexes are enzymatically inactive. The second part of the cascade couples on fXa. fXa activates the third key player, prothrombin (fII). fIIa has its own positive feedback: fIIa activates the conversion of fV to fVa, which forms a complex with fXa. The complex fXa/fVa is much more potent in activating fII then fXa alone. Furthermore, it activates fVIII, which forms a complex with fIX (which is activated by TF/fVIIa). This complex activates fX, resulting in higher concentrations of fXa and fXa/fVa complexes, which in turn activate more fII. Finally Thrombin (fIIa) induces fIa production. fIa (also called fibrin) produces the thrombus and "glues" the lesion. The anticoagulant ATIII forms complexes with almost all activated factors and deactivates them in this way; furthermore, on a slow time scale, the density of ATIII is increased by fIIa (e.g. upregulated by heparin). fIIa is also able to cleave PC to APC, which deactivates the factors fVa and fVIIIa by cleavage, resulting in the inhibition of the positive feedback loop. Most of these reactions take place on a cell membrane, i.e; either on the surface of tissue cells or on the surface of platelets. Only fXa and fIIa are able to diffuse freely.

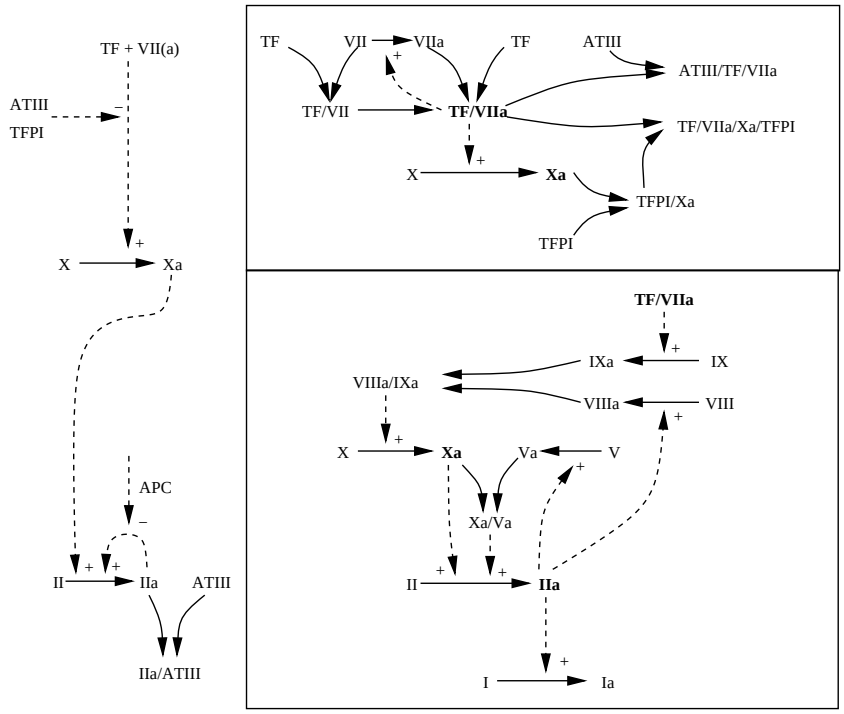

Figure 7.1: Scheme of the most important processes of the coagulation cascade. Left hand side: only most important processes; right hand side: more detailed system.

7.3 Threshold Behavior: A Minimal Model

In this section, we develop a toy model for the coagulation system. We will perform an analysis of this model. These results will guide us when considering large, more realistic models in Section 7.5. Let x be the amount of II, and y the amount of activated enzyme IIa. The primary pathway allows a positive auto-feedback at rate r, i.e. (see Fig 7.2)

$$\dot{x} = -rx\,y, \qquad \dot{y} = rx\,y.$$

We now add an anticoagulative substance z (e.g., ATIII). This substance forms a complex with IIa at rate b, ultimately resulting in the inactivation of this substance. In addition to purely biochemical processes, we also consider a biophysical process: blood flow. This effect is introduced by defining in- and outflow rates. I.e., we assume that there is a small region (at the surface of a lesion) where the reaction takes place. We assume that the substances are homogeneously mixed in this region, such that we are allowed to assume mass action dynamics. Substances x and z are washed in at their natural density, and all substances (x, y and z) are washed out at the same rate. The flow rate depends on the location of the region of interest: as a rule, the smaller the vessel, the smaller is the flow velocity. In order to concentrate on the most basic effects of blood flow (transport of substances), we deliberately neglect spatial effects. These effects sometimes have surprising consequences. E.g., many enzymes are located at the surface of cells. In this case, the rate limiting step sometimes is the transport of substrate to the surface rather then the reaction rates [18]. Basically, our region of interest is this small that density gradients can be neglected. Let the mean time a particle stays within the region of interest be $1/\zeta$, i.e. the average flow rate is ζ. Let furthermore μ_x resp. μ_z be the natural densities of coagulation factors resp. anticoagulant substances in the plasma. The equations for the minimal model read

$$\begin{aligned} x' &= -rxy + \zeta\mu_x - \zeta x \\ y' &= rxy - by\,z - \zeta y \\ z' &= -by\,z + \zeta\mu_z - \zeta z. \end{aligned} \tag{7.1}$$

We first investigate this model with fixed rates; in Section 7.4, we add a slow increase of anticoagulant substances triggered by activated zymogen. In the following we consider model (7.1) and investigate the stationary points, the local stability analysis of these points and perform a global analysis that shows that any trajectory eventually tends to one of these stationary points.

Stationary States

First note that a stationary solution of system (7.1) with a non-negative y-component also has non-negative x- and z-components – we may solve the equations $x' = 0$ and $z' = 0$ for x and z, respectively. It is thus sufficient to concentrate on y. The trivial

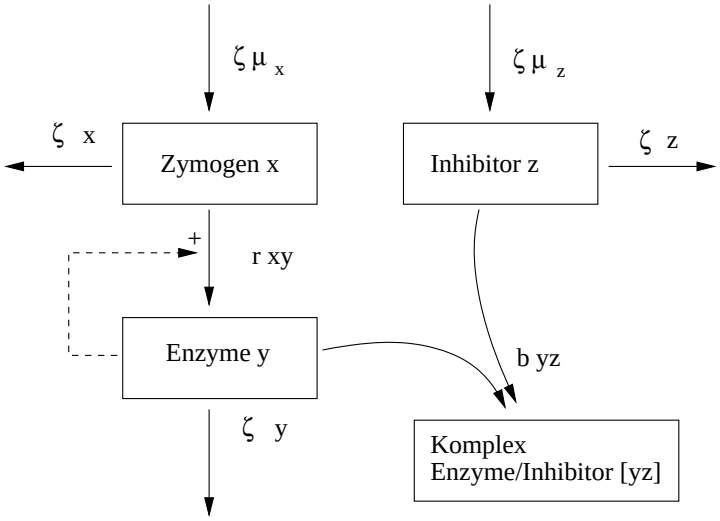

Figure 7.2: Flow diagram of the minimal model.

stationary point is given if $y = 0$. Then, we find $x = \mu_x$ and $z = \mu_z$.

Let $y \neq 0$. Under this circumstance

$$\begin{aligned} &rx - bz - \zeta = 0 \\ &0 = x' + y' - z' = \zeta\mu_x - \zeta\mu_z - \zeta(x + y - z). \end{aligned}$$

Let us assume that $\zeta \neq 0$ (for $\zeta = 0$ see below)

$$\begin{aligned} z &= (rx - \zeta)/b, \\ 0 &= \mu_x - \mu_z - (x + y + (\zeta - rx)/b) \\ &= \mu_x - \mu_z - ((1 - r/b)x + y + \zeta/b) \\ &= \mu_x - \mu_z - \zeta/b - (x(b - r)/b + y) \\ x &= \tfrac{b(\mu_x - \mu_z) - \zeta}{b - r} - \tfrac{b}{(b-r)}\, y \end{aligned}$$

Let

$$A = \tfrac{b(\mu_x - \mu_z) - \zeta}{b - r}, \qquad B = 1 - r/b = (b - r)/b$$

then $x = A - y/B$. Thus, we find for y (from $x' = 0$)

$$-ry(A - y/B) + \zeta\mu_x - \zeta A + \zeta y/B = 0 \quad \Rightarrow \quad r/B\ y^2 - (rA - \zeta/B)y + \zeta\mu_x - \zeta A = 0,$$

i.e.

$$y^2 - (AB - \zeta/r)y + \zeta(\mu_x\, B\ - AB)/r = 0.$$

Thus, the nontrivial stationary points read $(x_\pm, y_\pm, z_\pm)^T$ where the y-component is given by

$$\begin{aligned} y_\pm &= \tfrac{1}{2}\left(AB - \zeta/r \pm \sqrt{(AB-\zeta/r)^2 - 4\zeta(\mu_x B - AB)/r}\right) \\ &= \tfrac{1}{2}\left(AB - \zeta/r \pm \sqrt{(AB+\zeta/r)^2 - 4\zeta\mu_x B/r}\right). \end{aligned}$$

We now find $AB - \zeta/r = \mu_x - \mu_z - \zeta/b - \zeta/r$, $AB + \zeta/r = \mu_x - \mu_z - \zeta/b + \zeta/r$, $\zeta\mu_x B/r = \zeta\mu_x(b-r)/(br) = \zeta\mu_x(1/r - 1/b)$ i.e.

$$y_\pm = \tfrac{1}{2}\left[\mu_x - \mu_z - \tfrac{\zeta}{b} - \tfrac{\zeta}{r} \pm \sqrt{\left(\mu_x - \mu_z - \tfrac{\zeta}{b} + \tfrac{\zeta}{r}\right)^2 - 4\zeta\tfrac{(b-r)}{br}\mu_x}\,\right] \tag{7.2}$$

We use μ_z as bifurcation parameter, $y_\pm = y_\pm(\mu_z)$. Interesting effects (i.e. stationary solutions in the positive octant) are only possible for $y_+(0) > 0$. Under this condition, there are three cases to distinguish:

Case 1: $b = r$.

Then, $y_+ = \mu_x - \mu_z - \zeta/b$, $y_- = -\zeta/r < 0$. I.e., we have at most one non-negative solution apart from $y = 0$, and this solution is linearly decreasing in μ_z and is only non-negative if μ_z is small.

Case 2: $b < r$.

For all values of μ_z, there are two real branches $y_\pm(\mu_z)$. $y_-(\mu_z) < 0$ is always negative and thus not interesting for the dynamics in the positive octant. $y_+(\mu_z)$ is decreasing in μ_z. Thus, also in this case there is (like in case 1) at most one more non-negative solution apart of $y = 0$. We cannot expect bistable behavior in the positive octant.

Case 3: $b > r$.

There is an interval for μ_z, where we do not find real solutions $y_\pm(\mu_z)$. At the boundaries of this interval where no real solutions exist, two saddle-node bifurcations (one sub- and one supercritical) occur. These bifurcation points are located at the μ_z-values where the discriminant vanishes,

$$\mu_z = \mu_x - \tfrac{\zeta}{b} + \tfrac{\zeta}{r} \pm 2\sqrt{\tfrac{(b-r)}{br}\zeta\mu_x}.$$

The first (left) branch connects the positive value $y_+(0)$ with the negative value $y_-(0)$, i.e. crosses necessarily at least once $y_\pm(.) = 0$. Since there is only one value μ_z for that a solution $y_\pm = 0$, i.e. $\mu_x B - AB = 0$, there is only one value for μ_z s.t. $y_+(\mu_z) = 0$ or $y_-(\mu_z) = 0$. Since $B \neq 0$, in case 3, we find $A = \mu_x$, i.e. $\mu_z = \frac{r\mu_x - \zeta}{b}$. Thus, the second (right) branch does not change sign. Since $y_-(\mu_z) < 0$ if μ_z is large, the right branch is completely below zero. The only interesting manifold of stationary points is the positive

part of the left branch. This raises the question, if always $y_-(\mu_z) < 0$. The value of $y_\pm$ at the left bifurcation point reads

$$y_\pm = \sqrt{\tfrac{(b-r)}{br}\zeta\,\mu_x} - \tfrac{\zeta}{r}$$

i.e. is positive, if $\left(1 - \frac{r}{b}\right)\ \mu_x > \frac{\zeta}{r}$. Thus, we find two subcases.

Case 3(a): $b > r$, $(1 - r/b)\mu_x < \zeta/r$.

There is at most one more non-negative stationary solution in the positive octant apart of $y = 0$. Bistability is not possible.

Case 3(b): $b > r$, $(1 - r/b)\mu_x > \zeta/r$.

Hence, if

$$\mu_z \in \left(\mathrm{Max}\{0, (r\mu_x - \zeta)/b\},\ \ \mu_x - \tfrac{\zeta}{b} + \tfrac{\zeta}{r} - 2\sqrt{\tfrac{(b-r)}{br}\zeta\mu_x}\right),$$

there are the trivial and two further strictly positive stationary points. In this parameter region is bistability possible (see stability analysis below). For

$$\mu_z = \mu_x - \tfrac{\zeta}{b} + \tfrac{\zeta}{r} - 2\sqrt{\tfrac{(b-r)}{br}\zeta\mu_x}$$

a saddle-node bifurcation takes place, while at $\mu_z = 0$ and $\mu_z = (r\mu_x - \zeta)/b$ (if positive) transcritical bifurcations happen.

Local Stability Analysis

The Jacobian reads

$$J = \begin{pmatrix} -ry - \zeta & -rx & 0 \\ ry & rx - bz - \zeta & -by \\ 0 & -bz & -by - \zeta \end{pmatrix} = \begin{pmatrix} -ry & -rx & 0 \\ ry & rx - bz & -by \\ 0 & -bz & -by \end{pmatrix} \ - \ \zeta\, I.$$

Consider the trivial stationary point, $(x, y, z) = (\mu_x, 0, \mu_z)$. The Jacobian reads

$$J_0 = \begin{pmatrix} 0 & -r\mu_x & 0 \\ 0 & r\mu_x - b\mu_z & 0 \\ 0 & -b\mu_z & 0 \end{pmatrix} \ - \ \zeta I.$$

Due to the simple structure of this matrix, we directly find a double eigenvalue $\lambda_{1,2} = -\zeta$ and one eigenvalue $\lambda_3 = r\mu_x - b\mu_z - \zeta$. The last one determines the stability of the trivial

solution. If $r\mu_x - b\mu_z - \zeta < 0$, the trivial solution is stable, and $r\mu_x - b\mu_z - \zeta > 0$ implies instability. Now we return to the general case and consider the spectrum of the matrix $\hat{J} = J + \zeta I$. We find for the characteristic polynomial

$$p(\lambda) = \det(\hat{J} - \lambda I) = -\lambda\{\lambda^2 + \lambda[(r+b)y - rx + bz] + rby[y + z - x]\},$$

i.e. we have one zero eigenvalue for $\hat{J}$, corresponding to one eigenvalue $-\zeta$ for J. To find the remaining eigenvalues, we use the fact that we consider a non-trivial stationary point, i.e. $rx - bz = \zeta$ and $x - z = \mu_x - \mu_z - y$,

$$p(\lambda) = -\lambda q(\lambda), \qquad q(\lambda) = \{\lambda^2 + \lambda[(r+b)y - \zeta] + rby[2y + \mu_z - \mu_x]\}.$$

Now consider the negative branch of nontrivial stationary points, corresponding to y_-. Here, we know that

$$\begin{aligned} q(\zeta) &= y_-[(r+b)\zeta + rb(2y_- + \mu_z - \mu_x)] \\ &= y_- \left[(r+b)\zeta + rb\left(-\tfrac{\zeta}{b} - \tfrac{\zeta}{r} - \sqrt{\left(\mu_x - \mu_z - \tfrac{\zeta}{b} + \tfrac{\zeta}{r}\right)^2 - 4\tfrac{(b-r)}{br}\mu_x\,\zeta}\right)\right] \\ &= -\,y_-\; rb\,\sqrt{\left(\mu_x - \mu_z - \tfrac{\zeta}{b} + \tfrac{\zeta}{r}\right)^2 - 4\tfrac{(b-r)}{br}\mu_x\,\zeta}. \end{aligned}$$

Thus $q(\zeta) < 0$ if the stationary point lies within the positive octant ($y_- > 0$). Since $q(\lambda) \to +\infty$ for $|\lambda| \to \infty$, the polynomial $q(.)$ has one eigenvalue below and one above ζ. Thus, the spectrum of the stationary point corresponding to y_- has two negative eigenvalues and one positive eigenvalue. If the stationary point $(x_-, y_-, z_-)^T$ is in the positive octant, it is always unstable. Last, we inspect the stationary point corresponding to y_+. Here we find

$$q(\zeta) \;=\; y_+\, rb\,\sqrt{\left(\mu_x - \mu_z - \tfrac{\zeta}{b} + \tfrac{\zeta}{r}\right)^2 - 4\tfrac{(b-r)}{br}\mu_x\;\zeta} > 0.$$

Furthermore, $q(0) = rby_+[2y_+ + \mu_z - \mu_x] < y_+[\zeta(r+b) + rb(2y_+ + \mu_z - \mu_x)] = q(\zeta)$. Since $q(.)$ is only a quadratic polynomial, all real roots are left of $\lambda = \zeta$. In any case, the minimum of $q(.)$ is left to $\lambda = 1$, and thus also the real part of the roots are left to ζ. Thus, the stationary point corresponding to y_+ is always locally asymptotically stable, if we are not in a saddle-node or transcritical bifurcation.

Global analysis

We will show that any trajectory tends to an equilibrium point. We first observe that the system preserves positivity and that $x + y - z$ satisfies a closed equation,

$$\tfrac{d}{dt}\,(x + y - z) = \zeta(\mu_x - \mu_z) - \zeta(x + y - z).$$

Thus,

$$x(t) + y(t) - z(t) \to \mu_x - \mu_z$$

exponentially fast for $\zeta > 0$. From the theory of asymptotically autonomous systems we know that any ω-limit set will be obtained in the plane $x + y - z = \mu_x - \mu_z$, i.e. satisfies the two-dimensional set of equations

$$\begin{aligned} \dot{x} &= -rxy + \zeta\mu_x - \zeta x \\ \dot{y} &= (r-b)xy - by^2 - by(\mu_z - \mu_x) - \zeta y. \end{aligned}$$

Thus, we know from the theorem of Poincaré-Bendixon that the ω-limit sets are either stationary points, or periodic orbits or a cycle of heteroclinic/homoclinic orbits. We apply the negative criterion of Bendixon in order to exclude the last two options: If we rescale the vector field by $1/y$ (we may do that since $y > 0$ is invariant as well as the line $y = 0$), we find for the divergence of the resulting vector field

$$\left(\tfrac{-rxy+\zeta\mu_x-\zeta x}{y}\right)_x + \left(\tfrac{(r-b)xy-by^2-by(\mu_z-\mu_x)-\zeta y}{y}\right)_y = \left(-r - \tfrac{\zeta}{y}\right) - b < 0.$$

The divergence of the rescaled vector field does not change sign, and thus neither a periodic orbit nor a cycle of heteroclinic/homoclinic orbits may appear. Hence, any trajectory eventually tends to a stationary point.

Flow Rate As Bifurcation Parameter

In order to keep the analysis simple, we used μ_z as bifurcation parameter. However, we rather aim at the analysis of the behavior w.r.t. ζ. We thus need to rearrange the considerations from above in terms of ζ. First of all, $r \geq b$, no bistable behavior is possible. Now let's assume $r < b$. If ζ is small, then we are automatically in case 3(b), s.t. in principle we could have bistable behavior. If μ_z satisfies the inequalities

$$(r\mu_x - \zeta)/b \quad < \quad \mu_z \qquad \text{and} \qquad \mu_z \quad < \quad \mu_x - \tfrac{\zeta}{b} + \tfrac{\zeta}{r} - 2\sqrt{\tfrac{(b-r)}{br}\zeta\mu_x}$$

we do have this behavior. If we solve the inequalities for ζ, we find

$$r\mu_x - b\mu_z \quad < \quad \zeta \quad < \quad \tfrac{br}{b-r}(\sqrt{\mu_z} - \sqrt{\mu_x})^2.$$

Please note, that these two inequalities always can be satisfied simultaneously if $r^2\mu_x \neq b^2\mu_z$, since under this condition

$$\begin{aligned} & -(\sqrt{r^2\mu_x} - \sqrt{b^2\mu_z})^2 && < && 0 \\ \Rightarrow \quad & -r^2\mu_x - b^2\mu_z && < && -2br\sqrt{\mu_x\mu_z} \\ \Rightarrow \quad & br\mu_x - r^2\mu_x + br\mu_z - b^2\mu_z && < && br(\mu_x + \mu_z - \sqrt{\mu_x\mu_z}) \\ \Rightarrow \quad & r\mu_x - b\mu_z && < && \tfrac{br}{b-r}(\sqrt{\mu_z} - \sqrt{\mu_x})^2. \end{aligned}$$

If $r^2\mu_x = b^2\mu_z$ and $b < r$, the transcritical and the saddle-node-bifurcation happen at the same location, i.e. the trivial solution is involved. Thus, also under this non-generic condition we do not have a bistable behavior.

The degenerate case: $\mu_z = 0$ or $\zeta = 0$

In this section we will investigate the degenerate cases, $\zeta = 0$ and $\mu_z = 0$. Since the two cases require slightly different methods, we look at them separately.

Case 1: $\zeta = 0$.

We may follow the argumentation of the global analysis and find that

$$x(t) + y(t) - z(t) = a$$

where $a = x(0) + y(0) - z(0)$. Thus, we again derive a two-dimensional system, where we again may rescale time by $1/y(t)$. Let τ be the rescaled time, then

$$\begin{aligned} \tfrac{d}{d\tau}x &= -rx \\ \tfrac{d}{d\tau}y &= (r-b)x - by + ba. \end{aligned}$$

These two equations can be solved explicitly. First, we note that $x(\tau) = x(0)\exp(-r\tau)$. Next, we find

$$\begin{aligned} y(\tau) &= y(0)e^{-b\tau} + (r-b)x(0)\textstyle\int_0^\tau e^{-b(\tau-\sigma)}e^{-r\sigma}\,d\sigma + b\,a\int_0^\tau e^{-b(\tau-\sigma)}\,d\sigma \\ &= y(0)e^{-b\tau} + x(0)e^{-b\tau}\left(1 - e^{-(r-b)\tau}\right) + a\left(1 - e^{-b\tau}\right). \end{aligned}$$

Thus, $y(\tau) \to a$ if $a > 0$ and, since $y = 0$ is a singularity in the time transformation, $y(\tau) \to 0$ if $a \leq 0$. Thus, if at time $t = 0$ more z than x and y together is present in the system, z will "eat up" all zymogenes, otherwise the surplus of zymogenes will be left. There is no bistability present in the system.

Case 2: $\mu_z = 0$.

The analysis of $\mu_z = 0$ is the same like that for $\mu_z > 0$. If we consider the stationary points $y_\pm$ for $\mu_z = 0$, we find

$$\begin{aligned} y_\pm &= \tfrac{\zeta}{2}\left[\tfrac{\mu_x}{\zeta} - \tfrac{1}{b} - \tfrac{1}{r} \pm \sqrt{\left(\tfrac{\mu_x}{\zeta} - \tfrac{1}{b} + \tfrac{1}{r}\right)^2 - 4\tfrac{(b-r)}{br}\tfrac{\mu_x}{\zeta}}\,\right] \\ &= \tfrac{\zeta}{2}\left[\tfrac{\mu_x}{\zeta} - \tfrac{b+r}{br} \pm \sqrt{\left(\tfrac{\mu_x}{\zeta} - \tfrac{b-r}{br}\right)^2}\,\right], \end{aligned}$$

i.e. $y_+ = \mu_+ - \zeta/r$ and $y_- = -\frac{\zeta}{b}$. Thus, apart form the trivial stationary point, there is only one more non-negative stationary point, s.t. no bistable behavior is possible.

Bifurcation behaviour

One of the main outcomes of the analysis is that threshold behavior occurs only if the coagulation system is modelled within its physiological context, i.e. if physiological phenomena like blood flow are taken into account. We postpone the proof of the following result to the next subsection.Let us now concentrate on the case $\zeta > 0$ and $\mu_z > 0$, i.e. at the situation where blood flow as well as anticoagulant are present; the situations for $\zeta = 0$ or $\mu_z = 0$ are only discussed the last subsection.

Result of the bifurcation analysis:

(I) All trajectories tend to stationary points (see global analysis).

(II) Trivial stationary point: There is always a trivial stationary state ($y = 0$) present. At $\zeta = 0$, this trivial state undergoes a transcritical bifurcation (see last subsection).

(III) Non-trivial stationary states: There may be no, one or two positive stationary points. We find three scenarios (see Fig. 7.3).

(III.a) Assume $b \leq r$ or assume $b < r$ and $b^2\mu_z = r^2\mu_x$: No bistable behavior is possible. For $\zeta < r\mu_x - b\mu_z$ the trivial stationary point is unstable and there is a non-trivial, locally asymptotically stable stationary point. At $\zeta = r\mu_x - b\mu_z$, these two stationary points undergo a transcritical bifurcation; the non-trivial stationary point vanishes from the positive octant and the non-trivial stationary point becomes locally asymptotically stable.

(III.b) Assume $b > r$, $b^2\mu_z \neq r^2\mu_x$ and $r\mu_x > b\mu_z$: In this case, two bifurcations take place if we vary ζ: for $\zeta \in (0, r\mu_x - b\mu_z)$ the trivial stationary point is unstable while we have a positive, non-trivial, locally asymptotically stable stationary point. At $\zeta = r\mu_x - b\mu_z$ a transcritical bifurcation happens, and the trivial stationary state becomes locally asymptotically stable (and stays locally stable for all $\zeta > r\mu_x - b\mu_z$), while a saddle invades the positive octant. We observe a bistable behavior until the saddle and the locally asymptotically stable, nontrivial stationary point undergo a saddle-node bifurcation at $\zeta = br(\sqrt{\mu_x} - \sqrt{\mu_z})/(b - r)$ and vanish from the system.

(III.c) Assume $b > r$, $b^2\mu_z \neq r^2\mu_x$ and $r\mu_x \leq b\mu_z$: Then, for

$$0 < \zeta < \tfrac{br}{b-r}(\sqrt{\mu_x} - \sqrt{\mu_z})$$

we have a bistable behavior: the trivial stationary point and a positive, non-trivial stationary point are both locally asymptotically stable, while we have a second positive, non-trivial stationary point that is a saddle. At $\zeta = br(\sqrt{\mu_x} - \sqrt{\mu_z})/(b-r)$, the two non-trivial points are annihilated in a saddle-node bifurcation.

Especially in case (b) we find distinctly that the anticoagulant has in some sense similar effects like the blood flow: since $r\mu_x > b\mu_z$, the anticoagulant is not able to control

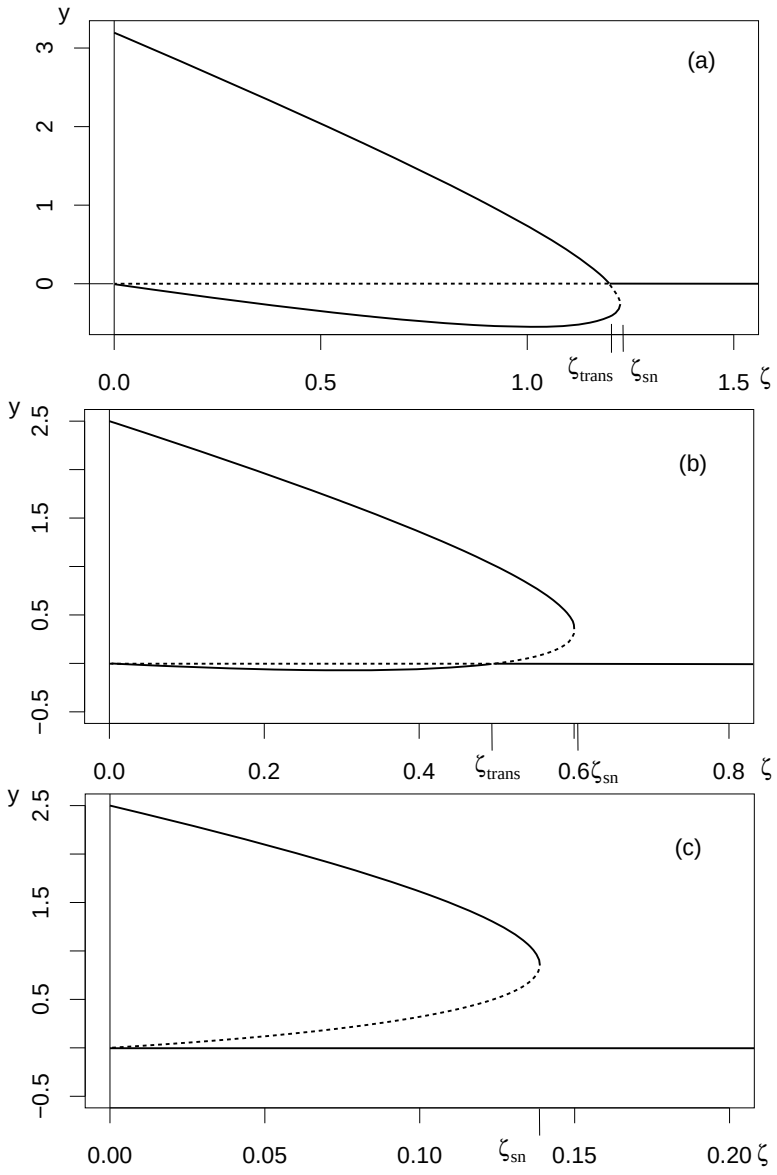

Figure 7.3: y-components of stationary points over ζ for the three cases (see text). Locally stable stationary points are indicated by a bold line, unstable stationary points by a dashed line. Negative values have no physiological meaning and are added only for better comprehensibility. The location of the saddle-node and the transcritical bifurcation on the ζ-axis are denoted by ζ_{sn} and ζ_{trans}, respectively. Parameters: (a) $\mu_x = 4$, $\mu_z = 0.8$, $b = 1$, $r = 0.5$, (b) $\mu_x = 4$, $\mu_z = 1.5$, $b = 1$, $r = 0.5$, (c) $\mu_x = 4$, $\mu_z = 1.5$, $b = 1.5$, $r = 0.2$.

the system, and the trivial stationary state is unstable. If, however, the blood flow is strong enough, then the combined effect of anticoagulant and wash-out stabilizes the non-activated state. The positive feedback loop for y increases pro-coagulative forces s.t. nevertheless an activated stationary state can exist (bistable behavior) as long as the blood flow is not too strong.

7.4 Minimal Model For The Whole Story

We now consider a fixed blood flow rate ζ. For appropriate parameter settings, we find a bistable regime: the trivial state is locally stable and a certain strength of the initial stimulus is necessary to activate the system. If the stimulus is above this threshold, the system eventually is completely activated. We now add a further process on a slow time scale, the increase of the density of anticoagulant. E.g., fIIa cleaves protein C to activated protein C, which suppresses the positive feedback loop of fIIa. Or, heparin is released that enhances the effect and the amount of ATIII. Thus, one may add to system (7.1) the differential equation

$$\dot{\mu}_z = \varepsilon(y - k\,(\mu_z - \mu_z^*)), \tag{7.3}$$

where ε is a small constant that separates time scales, μ_z^* denotes the density of anti-coagulants in the resting state and k the strength of the force that moves the system back in the resting state. Time scale arguments give an impression of the life cycle of the clot formation (see Fig. 7.4, "one spike"): a subcritical stimulus yields to the activation of the system. On the fast time scale, the system is completely activated and settles on the activated, stationary point. Then the slow time scale takes over and μ_z increases until the point of the saddle-node bifurcation is reached. Here, the coagulation process breaks down, and consequently the amount of anti-coagulants is reduced until the system reaches the resting state. There are three pathologic situation possible:

(1) The line $y = k(\mu_z^* - \mu_z)$ hits the (w.r.t. the fast field) stable branch of the stationary points. In this case, this intersection point is a locally stable stationary point of the complete system, and - once activated - the trajectory will tend to this point and settle there. The system never returns to the resting state but stays activated.

(2) μ_z^* is left of the transcritical bifurcation at $r\mu_x - b\mu_z$. We then find relaxation oscillations: after activation, the trajectory follows the locally stable branch of stationary points until it reaches the saddle-node-bifurcation, where the trajectory jumps to the resting state $y \approx 0$. Here, μ_z slowly proceeds towards μ_z^*. On this way, however, the trajectory crosses the stability change of the trivial solution, i.e. the point of the transcritical bifurcation. The trivial solution becomes locally unstable, s.t. the system eventually is repelled from the trivial branch and jumps to the activated branch again.

(3) μ_z^* is right of the saddle-node bifurcation. Then, the system cannot be activated. This may (*cum grano salis*) correspond to diseases like haemophilia.

It would be interesting to see, if the case (2) can appear in a well stirred flow reactor that works with "artificial plasma". As the assumptions underlying these mechanisms are very fundamental and structural stability can be assumed these phenomena might be amenable to experimental validation. Scenario (2) is close to the non-stirred reactor with only weak anti-coagulant substances, e.g. with only TFPI and no ATII or PC. In this case, we find complete, sustained activation. Only limited resources are able to stop the coagulation. Normally, the experiments are finished before this time is reached.

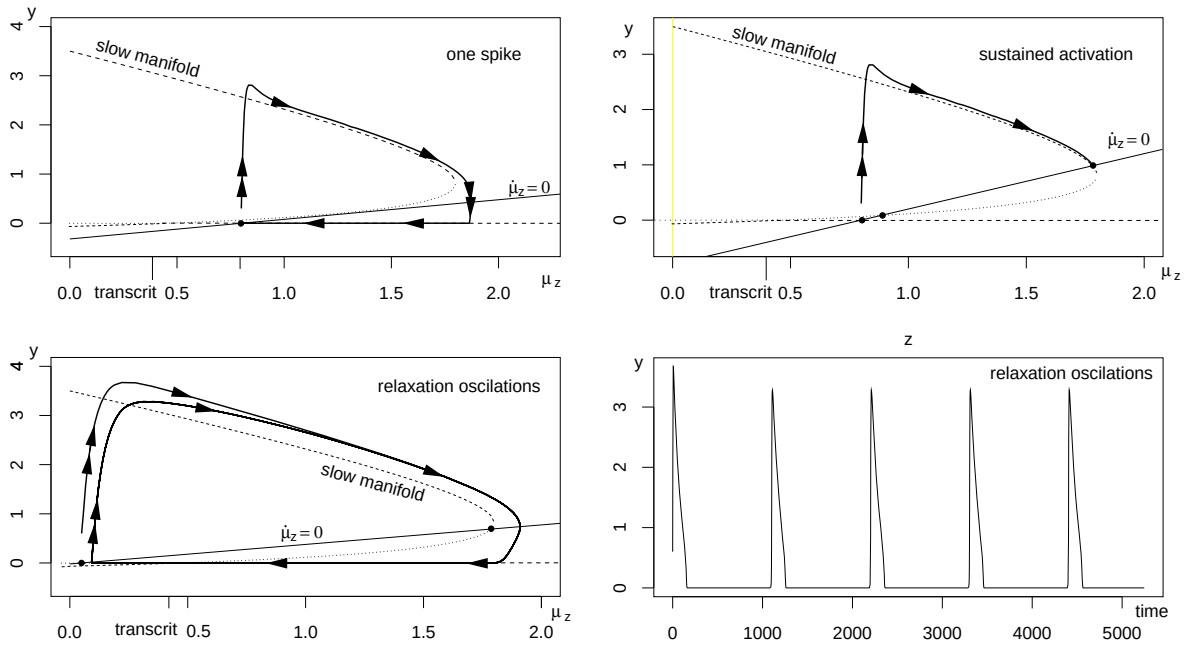

Figure 7.4: Time course of the complete model (7.1), (7.3) with flow and activation of anti-coagulatory substances. We find three cases: one spike only ($b = 1.5$, $r = 0.2$, $\mu_x = 4$, $\mu_z^* = 0.8$, $\epsilon = 0.02$, $k = 0.4$, $\zeta = 0.1$), sustained activation ($b = 1.5$, $r = 0.2$, $\mu_x = 4$, $\mu_z^* = 0.8$, $\epsilon = 0.02$, $k = 1.0$, $\zeta = 0.1$), and relaxation oscillations ($b = 1.5$, $r = 0.2$, $\mu_x = 4$, $\mu_z^* = 0.05$, $\epsilon = 0.01$, $k = 0.4$, $\zeta = 0.1$). Upper row and lower, left panel: the three situations are presented in the phase plane (y over μ_z). The bold line denotes the trajectory, the stationary points are indicated by filled circles. Furthermore, the slow manifold (stable: dashes, unstable: dots) and the isocline of μ_z are shown. Panel at the lower r.h.s: the time course of y for relaxation oscillations.

Time Scale Analysis

In this section we briefly sketch the bifurcation analysis of the model (7.1), (7.3) by means of time scale arguments and their results. In order to use the established theory of fold points here, the system is reduced to two dimensions by center manifold techniques. Consequently, fast solutions and slow manifold are identified. The orbit for $0 < \varepsilon \ll 1$ follows closely singular orbits, i.e. orbits that are concatenated by pieces of the slow manifold and jumps through the fast field. In order to identify parameter regions that induce one of the three patterns (one spike, sustained activation, relaxation oscillations) it is necessary to inspect (a) the location of the intersection point of the line given by $\dot{\mu}_z = 0$ with the slow manifold and (b) the stability of the resting state. If the line $\dot{\mu}_z = 0$ crosses the slow manifold in its stable region, then we always find sustained activation. If this intersection point is in the unstable part, the trajectory jumps through the fast field (close) to the μ_z-axis and drifts slowly towards the resting state. If the resting state is stable, it will finally stay there and we get one spike. If the resting state is unstable, the trajectory is eventually repelled from the μ_z-axis and the trajectory will oscillate.

The corresponding parameter regions can be thus identified as given in Figure 7.5. The extended Jacobian (see also local stability) for the trivial stationary point $(x, y, z, \mu_z) = (\mu_x, 0, \mu_z^*, \mu_z^*)$ and $\varepsilon > 0$ reads

$$J_{0,\varepsilon} = \begin{pmatrix} -\zeta & -r\mu_x & 0 & 0 \\ 0 & r\mu_x - b\mu_z^* - \zeta & 0 & 0 \\ 0 & -b\mu_z^* & -\zeta & \zeta \\ 0 & \varepsilon & 0 & -k\varepsilon \end{pmatrix}.$$

The eigenvalues are $\lambda_{1,2} = -\zeta$, $\lambda_3 = r\mu_x - b\mu_z^* - \zeta$ and $\lambda_4 = -k\varepsilon$. Therefor the resting state is stable if $\mu_z^* > \frac{r\mu_x - \zeta}{b}$ and unstable if $\mu_z^* < \frac{r\mu_x - \zeta}{b}$. The saddle-node bifurcation is located at (see stationary points)

$$(y, \mu_z) = (\sqrt{\tfrac{b-r}{br}\zeta\mu_x} - \tfrac{\zeta}{r}, \mu_x - \tfrac{\zeta}{b} - \tfrac{\zeta}{r} - 2\sqrt{\tfrac{b-r}{br}\zeta\mu_x}).$$

We assume that the resting state is left of the saddle-node bifurcation point, i.e. $\mu_z^* < \mu_x - \frac{\zeta}{b} - \frac{\zeta}{r} - 2\sqrt{\frac{b-r}{br}\zeta\mu_x}$, as only under this condition interesting behavior occurs (existence of non-trivial stationary points). The line $\dot{\mu}_z = 0$ crosses the slow manifold in its stable region if

$$k(\mu_x - \tfrac{\zeta}{b} - \tfrac{\zeta}{r} - 2\sqrt{\tfrac{b-r}{br}\zeta\mu_x} - \mu_z^*) > \sqrt{\tfrac{b-r}{br}\zeta\mu_x} - \tfrac{\zeta}{r}.$$

In terms of μ_z^*, this happens if

$$\mu_z^* < \mu_x + (1 + \tfrac{1}{k})\tfrac{\zeta}{r} - \tfrac{\zeta}{b} - (2 + \tfrac{1}{k})\sqrt{\tfrac{b-r}{br}\zeta\mu_x}.$$

	$\mu_z^* > \frac{r\mu_x - \zeta}{b}$	$\mu_z^* < \frac{r\mu_x - \zeta}{b}$
$\mu_z^* < \mu_x + (1+\frac{1}{k})\frac{\zeta}{r} - \frac{\zeta}{b} - (2+\frac{1}{k})\sqrt{\frac{b-r}{br}\zeta\mu_x}$	sustained activation	sustained activation
$\mu_z^* > \mu_x + (1+\frac{1}{k})\frac{\zeta}{r} - \frac{\zeta}{b} - (2+\frac{1}{k})\sqrt{\frac{b-r}{br}\zeta\mu_x}$	one spike	relaxation oscillation

Figure 7.5: Table of parameter regions.

Transient Behavior And Clot-Formation

From the practical point of view, the bifurcation structure gives a certain hint about the behavior we shall expect, but perhaps even not the most important hint: bifurcation analysis focuses on asymptotic analysis. However, even if the system eventually becomes completely activated, but this activation takes a very long time (which may be the case for $y(0)$ small), the result may be not different to that of a system that cannot be activated at all. Also relaxation oscillations may not play any role, if the time period between the localized spike-like bursts of activation is very long. In order to get an idea about the transient behavior and the performance of the system for different values of ζ, we focus on the situation that may reflect the physiological situation, i.e. those parameters that guarantee that one spike occurs. We are especially interested in the overall strength of the response on a given stimulus.

We compare on the one hand the time course of $y(t)$ for different parameters and different initial activation (i.e. different size of $y(0)$) and different flow rates (see Fig. 7.6). We find that the system may be activated if the initial condition is above the threshold that separates the trivial stationary point form the activated state. In the simulations, this threshold is close to the y-component of the unstable stationary point. The magnitude of the activation depends on the flow and is lower for higher flow. This fact is also observed in experiments [18]. This finding reflects the simple fact that the average time the zymogen is presented to the active zymogen becomes shorter if the blood flow is faster. If a certain threshold is exceeded, this washing-out effect is strong enough to break the positive feedback loop.

Another magnitude of interest is the total yield of fIa. Since factor IIa cleaves factor I to factor Ia, this amount is more or less proportional to the integral of IIa formed during the whole time; of course, this magnitude only takes into account the cleavage process and not the amount of fI available for cleavage; the latter may strongly depend on the flow. We thus determine this integral for different values of ζ and different values of $y(0)$. This integral is closely related to the time the system stays activated, i.e.

the relaxation time. We will compare these findings with similar computations of more realistic models. In Fig. 7.7 the result is drawn. We find, that - on a logarithmic scale - the flow rate resp. the initial condition influence the result rather weakly, as long as we are above (resp. below) the activation threshold. Below this threshold, the yield is one to two magnitudes less. This threshold nicely agrees with the analysis of stationary points: if we consider the y-component of the saddle point y_-, then this line (shown at the bottom of the graph) agrees with the activation threshold.

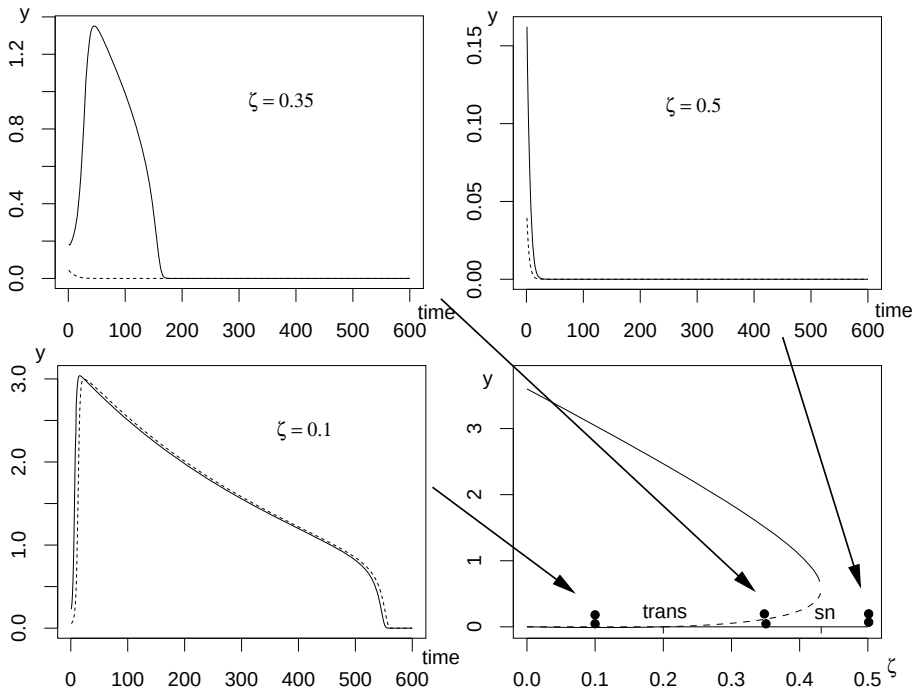

Figure 7.6: Time course of the complete model (7.1), (7.3) with flow and activation of anti-coagulatory substances. The trajectory for $\zeta \in \{0.1, 0.35, 0.5\}$ and $y(0) = 0.05$ (dashed line) resp. $y(0) = 0.2$ (solid line) are shown. The structure of the stationary points in the fast system (together with the initial conditions for y are presented in the left, lower corner (parameter values: $b = 1.5$, $r = 0.2$, $\mu_x = 4$, $\mu_z^* = 0.8$, $\epsilon = 0.02$, $k = 0.4$).

7.5 Realistic coagulation models

The basis of the present section is a large simulation model introduced by Hockin et al. [26]. The model has 29 players and describes the most important pathways of the intrinsic coagulation system. We adapt the model to our needs: we added the APC-inhibitory pathway to this model and we introduce the blood flow formulated as inflow and outflow rates. Here, we need to distinguish between molecules bound to surfaces (cell surfaces resp. PSPL-particle surface) and factors that diffuse freely (for details of

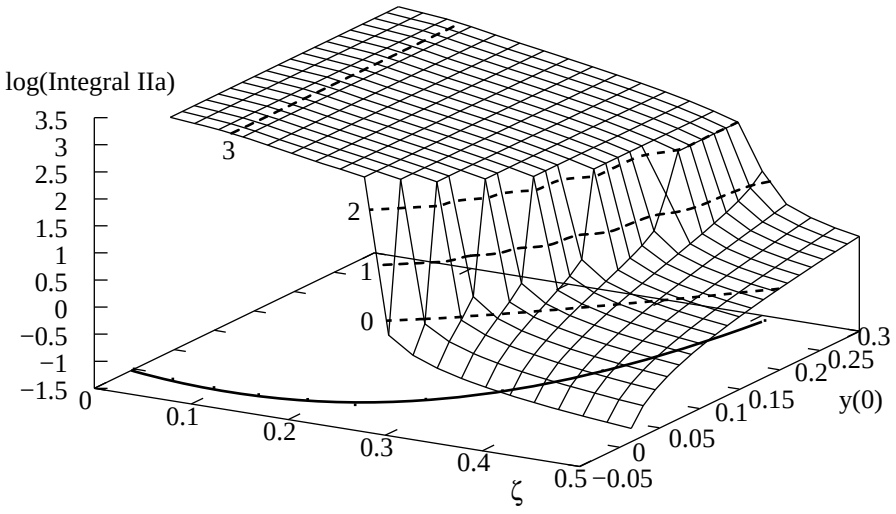

Figure 7.7: Logarithm over the integral over $y(t)$ for $t \in [0, 600]$ for different initial conditions and different flow rates ζ. The level curves for 3,, 2, 1 and 0 are indicated by dashed curves on the surface of the graph. The solid line at the base of the graph represents the stationary point y_- in dependence of ζ. Above this line, the initial condition is able to activate the system, below this line this is not possible. ($b = 1.5$, $r = 0.2$, $\mu_x = 4$, $\mu_z^* = 0.8$, $\epsilon = 0.02$, $k = 0.4$).

this model see the article of Hockin [26]). Of course, this simple way to introduce the blood flow is perhaps not able to model the situation in a vessel. We rather model a well stirred flow reactor, that parallels the well stirred tank reactors for the "artificial plasma". We nevertheless expect the system to have enough properties in common with the physiologic situation, s.t. the overall outcome allows to gain insight in mechanisms of the *in vivo* situation.

If we first consider the model only for the first part of the pathway, from TF to Xa, we do not find a sign for an activation threshold (see Fig. 7.8, upper panel). Also the stability analysis of the trivial stationary state (TF=0, all other substances like indicated in Tab. 7.4, third column) yields the stability of the trivial stationary state for $\zeta > 0$. Like in the small model above, the stationary point undergoes at $\zeta = 0$ always a stability change. Since TF vanishes in the long run (due to the fact that ATIII withdraws the system irreversibly TF-VIIa), the feedback has no chance to reach a self sustained state. Nevertheless, and this is the important finding, there is no threshold for the minimal amount of TF present. The efficacy, i.e. amount of Xa per amount of TF is about the same range – a detailed analysis shows a variation of this ratio of at most two if we vary the initial amount of TF in a reasonable manner. This is in accordance to dose-dependency curves measured in a system without flow [5].

Now we go to the full model in order to investigate the threshold behavior of IIa. If

Reaction			Rate
TF + VII	→	TF-VII	$3.2 \cdot 10e5/(\text{Mol} \cdot \text{sec})$
TF-VII	→	TF + VII	$3.1 \cdot 10e\text{-}4/\text{sec}$
TF + VIIa	→	TF-VIIa	$2.3 \cdot 10e6/(\text{Mol} \cdot \text{sec})$
TF-VIIa	→	TF + VIIa	$3.1 \cdot 10e\text{-}4/\text{sec}$
TF-VIIa + VII	→	TF-VIIa + VIIa	$4.4 \cdot 10e4/(\text{Mol} \cdot \text{sec})$
Xa + VII	→	Xa + VIIa	$1.3 \cdot 10e6/(\text{Mol} \cdot \text{sec})$
IIa + VII	→	IIa + VIIa	$2.3 \cdot 10e3/(\text{Mol} \cdot \text{sec})$
TF-VIIa + X	→	TF-VIIa-X	$2.5 \cdot 10e6/(\text{Mol} \cdot \text{sec})$
TF-VIIa-X	→	TF-VIIa + X	$1.05/\text{sec}$
TF-VIIa-X	→	TF-VIIa-Xa	$6/\text{sec}$
TF-VIIa + Xa	→	TF-VIIa-Xa	$2.2 \cdot 10e6/(\text{Mol} \cdot \text{sec})$
TF-VIIa-Xa	→	TF-VIIa + Xa	$19/\text{sec}$
TF-VIIa + IX	→	TF-VIIa-IX	$1.0 \cdot 10e6/(\text{Mol} \cdot \text{sec})$
TF-VIIa-IX	→	TF-VIIa + IX	$2.4/\text{sec}$
TF-VIIa-IX	→	TF-VIIa + IXa	$1.8/\text{sec}$
Xa + II	→	Xa + IIa	$7.5 \cdot 10e2/(\text{Mol} \cdot \text{sec})$
IIa + VIII	→	IIa + VIIIa	$2.0 \cdot 10e6/(\text{Mol} \cdot \text{sec})$
VIIIa + IXa	→	IXa-VIIIa	$1.0 \cdot 10e6/(\text{Mol} \cdot \text{sec})$
IXa-VIIIa	→	VIIIa + IXa	$5.0 \cdot 10e\text{-}4/\text{sec}$
IXa-VIIIa + X	→	IXa–VIIIa-X	$1.0 \cdot 10e7/(\text{Mol} \cdot \text{sec})$
IXa–VIIIa-X	→	IXa-VIIIa + X	$1.0 \cdot 10e\text{-}4/\text{sec}$
IXa–VIIIa-X	→	IXa-VIIIa + Xa	$8.2/\text{sec}$
VIIIa	→	$2 \cdot$ VIIIa1-L	$6.0 \cdot 10e\text{-}4/\text{sec}$
$2 \cdot$ VIIIa1-L	→	VIIIa	$2.2 \cdot 10e3/(\text{Mol} \cdot \text{sec})$
IXa–VIIIa-X	→	$2 \cdot$ VIIIa1-L + X + IXa	$1.0 \cdot 10e\text{-}4/\text{sec}$
IXa-VIIIa	→	$2 \cdot$ VIIIa1-L + IXa	$1.0 \cdot 10e\text{-}4/\text{sec}$
IIa + V	→	IIa + Va	$2.0 \cdot 10e6/(\text{Mol} \cdot \text{sec})$
Xa + Va	→	Xa-Va	$4.0 \cdot 10e7/(\text{Mol} \cdot \text{sec})$
Xa-Va	→	Xa + Va	$0.2/\text{sec}$
Xa-Va + II	→	Xa-Va-II	$1.0 \cdot 10e7/(\text{Mol} \cdot \text{sec})$
Xa-Va-II	→	Xa-Va + II	$103/\text{sec}$
Xa-Va-II	→	Xa-Va + mIIa	$63.5/\text{sec}$
mIIa + Xa-Va	→	IIa + Xa-Va	$1.5 \cdot 10e6/(\text{Mol} \cdot \text{sec})$
Xa + TFPI	→	Xa-TFPI	$9.0 \cdot 10e4/(\text{Mol} \cdot \text{sec})$
Xa-TFPI	→	Xa + TFPI	$3.6 \cdot 10e\text{-}5/\text{sec}$
TF-VIIa-Xa + TFPI	→	TF-VIIa-TFPI-Xa	$3.2 \cdot 10e7/(\text{Mol} \cdot \text{sec})$
TF-VIIa-TFPI-Xa	→	TF-VIIa-Xa + TFPI	$1.1 \cdot 10e\text{-}5/\text{sec}$
TF-VIIa + Xa-TFPI	→	TF-VIIa-TFPI-Xa	$5.0 \cdot 10e6/(\text{Mol} \cdot \text{sec})$
Xa + ATIII	→		$1.5 \cdot 10e2/(\text{Mol} \cdot \text{sec})$
mIIa + ATIII	→		$7.1 \cdot 10e2/(\text{Mol} \cdot \text{sec})$
IXa + ATIII	→		$4.9 \cdot 10e1/(\text{Mol} \cdot \text{sec})$
IIa + ATIII	→		$7.1 \cdot 10e2/(\text{Mol} \cdot \text{sec})$
TF-VIIa + ATIII	→		$2.3 \cdot 10e1/(\text{Mol} \cdot \text{sec})$

Table 7.1: Reactions of the simulation original model of Hockin [26]. All reaction products withdrawn from the system do not appear on the right hand side.

Reaction			Rate	Source
PC	→	APC	$480/\text{min} \cdot \text{muMol} \cdot \text{IIa}/(6.1 \cdot \text{muMol}+\text{PC})$	[22]
PC	→	APC	$480/\text{min} \cdot \text{mIIa}/(6.1 \cdot \text{muMol}+\text{PC})$	[22]
Va + APC	→	APC	$10e5/(\text{Mol} \cdot \text{sec})$	[40]
Xa-Va + APC	→	APC	$10e5/(\text{Mol} \cdot \text{sec})$	[40]
Xa-Va-II + APC	→	APC	$10e5/(\text{Mol} \cdot \text{sec})$	[40]
APC	→		$1/(18 \cdot \text{min})$	[25]
VIII + APC	→	APC	$1/(1.25 \cdot \text{muMol} \cdot \text{sec})$	[11]
VIIIa + APC	→	APC	$1/(\text{muMol} \cdot \text{min})$	[11]
IXa-VIIIa + APC	→	APC	$1/(\text{muMol} \cdot \text{min})$	[11]
IXa–VIIIa-X + APC	→	APC	$1/(\text{muMol} \cdot \text{min})$	[11]
VIIIa1-L + APC	→	APC	$1/(\text{muMol} \cdot \text{min})$	[11]

Table 7.2: APC-pathway added to the model. We assumed that rates for complexes are the same like the rates for single zymogenes. Note, that we assumed here for the activation of PC Michaelis-Menten kinetics.

we incorporate the flow we find a strong dependency of the amount of IIa produced on the initial amount of TF. This effect is not present for $\zeta = 0$. This finding indicates that there is a flow-dependent activation threshold in the coagulation system. In the first step, TF will always create a small amount of Xa. The strength of the local loss of Xa by washing out will determine if or if not the motor of positive feedback loop (IIa produces Va and VIIIa, Va-Xa and VIIIa-IXa produce Xa that again produces IIa) is able to be activated such that this loop can life self-sustained. Of course, the activation of APC by IIa will finally shut down this motor and bring the system to rest again.

The simple model of section three seems to catch most aspects of this finding. However, there are some differences that do not allow a direct analysis of the complete system by means of the methods used for the minimal model (also not by means of numerical bifurcation tools). According to the model used, the factors VIIIa and Va resp. the complexes they are part of will accumulate on the cell wall if no PC and APC is present in the system. Since we did not introduce a bounded capacity of the cell wall, we cannot prevent this to happen. In order to obtain an impression about the behavior of the system, this bounded carrying capacity is not important, since APC will destroy these complexes before they start to grow unlimited. However, if one desires to perform a bifurcation analysis it may be desirably to find stationary states in absence of PC, i.e. to investigate the fast system alone. In this case we would need the bounded carrying capacity.

Substance			Rate
VIIa	→		ζ
	→	VIIa	ζ*VIIa0
Xa	→		ζ
X	→		ζ
	→	X	ζ*X0
IX	→		ζ
	→	IX	ζ*IX0
II	→		ζ
	→	II	ζ*II0
VIII	→		ζ
	→	VIII	ζ*VIII0
V	→		ζ
	→	V	ζ*V0
mIIa	→		ζ
IIa	→		ζ
TFPI	→		ζ
	→	TFPI	ζ*TFPI0
ATIII	→		ζ
	→	ATIII	ζ*ATIII0
Xa-TFPI	→		ζ
PC	→		ζ
	→	PC	ζ*PC0

Table 7.3: Effect of blood flow added to the model. If a substance flows into the system, the left hand side is left blank, if a substance flows out of the system, the right hand side is left blank. The constants in the rates are the plasma concentrations of different substances (see also Table 7.4).

Substance	scale	Initialvalue (TF to Xa)	initial value (complete model)
TF	pMol	25 pMol (varied)	25 pMol (varied)
VII	nMol	10 nMol	10 nMol
TF–VII	pMol	0 nMol	0 nMol
VIIa	nMol	0.1 nMol=VIIa0	0.1 nMol=VIIa0
TF–VIIa	pMol	0 Mol	0 Mol
Xa	nMol	0 Mol	0 Mol
IIa	muMol	0 Mol	0 Mol
X	nMol	0.16 muMol=X0	0.16 muMol=X0
TF–VIIa–X	pMol	0 Mol	0 Mol
TF–VIIa–Xa	pMol	0 Mol	0 Mol
IX	nMol	0 nMol=IX0	90 nMol=IX0
TF–VIIa–IX	nMol	0 Mol	0 Mol
IXa	nMol	0 Mol	0 Mol
II	muMol	0 muMol=II0	1.4 muMol=II0
VIII	nMol	0 nMol=VIII0	0.7 nMol=VIII0
VIIIa	nMol	0 Mol	0 Mol
IXa–VIIIa	nMol	0 Mol	0 Mol
IXa–VIIIa–X	nMol	0 Mol	0 Mol
VIIIa1–L	nMol	0 Mol	0 Mol
V	nMol	0 nMol=V0	20 nMol=V0
Va	nMol	0 nMol	0 nMol
Xa–Va	nMol	0 Mol	0 Mol
Xa–Va–II	nMol	0 Mol	0 Mol
mIIa	muMol	0 Mol	0 Mol
TFPI	nMol	2.5 nMol=TFPI0	2.5 nMol=TFPI0
Xa–TFPI	nMol	0 Mol	0 Mol
TF–VIIa–TFPI–Xa	nMol	0 Mol	0 Mol
ATIII	muMol	3.4 muMol=ATIII0	3.4 muMol=ATIII0
PC	muMol	0 muMol=PC0	0.08 muMol=PC0
APC	nMol	0 nMol	0 nMol
time	10 sec	0 sec	0 sec

Table 7.4: Initial conditions for the system. The second column has been used for the investigation of the production of Xa by TF, the third column for the simulation of the complete model. The scale gives the information hw to relate the de-demensionalized magnitude to their dimensional counterpart. E.g, if, in the de-demensionalized ODE we have $t = 10$, then time is $10 \cdot 10$ sec $=$ 100 sec.

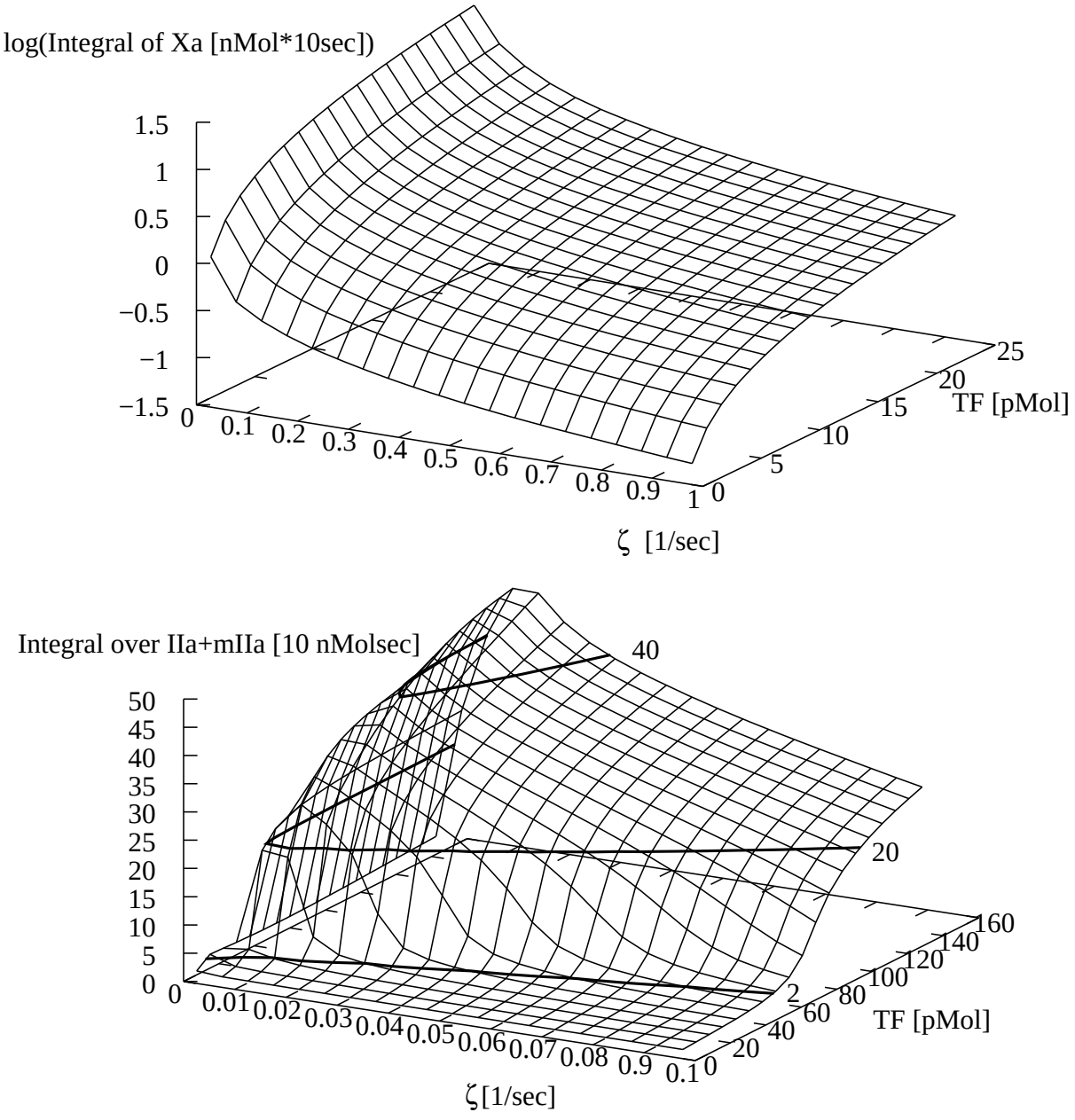

Figure 7.8: Upper panel: Logarithm over the integral of $Xa(t)$ for $t \in [0, 5000 \text{ sec}]$ for different initial conditions in TF and different flow rates ζ. Lower panel: Yield of IIa+mIIa in dependence of the initial amount of TF and the flow rate. The level sets for 2, 20 and 40 are indicated by bold lines.

7.6 Discussion

To better understand the basic mechanisms that may be responsible for threshold behavior of the coagulation cascade we investigated a minimal model of the coagulation pathway. This minimal model consists of a coagulation factor (fII) that is able to activate itself, blood flow that transports new coagulation factors into the region of interest resp. washes away activated coagulation factors and an anticoagulatorive substance (AT III). Additionally the density of anticoagulative (ATII and APC) is increased by activated fII.

Under some circumstances "blood flow" may be replaced by biochemical reactions that sustain the process in making new zymogen available and suppress the process in eliminating all three kinds of molecules, the zymogen, the activated zymogen and the inhibitor. This observation may be of value if one addresses the question why sTF alone does not activate the coagulation system. Since sTF is in the whole blood, the blood flow is not of outstanding importance for tolerance in this case, but rather the limited halftime of the sTF-VII-complex and its low affinity to the cell wall [46, 14]. These properties together with the low density of sTF and the overall structure exploited here may provide an explanation.

We used time scale arguments in order to reveal the basic dynamics. If the anticoagulatorive substances are assumed to be increased on a slow time scale, we find parameter regions with the desired bistable behavior, i.e. with threshold behavior. Both, the blood flow as well as the anticoagulatorive substance are needed to produce this behavior. If the system can be activated at all, and no flow is present, we then find that the resting state is unstable. This behavior is in accordance with experimental findings [38]. The blood has a detractive as well as a beneficial effect on the activation of the system: blood flow transports new raw material to the region of interest. On the other hand the wash-out effect reduces the efficiency of the auto-feedback loop. This is reflected by a steep increase of the yield for very small flow rates, followed by a slow decrease for higher flow rates (if the system is subcritical). The latter observation is supported by experimental evidence [18] as well as clinical knowledge as a reduced blood flow is a known risk factor for the development of thrombosis.

Adding the slow time scale, we find four classes of behavior: (1) after a complete activation of the coagulation cascade, the system will be finally deactivated by the increasing amount of anticoagulants. This may describe the physiological situation. (2) The anticoagulants are not able to shut down the system; once the system has been activated it stays activated. (3) Relaxation oscillations occur. However, the outbreaks of activated zymogen are quite localized, and the time between two outbreaks is long enough s.t. they perhaps play no larger role. From a practical point of view, they may be indistinguishable from the first scenario. Nevertheless, the phenomenon that some patients develop a thrombosis without any elicitating event and with no abnormalities concerning the densities and activities of coagulation factors might be explained by this

mechanism. (4) The system is not able to be activated, either because the blood flow is too high or because the concentrations of anticoagulative substances are to high. This scenario may correspond to coagulation failures like haemophilia. This effect might also be of interest in a situation of hyperdynamic hemodynamics like in hemorrhagic shock or sepsis.

In a second step we investigated a simulation model of the coagulation cascade. It is not the aim of this model to provide an exact picture of the coagulation cascade *in vivo*. The aim was to analyze the overall mechanisms governing the activation behavior in a physiologic context, i.e. the dependence of the coagulation process from blood flow. Thus certain simplifications had to be accepted. Consequently the model is not sophisticated enough to allow quantitative conclusions; however, qualitative conclusions can be drawn.

We find that the first step, from TF to the initially triggered fXa, does not exhibit a threshold but is completely driven by TF: the more TF, the more fXa will appear. The connection between TF and fXa is approximately linear. This finding is supported by experiments [5], where the time course of fXa does not show exponential growth in time, which would be expected for an unstable resp. subcritical situation. Since blood flow affects rather fXa than the membrane bound TF-fVII(a), it is reasonable that the mechanism under consideration (the blood flow) does not affect to system behavior at this point.

This is different if we consider the complete cascade. The positive auto-feedback loop relays on fIIa and fXa. Hence, the wash out of these two substances critically affects this feedback loop. With respect to the complete cascade threshold behavior can be observed. Since the first step of the cascade does not show this threshold behavior, we conclude that this observation is caused by the wash out of fXa resp. fIIa, and takes only place in the second part of the coagulation system.

In accordance with our minimal model we conclude that the threshold behavior is created by the interplay of blood flow and ATIII, while the deactivation of the system basically is due to the activation of PC to APC and the effect of APC on the feedback loop (via fVa and fXIIIa). Also in accordance with feedback the minimal model as well as with the experiments we find a sharp increase of the yield (total fIIa produced) for very small flow rates that slowly decreases for higher flow rates.

From the clinical point of view the model presented here offers several interesting aspects that warrant further investigation. The effects of blood flow are of special interest in trauma patients, as these patients typically present with severe coagulation disorders. The blood loss by itself as well as the therapeutic interventions (e.g. infusion of large amounts of fluids) result in marked alterations of tissue blood flow. The model presented here might be a valuable tool to analyze the interactions of these phenomena, which are difficult to analysis experimentally. Emerging therapeutic concepts for trauma

associated coagulation disorders, which mostly rely on substitution of fVIIa, can also be evaluated, or optimized, on the basis of the present model of coagulation.

Bibliography

[1] U. Alon. Network motifs: theory and experimental approaches. *Nat. Rev. Genet.*, 8:450–461, 2007.

[2] M. Anand, K. Rajagopal, and K.R. Rajagopal. A model incorporating some of the mechanical and biochemical factors underlying clot formation and dissolution in flowing blood: review article. *J. Theoret. Med.*, 5:183–218, 2003.

[3] M. Anand, K. Rajagopal, and K.R. Rajagopal. A model for the formation and lysis of blood clots. *Pathophys. Haemost. Thromb.*, 34:109–120, 2005.

[4] S. Banerjee and I. Bose. Functional characteristics of a double positive feedback loop coupled with autorepression. *Phys. Biol.*, 5, 2008.

[5] R. Baugh, G. Bronze, and S. Krishnaswamy. Regulation of extrinsic pathway factor Xa formation by tissue factor pathway inhibitor. *J. Biol. Chem.*, 273:4378–4386, 1998.

[6] E. Benoit, J.F. Callot, F. Diener, and M. Diener. Chasse au canard. *Collectanea Mathematica*, 31-32:37–119, 1981.

[7] S. Butenas and K.G. Mann. Blood coagulation. *Biochem.*, 67:5–15, 2002.

[8] S-N. Chow, C. Li, and D. Wang. *Normal Forms and Bifurcations of Planar Vector Fields*. Cambridge University Press, 1994.

[9] E.A. Ermakova, M.A. Panteleev, and E.E. Shnol. Blood coagulation and propagation of autowaves in flow. *Pathophys. Haemost. Thromb.*, 34:135–142, 2005.

[10] B. Ermentraut. XPPAUT 5.85 the differential tool. 2003.

[11] P. Fay, T.M. Smudzin, and F.J. Walker. Activated protein c-catalyzed inactivation of human factor viii and factor viiia. *J. Biol. Chem.*, 266:20139–20145, 1991.

[12] N. Fenichel. Persistence and smoothness of invariant manifolds for flows. *Math. J., Indiana Univ.*, 21:193–226, 1971.

[13] N. Fenichel. Geometric singular perturbation theory. *J. Diff. Equ.*, 31:53–98, 1979.

[14] M.M. Fiore, P.F. Neuenschwander, and J.H. Morrissey. The biochemical basis for the apparent defect of soluble mutant tissue factor in enhancing the proteolytic activities. *J. Biol. Chem.*, 269:143–149, 1994.

[15] R. FitzHugh. Impulses and physiological states in theoretical models of nerve membranes. *Biophys J.*, 1:445–466, 1961.

[16] A.L. Fogelson and N. Tania. Coagulation under flow: The influence of flow-mediated transport on the initiation and inhibition of coagulation. *Pathophys. Haemost. Thromb.*, 34:91–108, 2005.

[17] F.R. Gantmacher. *Matrizentheorie*. Springer: New York, Berlin, Heidelberg, 1986.

[18] C.H. Gemmell, V.T. Turitto, and Y. Nemerson. Flow as a regulator of the activation of factor X by tissue factor. *Blood*, 72:1404–1406, 1988.

[19] B.C. Goodwin. Oscillatory behavior in enzymatic control processes. *Adv. in Enzyme Regulation*, 3:425–438, 1965.

[20] J.S. Griffith. Mathematics of cellular control processes i. *J. Theoret. Biol.*, 20:202–208, 1968.

[21] J.S. Griffith. Mathematics of cellular control processes ii. *J. Theoret. Biol.*, 20:209–216, 1968.

[22] B.W. Grinnell, J.D. Walls, and B.Gerli. Glycosylation of human protein c affects its secretion, processing, functional activities, and activation by thrombin. *J. Biol. Chem.*, 266:9778–9785, 1991.

[23] J. Guckenheimer and P. Holmes. *Nonlinear Oscillations, Dynamical Systems, and Bifurcations of Vector Fields*. Springer: New York, Berlin, Heidelberg, 1983.

[24] S.P. Hastings, J.J. Tyson, and D. Webster. Existence of periodic solutions for negative feedback control systems. *J. Diff. Eq.*, 25:39–64, 1977.

[25] M. Heerb, A. Gruber, and J. Griffin. Identification of divalent metal ion-dependent inhibition of activated protein c by alpha 2-macroglobulin and alpha 2-antiplasmin in blood and comparisons to inhibition of factor xa, thrombin, and plasmin. *J. Biol. Chem.*, 266:17606–17612, 1991.

[26] M.F. Hockin, K.C. Jones, S.J. Everse, and K.G. Mann. A model for the stoichiometric regulation of blood coagulation. *J. Biol. Chem.*, 277:18322–18333, 2002.

[27] C.K.R.T. Jones. Geometric singular perturbation theory. Johnson, Russell (ed.), Dynamical systems. Lectures given at the 2nd session of the Centro Internazionale Matematico Estivo (CIME) held in Montecatini Terme, Italy, June 13-22, 1994. Berlin: Springer-Verlag. Lect. Notes Math. 1609, 44-118 (1995)., 1995.

[28] C.K.R.T. Jones. A geometric approach to systems with multiple time scales. *Bull. JSIAM*, 7:No. 4, 1997.

[29] C.K.R.T. Jones, T. Kaper, and N. Kopell. Tracking invariant manifolds up to exponentially small errors. *SIAM J. Math. Analysis*, 27:558–577, 1996.

[30] C.K.R.T. Jones and N. Kopell. Tracking invariant manifolds with differential forms in singularly perturbed systems. *J. Diff. Eq.*, 108:64–88, 1994.

[31] D.S. Jones and B.D. Sleeman. *Differential equations and mathematical biology.* London: CRC Press, 2003.

[32] K.C. Jones and K.G. Mann. A model for the tissue factor pathway to thrombin. *J. Biol. Chem.*, 269:23367–23373, 1994.

[33] M.A. Khanin and V.V. Semenov. A mathematical model of the kinetics of blood coagulation. *J. Theor. Biol.*, 136:127–134, 1989.

[34] J.-R. Kim, Y. Yoon, and K.-H. Cho. Coupled feedback loops form dynamic motifs of cellular networks. *Biophys. J.*, 94(2):359–364, 2008.

[35] M. Krupa and P. Szmolyan. Extending singular perturbation theory to non-hyperbolic points - fold and canard points in two dimensions. *SIAM J. Math. Analysis*, 33:No. 2, 2001.

[36] M. Krupa and P. Szmolyan. Relaxation oscillation and canard explosion. *J. Diff. Equ.*, 174:312–368, 2001.

[37] Y. A. Kuznetsov. *Elements of Applied Bifurcation Theory.* Springer: New York, Berlin, Heidelberg, 1995.

[38] J.H. Lawson, M. Kalafatis, Sh. Stram, and K.G. Mann. A model for the tissue factor pathway to thrombin. *J. Biol. Chem.*, 269:23357–23366, 1994.

[39] A.I. Lobanov and T.K. Starozhilova. The effect of convective flows on blood coagulation processes. *Pathophys. Haemost. Thromb.*, 34:121–134, 2005.

[40] L.Yang, C. Manithody, and A. Rezale. The functional significance of the autolysis loop in protein c and activated protein c. *Thromb. Haemost.*, 94:60–68, 2005.

[41] K. Mann, S. Butenas, and K. Brummel. The dynamics of thrombin formation. *Arterioscler. Thromb. Vasc. Biol.*, 23:17–25, 2003.

[42] K. Mann, M. Nesheim, W. Church, P. Haley, and S. Krishnaswamy. Surface-dependent reactions of the vitamin k-dependent enzyme complexes. *Blood*, 76:1–16, 1990.

[43] J.D. Murray. *Mathematical Biology I: An Introduction.* Springer: New York, Berlin, Heidelberg, 2002.

[44] J.D. Murray. *Mathematical Biology II: Spatial Models and Biomedical Applications.* Springer: New York, Berlin, Heidelberg, 2002.

[45] J.S. Nagumo, S. Arimoto, and S. Yoshizawa. An active pulse transmission line simulating nerve axon. *Proc. IRE*, 50:2061–2071, 1962.

[46] L.V.M. Rao, O.Nordfang, A.D. Hoang, and U.R. Pendurthi. Mechanism of an-

tithrombin III inhibition of factor VIIa/tissue factor activity on cell surfaces. Comparison with tissue factor pathway inhibitodfactor Xa-induced inhibition of factor VIIa/tissue factor activity. *Blood*, 85:121–129, 1995.

[47] W. Sha, J. Moore, K. Chen, A.D. Lassaletta, C.-S. Yi, J.J. Tyson, and J.C. Sible. Hysteresis drives cell-cycle transitions in *xenopus iaevis* egg extracts. *Cell Biol.*, 100:975–980, 2003.

[48] H.L. Smith. Systems of ordinary differential equations which generate an order preserving flow. a survey of results. *SIAM Rev.*, 30:No. 1, 1988.

[49] J. Tsang, J. Zhu, and A.v. Oudenaarden. MicroRNA-mediated feedback and feedforward loops are recurrent network motifs in mammals. *Mol. Cell*, 26:753–767, 2007.

[50] J.J. Tyson. *What everyone should know about the Belousov-Zhabotinsky reaction*, volume 100 of *Lect. Notes in Biomathematics*, pages 569–587. Springer: New York, Berlin, Heidelberg, 1994.

[51] J.J. Tyson and H. Othmer. The dynamics of feedback control circuits in biochemical pathways. *Prog. Theor. Biol.*, 5:1–62, 1978.

[52] ABC News Internet Ventures. What is a "feedback loop"?, February 2006.

[53] Wolfram Research Inc. Mathematica 5.0. 1988-2003.

[54] C.Q. Xu, Y.J. Zeng, and H. Gregersen. Dynamic model of the role of platelets in the blood coagulation system. *Med. Engin. Phys.*, 24:587–593, 2002.